Copyright Warning & Restrictions

The copyright law of the United States (Title 17, United States Code) governs the making of photocopies or other reproductions of copyrighted material.

Under certain conditions specified in the law, libraries and archives are authorized to furnish a photocopy or other reproduction. One of these specified conditions is that the photocopy or reproduction is not to be "used for any purpose other than private study, scholarship, or research." If a, user makes a request for, or later uses, a photocopy or reproduction for purposes in excess of "fair use" that user may be liable for copyright infringement,

This institution reserves the right to refuse to accept a copying order if, in its judgment, fulfillment of the order would involve violation of copyright law.

Please Note: The author retains the copyright while the New Jersey Institute of Technology reserves the right to distribute this thesis or dissertation

Printing note: If you do not wish to print this page, then select "Pages from: first page # to: last page #" on the print dialog screen

Kuan, Chih-Ning

AN EXPERIMENTAL STUDY OF MULTIPLE STEADY STATES IN A PHOTOPOLYMERIZATION REACTOR

New Jersey Institute of Technology D.ENG.SC. 1982

AN EXPERIMENTAL STUDY OF MULTIPLE STEADY STATES IN A PHOTOPOLYMERIZATION REACTOR

by

Chih-Ning Kuan

A Dissertation submitted to the faculty of the Graduate School of the New Jersey Institute of Technology in partial fulfillment of the requirements for the degree of Doctoral of Engineering Science

1982

APPROVAL OF THESIS

Title of Thesis:

An Experimental Study of Multiple Steady States in a Photopolymerization Reactor

Name of Candidate: Chih-Ning Kuan
Doctor of Engineering Science, 1982

Thesis and Abstract Approved:

Professor C.R. Huang Assistant Chairman Chemical Engineering Department New Jersey Institute of Technology	Date
	Date
	Date
	Date
	Date

VITA

Name: Chih-Ning Kuan

Degree and Date to be Conferred: D. Eng. Sc., 1982.

Secondary Education: Hsu Hwei High School, Taiwan, June, 1970.

Collegiate Institutions Attended	Date	Degree	Date of Degree
Chung Yuan Christian College of Science and Engineering	Sep., 1970	B.S. in Ch.E	June, 1974
Tennessee Technological University	Jan., 1977	M.S. in Ch.E	June, 1979
New Jersey Institute of Technology	Jan., 1979	D. Eng. Sc. in Ch.E	May., 1982

Major: Chemical Engineering

Publications:

(1) "Determination of Thermal Conductivity of Heavy Hydrocarbons Using an Unguarded Concentric Cylinder Apparatus" - Master Thesis.

(2) "Photopolymerization in a Continuous Stirred Tank Reactor: Experiment" 672, 26, AIChE J. 1980.

(3) "Photopolymerization in an Isothermal and Continuous Stirred Tank Reactor: Concentration Stability" 214, 28, AIChE J. 1982.

Position Held: Process Design Engineer
The C-E Lummus Company
1515 Broad Street, Bloomfield,
New Jersey 07003

ABSTRACT

Title of Thesis: An experimental Study of Multiple Steady States in a Photopolymerization Reactor

Chih-Ning Kuan, Doctor of Engineering Science, 1982

Thesis directed by: Professor H.T. Chen (deceased) and Professor C.R. Huang

An experimental study of photosensitized free radical polymerization of styrene in both batch and continuous stirred tank reactors is presented. Each reactor was run under both adiabatic and isothermal conditions. Multiple steady states were investigated. Exact multiplicity and uniqueness criteria for the above systems were derived and a mathematical model developed to correlate the results.

For both adiabatic and isothermal continuous stirred tank reactors operating in the metastable state regions, the conversion and polymer molecular weight are greater than the corresponding lower steady state operations. At a given conversion level, the reaction time for both adiabatic and isothermal continuous stirred tank reactors is less than for an equivalent batch operation. This study indicates that for both isothermal and adiabatic continuous operations, the photopolymerization reactor can be accurately controlled through a simple on-off regulation of light intensity.

ACKNOWLEDGEMENT

I wish to express my sincere gratitute to my deceased thesis advisor, Professor H.T. Chen for his great enthusiasm, encouragement and inspiration. The author is also indebted to the other member of the doctoral committee, who have given valuable discussions and suggestions in the preparation of this work.

Greatful thanks are extended to Professor C.R. Huang who has shared with me the task of proofreading the manuscript in all its stages. Deep appreciation also goes to my coworkers for their experimental assistance.

Finally, this work is especially dedicated to my parents and my wife, for their understanding and constant spiritual support.

TABLE OF CONTENTS

Page

LIST OF FIGURES

Figure | Page

Figure | Page

Figure | Page

LIST OF TABLES

Table | Page

CHAPTER 1

INTRODUCTION

1-1. Background

The structure property relations of a polymer are in large measure determined by the molecular weight distribution of the polymer and its mean values, e.g. number and weight averaged degrees of polymerization. In most polymerization processes, high temperatures are required for high rates of polymerization, but in free radical chain growth polymerizations, a temperature increase will lead to a concomitant decrease in degree of polymerization (molecular weight). Conventionally, addition polymerizations are usually initiated through the use of catalyst. Alternate means of initiation are also available, including initiation by absorption of radiation (ionizing or ultraviolet). Both catalyst decomposition and radiation absorption lead to the production of free radicals which initiate the polymerization reaction. However, there are differences between the initiation modes which can profoundly affect the ease with which the reaction is carried out and the character of the product. Thus, in the case of radiation initiation, the rate of initiation is essentially independent of temperature, and because of the physical separation of radiation source and the reaction medium, the initiation rate may be changed very rapidly.

By contrast, the rate of initiation with chemical initiators is usually strongly temperature dependent, and because the chemical initiator is in solution in the reaction medium, the initiation rate can not be changed very rapidly. Because of these facts, radiation initiation may lead to greater reactor stability and a better reactor control. An important consequence of greater stability and ease of reactor control should be less frequent instances of runaway reactions and explosive decompositions, or the elimination of these events altogether. This consequence would result in greater safety of operation and loss of production.

Photochemical reactions are receiving increased attention in selective, nonthermal chemical processing routes are perceived as energy and material conservation possibilities. The application of this technology to the control of chemical reaction pathways promises to be an exciting area for chemical engineering in the 1980's. A number of studies of the design and analysis of photochemical reactors have appeared in the literatures during the last decade, with outstanding contributions in this area being made by J.M. Smith and J.S. Dranoff and their co-workers. The commercial applications of photochemistry have been somewhat slower to appear, however, some papers such as by Houston and Logan [13] and Klink et al. [14] signal an increasing industrial interest in photochemical processing. Among impediments to the commercial development

of photochemical processes have been a scarcity of reliable kinetic data, and the difficulty of accounting for imperfect mixing and nonuniform light absorption in the polymerization reactor. Some theoretical models have been proposed to describe these effects, but very few experimental results which might either confirm or invalidate the models.

1-2. Photopolymerization

Polymerization processes initiated by the thermal decomposition of a catalyst are well established. But very little work has been done on the engineering aspect of photopolymerizations (Yemin and Hill [22], Jain et al. [40], Chen and Hill [7], Hill and Chen [43], Sandru and Smith [41], Ibarra and Smith [42], Mendiratta and Felder [11] and Chen and Steenrod [6]), in part because of incomplete exploration of their characteristics and advantages.

In optically dense systems mixing effects may be distinguished which result from nonuniform depletion of reactant , or from nonuniform production of reactive intermediates. It is therefore that mixing phenomena are important in determining the observed reaction rate and product molecular weight distribution in the photoreaction mixtures. The accurate prediction of mixing effect requires a detailed knowledge of the mechanism of the reaction of interest, the optical

properties of the system, the physics of the radiation used, and the mixing processes themselves. The observed rate of polymerization, when carried out with an initiation rate which is constant throughout the reactor volume, depends in general on the specific rate of diffusion or mixing. For radiation initiation polymerization, nonuniform initiation follows from radiation attenuation, and the nonuniformity in polymerization initiated by the decomposition of catalyst results from a nonuniform distribution of catalyst. Seldom will adequate information be available for a given system to permit prediction out of hand of the observed rate. Usually experimental characterization will be required. In addition, experimental studies are useful in understanding the nature of the interaction of chemical kinetics and mixing processes in the presence of nonuniform initiation.

1-3. Literature Review

A number of investigations have been made of the manner and extent to which chemical reaction rates are modified by the presence of spatial nonuniformities. Most of the experimental studies have been made at low conversion level, the theoretical approaches have been concerned with solution of the partial differential equation for reaction, flow, and radial diffusion or solution of two ordinary differential equations corresponding to the extremes of radial diffusion or mixing - no mixing (NM) and perfect mixing (PM).

Yemin and Hill [22] reported that the polymerization rate of methyl methacrylate in a partially illuminated reactor increases with agitation speed. Felder and Hill [12] have examined mixing effects in both batch and continuous systems. It is found that when radial mixing in a tubular reactor, the conversion is enhanced, while in a batch reactor, mixing can either increase or does not affect the overall conversion at a given time. Jacob and Dranoff [23] have theoretically and experimentally investigated the light intensity distribution in a perfectly mixed photoreactor. They proposed an empirical correction function which is in close agreement with the experimental results. Kawakami and Isbin [15] reported the effects of agitation on radiolysis of chloralhydrate aqueous solution under nonuniform dose rate distribution. They proposed a simplified analysis based mainly on the intermittent irradation of fluid elements caused by recirculating flow in a stirred tank reactor.

Chen and Hill [7] carried out a theoretical study on effects of nonuniform initiation on reaction rate and product molecular weight distribution in continuous stirred tank reactors. Their conclusions showed that nonuniformity of dose rate distribution and radical life time relative to mixing time have large effects on polymerization. The molecular weight distribution was calculated to be unimodal, and the position of the peak moves to the lower molecular weight with

increase of the nonuniform and/or the mixing time relative to the radical life time. Muller et al. [24] examined the molecular weight distribution of the polymer and observed a bimodal distribution. They also found that a low molecular weight species was appreciable at low stirring speed, and its amount became smaller with increasing agitation speed.

Chen and Steenrod [6] examined the effects of mixing on a batch reactor. In their study, two extreme mixing states, perfect and no mixing are considered. It shows that when nonuniform initiation exists, this can increase the polymerization rate and the number average molecular weight and decrease the weight molecular weight and thus the polydispersity. Mendirtta and Felder [11] have experimentally determined the kinetic parameters for several sensitized photopolymerization reactions. Their work is limited to very low conversion levels.

From the above literature survey, only scant experimental data exist and it is very difficult to draw any conclusions to evaluate currently proposed models. Further investigations of photopolymerization are obviously needed to establish reliable design information.

1-4. Multiple Steady States

The reaction being investigated in this work is styrene polymerization, which is an exothermic reaction. It is very

well known that this type of reaction under adiabatic operation may lead to more than one steady states under the same feed condition and that not all are naturally stable; that is, some states are metastable. The existence of this multiplicity of steady states has been demonstrated experimentally by Vejtasa and Schmitz [25], Ausikaitis and Engel [26], Guha et al. [27], and Chang and Schmitz [28] for oxidation of aqueous sodium thiosulfate by hydrogen peroxide. In polymerizations, certain of these metastable states offer increased conversion for the same residence time. Moreover, theoretical investigations have indicated that through the addition of controller actions, stable operation may be obtained in a continuous stirred tank reactor. Among these studies were those by Hoftyzer and Zwietering [29] and by Warden and Amundson [30] on thermal catalytic initiation in a continuous reactor. Comparable work on the other modes of initiation has not been done, although the recent study by Hashimoto and Kawakami [31] indicated that marked improvement in reactor response may be achieved through radiation dose rate regulation over that obtainable through the more conventional means of coolant flow rate regulation. No consideration was given to the enhancement of stability of the metastable state.

The above multiplicity behavior also exists in an isothermal and continuous polymerization reactor due to "gel" effect or Tromsdorff effect. It is inevitable in all kinds of

polymerization in which the reactions are accompanied by a rapid increase in viscosity [9]. This gel effect in polymerization reactions is due to a decrease in the mobility of long chain radicals with increasing viscosity and as a result, the termination reaction rate being diffusion controlled at that stage is greatly restricted. Therefore, in solution of high viscosity, the rate of free radical polymerization increases with conversion reaching a peak at very high viscosity and then falls off rapidly. From the behavior described above, Knorr and O'Driscoll [1] have mathematically demonstrated the steady state mass balances on bulk polymerization of styrene are possible at three conversion levels. A recent study by Schmidt and Ray [32] of solution polymerization of methyl methacrylate in an isothermal continuous stirred tank reactor, has theoretically and experimentally demonstrated this multiple steady state behavior. This multiplicity of steady state with its particular problems of stability is analogous to much studied phenomena of temperature stability characteristics of autocatalytic and heterogeneous catalytic reactions [1]. To the best of our knowledge, no experimental analysis has ever been done on the stability and control of photopolymerization reactor systems.

1-5. Summary

The use of ultraviolet light as a generator of free radicals offers a significant improvement in the control of

polymerization reactions and to determine the effect on molecular weight distribution of the polymer formed. Experimental measurements were undertaken in both batch and continuous systems to investigate steady state multiplicity, stability, and controllability of reaction systems. The overall objectives of this work are to add to the collection of experimental data that are available to the design of photopolymerization reactors. Exact multiplicity and uniqueness criteria for photopolymerization in both adiabatic and isothermal continuous operations are studied. An attempt is also made on development of a mathemetical model to correlate the mixing effects of photosensitized polymerizations due to nonuniform distribution of light intensity.

CHAPTER 2

MULTIPLICITY AND UNIQUENESS

A prior prediction of steady state multiplicity is important for the design and control of chemical reactors. In this chapter, exact multiplicity and uniqueness criteria are established for a photosensitized free radical polymerization in continuous stirred tank reactors through a simple tangent analysis. Three steady states are found to exist even under isothermal conditions, if gel effects become pronounced. Multiplicity is guaranteed by limiting the residence time in a proper range in addition to the necessary conditions.

2-1. Polymerization Mechanism

The reaction mechanism to be considered is addition polymerization in bulk:

Initiation by absorption of UV light by sensitizer

$$S \xrightarrow{\phi_s I_{as}} 2\,S\cdot$$

$$S\cdot + M \xrightarrow{k_d} R_1 \qquad \Omega_i = 2\,\phi_s\,I_{as}$$

Propagation

$$R_j + M \xrightarrow{k_p} R_{j+1} \qquad \Omega_p = k_p\,\Sigma R_i\,m$$

Termination

$$R_i + R_j \xrightarrow{k_{tc}} P_{i+j} \qquad \Omega_{tc} = k_{tc}\, \Sigma R_i^2$$

$$R_i + R_j \xrightarrow{k_{td}} P_i + P_j \qquad \Omega_{td} = k_{td}\, \Sigma R_i^2$$

By application of the stationary approximation [2,7], the rates of formation and destruction of free radicals are equal:

$$\Omega_i = k_t \quad \Sigma R_i^2$$

or
$$\Sigma R_i = \left(\frac{\Omega_i}{k_t} \right)^{1/2} \qquad (1)$$

the monomer consumption rate can be expressed as:

$$\Omega_m = k_p \left(\frac{\Omega_i}{k_t} \right)^{1/2} m \qquad (2)$$

The polymerization takes place in a continuous stirred tank reactor (either adiabatic or isothermal), as shown schematically in Figure 1. The reactor volume is illuminated with a parallel, monochromatic and uniform beam of radiation through a window in the bottom of the reactor. If I_o is the flux of light incident upon the reactor, the total amount of light absorbed by the sensitizer is [11],

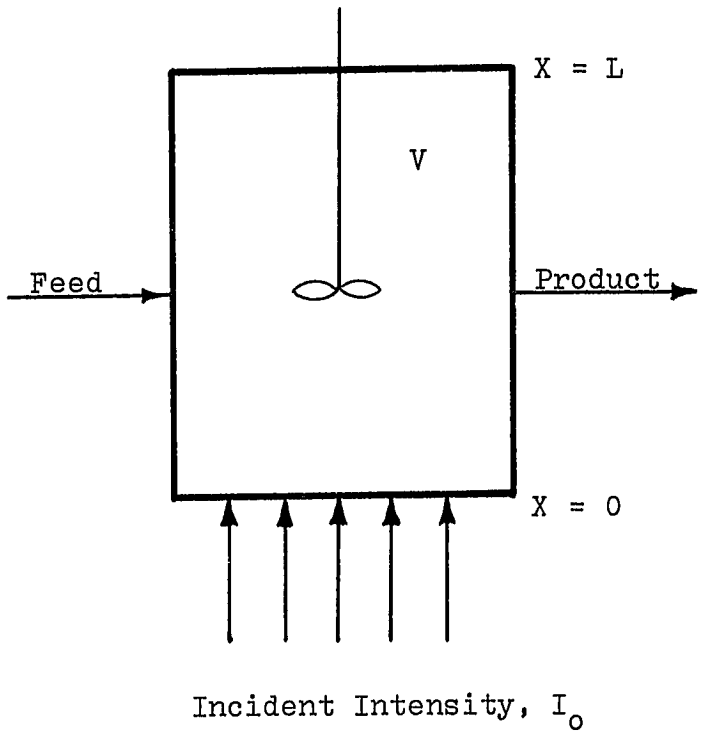

Figure 1. Schematic Diagram of a Photo Reactor

$$I_{as} = I_o \frac{\epsilon_s S}{\epsilon_s S+\epsilon_m m+\Sigma\epsilon_{p_i} P_i} \frac{1-Exp[-(\epsilon_s S+\epsilon_m m+\Sigma\epsilon_{p_i} P_i)L]}{L} \quad (3)$$

The feed consists of monomer and sensitizer. The reactor is assumed to be perfectly mixed so that the composition is uniform throughout. In addition, the following assumptions are made:

1. The feed stream consists of excess amount of sensitizer and its concentration in the product is essentially identical to that in the feed.
2. The light absorbed by the monomer and the sensitizer is negligible, that is,

   $$\epsilon_s S \gg \epsilon_m m + \Sigma\epsilon_{p_i} P_i$$

   Thus, equation (3) becomes

   $$I_{as} = \frac{I_o}{L} [1-Exp(-\epsilon_s S)L] \quad (4)$$

By applying assumptions 1 and 2, one may consider that the initiation rate via absorption of ultraviolet light by sensitizer is insensitive to detailed chemical composition, i.e.,

$$\Omega_i = I_{as} \phi_s = \text{constant} \quad (5)$$

3. Consider the case of styrene polymerization, that is

   $$k_{tc} \gg k_{td}$$ [2]

4. The volume change involved in polymerization is small, this is to say that the volumetric flow rate for the feed is identical to that for the product.
5. The rate constants are independent of chain length, The kinetic data due to "gel effect" is based on the work by Hui and Hamielec [2], i.e., $(k_p/k_t^{1/2})$ is allowed to vary with conversion as follows:

$$\left(\frac{k_p}{k_t^{1/2}}\right) = \left(\frac{k_p}{k_t^{1/2}}\right)_o \mathrm{Exp}(A_1X+A_2X^2+A_3X^3) \qquad (6)$$

The subscript "o" means values at zero conversion, A_1, A_2, A_3 and $(k_p/k_t^{1/2})_o$ are independent of conversion at any given temperature.

As mentioned in chapter 1, gel effect or Trommsdorff effect [17,18] in free radical chain growth polymerizations, the rate of reaction increases with an increase in conversion instead of decrease as monomer is consumed. This increase is attributed to a decrease in the rate of termination and consequently an increase in the macro-radical concentration. The decrease in termination rate can be related to the restricted diffusion of macro-radicals in the polymerization system of high viscosity. The rate of the propagation reaction, which involves only one large radical, will be less effected, hence the net result will be a progressive increase in the rate of polymerization.

2-2. Reactor Equations

Steady state CSTR models are useful in quantifying operating parameters such as the maximum adiabatic temperature rise, multiple steady state operating conditions, stability of the steady states and sensitivity to flow rate, sensitizer concentration, light intensity, etc. The reactor performance equation from material and energy balances can be described as:

The material balance for monomer is

$$\frac{dm}{dt} = \frac{m_o - m}{\theta} - \Omega_i^{1/2}\, m\, (k_p/k_t^{1/2}) \qquad (7)$$

Two exterme conditions will be considered, isothermal and adiabatic. For an adiabatic process, the energy balance equation around the reactor is

$$V \rho C_p \frac{dT}{dt} = Q \rho C_p\, (T_o - T) + (-\Delta H)\, V\, \Omega_m \qquad (8)$$

In the steady state, equation (7) and (8) become,

$$\frac{X}{\theta} = \Omega_i^{1/2}\, (1-X)\left(\frac{k_p}{k_t^{1/2}}\right) \qquad (9)$$

and

$$T_o - T = \frac{-(-\Delta H)\,\theta\,\Omega_m}{\rho\, C_p} \qquad (10)$$

Note that in the case of adiabatic operation, concentration and temperature in the reactor can be expressed in

terms of the single variable - conversion by substituting equation (10) into equation (9).

2-3. Multiplicity Analysis

The analysis described below is based on a method developed by Lin [8]. However, he is concerned with exothermic binary reactions, this analysis is dealing with polymerization systems.

2-3-1. Isothermal Process

By combining equations (6) and (9)

$$\frac{X}{\theta} = \alpha(1-X)\ \mathrm{Exp}(A_1X+A_2X^2+A_3X^3) \tag{11}$$

where

$$\alpha = \left(\frac{k_p}{k_t^{1/2}} \right)_o (2\ \phi_s I_{as})^{1/2} \tag{12}$$

let

$$Q_c(X) = \alpha(1-X)\ \mathrm{Exp}(A_1X+A_2X^2+A_3X^3) \tag{13}$$

$$Q_s(X) = \frac{X}{\theta} \tag{14}$$

The derivatives of Q_c with respect to X are,

$$Q_c'(X) = \alpha\ \mathrm{Exp}(A_1X+A_2X^2+A_3X^3)\ \beta(X) \tag{15}$$

$$Q_c''(X) = \alpha\ \mathrm{Exp}(A_1X+A_2X^2+A_3X^3)\ \beta'(X) + \alpha\beta(X)\ \mathrm{Exp}(A_1X+A_2X^2+A_3X^3)(A_1+2A_2X+3A_3X^2) \tag{16}$$

where

$$\beta(X) = -3A_3X^3 + (3A_3-2A_2)X^2 + (2A_2-A_1)X + (A_1-1) \quad (17)$$

and

$$\beta'(X) = -9A_3X^2 + 2(3A_3-2A_2)X + (2A_2-A_1) \quad (18)$$

The equation $\beta(X)=0$ will have one or three real roots, depending on the parameters A_1, A_2, and A_3. Also, the equation $\beta'(X)=0$ will have two roots:

$$\begin{matrix} X_A \\ X_B \end{matrix} = \frac{\sqrt{(3A_3-2A_2) \pm (3A_3-2A_2)^2 + 9A_3(2A_2-A_1)}}{9A_3} \quad (19)$$

Q_s (equation (14)) is a linear function of conversion with a slope of $1/\theta$. At steady state, $Q_c=Q_s$. Examination of $\beta(\infty)$, $\beta(-\infty)$, $\beta(0)$, $\beta(1)$, X_A and X_B reveals that there are four possible cases for which the two steady states can exist (Figure 2). The existence of the two steady states requires Q_c and Q_s curves be tangent at one point, i.e.,

$$Q_c'(X) = Q_s'(X) = \frac{1}{\theta} \quad (20)$$

From Figure 2, there are an upper and lower limits for the holding time θ_1 and θ_2. for values θ over a range from θ_2 to θ_1, three steady states are possible of which the highest and lowest ones are stable steady states, and the middle one is unstable [1]. The Q_c curve can vary with its

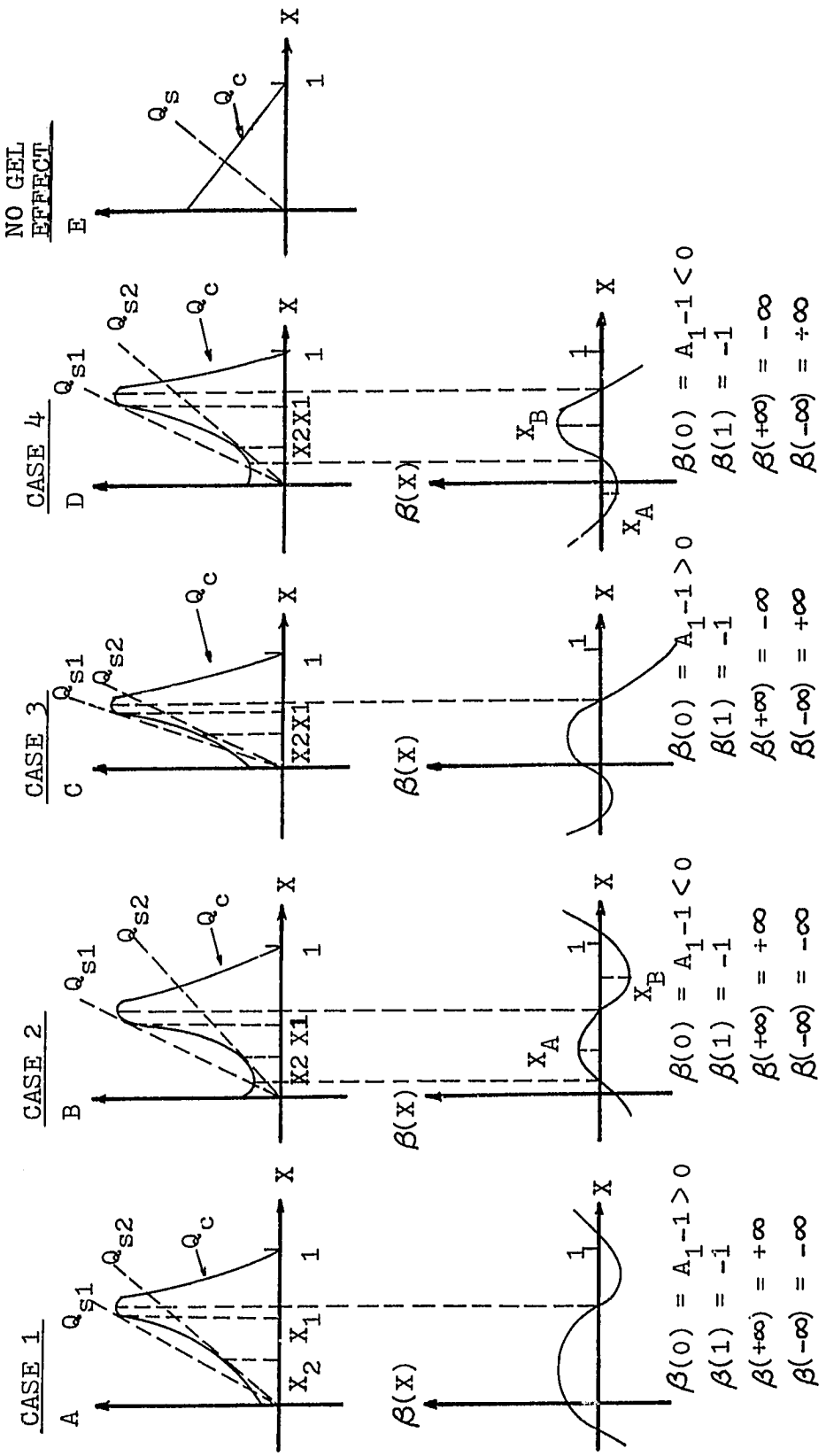

Figure 2. Schematic Plots of Q_c and Q_s vs. X - Isothermal Conditions

parameters A_1, A_2, and A_3. In the absence of gel effect ($A_1=A_2=A_3=0$), equation (13) becomes

$$Q_c(X) = \alpha(1-X) \tag{21}$$

As shown in Figure 2E, Q_c decreases linearly with the increase of conversion, and there is only a single intersection of Q_c and Q_s. Single intersection always produces one stable point. Only those four cases shown in Figure 2A to 2D may produce three steady states. Their necessary conditions are shown in Table 1. For all other cases, uniqueness is assured.

To fulfill the necessary conditions implies that the system exists two tangent points X_1 and X_2 as shown in Figure 2, at tangent point, both the slopes and the ordinates of $Q_c(X)$ and $Q_s(X)$ should be equal;

$$G(X) = Q_c'(X) - Q_s'(X) = 0$$

or

$$F(X) = -3A_3X^4 + (3A_3-2A_2)X^3 + (2A_2-A_1)X^2 + A_1X - 1 = 0 \tag{22}$$

and

$$\begin{matrix} F(X_1) = 0 \\ F(X_2) = 0 \end{matrix} \tag{23}$$

where

$$0 < X_2 < X_1 < 1$$

TABLE 1

MULTIPLICITY CRITERIA FOR ISOTHERMAL CONDITIONS

	Case 1	Case 2	Case 3	Case 4
Necessary Conditions	$A_3 < 0$ $A_1 - 1 > 0$ $Q_c''(0) > 0$	$A_3 < 0$ $A_1 - 1 < 0$ X_A and X_B must be real and greater than zero; either X_A or both X_A and X_B must be between 0 and 1.	$A_3 > 0$ $A_1 - 1 > 0$ $Q_c''(0) > 0$	$A_3 > 0$ $A_1 - 1 < 0$ X_A and X_B must be real and less than one; either X_B or both X_A and X_B must be between 0 and 1.
Sufficient Condition	$\theta_1 < \theta < \theta_2$			

For the system satisfying the necessary conditions for multiplicity, the sufficient condition is,

$$\theta_1 < \theta < \theta_2 \tag{24}$$

where

$$\theta_1 = \frac{X_1}{\alpha(1-X_1)\ \mathrm{Exp}(A_1X_1 + A_2X_1^2 + A_3X_1^3)}$$

$$\theta_2 = \frac{X_2}{\alpha(1-X_2)\ \mathrm{Exp}(A_1X_2 + A_2X_2^2 + A_3X_2^3)} \tag{25}$$

A sample calculation based on the derived multiplicity criteria for photopolymerization in an isothermal CSTR is illustrated in Appendix A.

2-3-2. Adiabatic Process

In this case, A_1, A_2, A_3, and $(k_p/k_t^{1/2})_o$ are dependent of temperature. Let

$$\begin{aligned} A_1 &= a_{11} + a_{12}T \\ A_2 &= a_{21} + a_{22}T \\ A_3 &= a_{31} + a_{32}T \end{aligned} \tag{26}$$

also,

$$\left(\frac{k_p}{k_t^{1/2}}\right)_o = \left(\frac{A_p}{A_t^{1/2}}\right) \mathrm{Exp}\left(\frac{E}{T}\right) \tag{27}$$

where

$$E = (E_t - 2E_p)/2$$

then, equation (9) becomes

$$\frac{X}{\theta} = \frac{A_p}{A_t^{1/2}} (2\phi_s I_{as})^{1/2} \mathrm{Exp}[(a_{11}+a_{12}T)X + (a_{21}+a_{22}T)X^2 + (a_{31}+a_{32}T)X^3 + \frac{E}{T}](1-X) \quad (28)$$

Equations (9) and (10) may be written as,

$$\frac{X}{\theta} = \frac{\Omega_m}{m_o} \quad (29)$$

and

$$T_o - T = \frac{-(-\Delta H)m_o X}{\rho C_p} = -\lambda X$$

or

$$T = T_o + \lambda X \quad (30)$$

By substituting equation (30) into (28)

$$\frac{X}{\theta} = b\ \mathrm{Exp}(C_1X+C_2X^2+C_3X^3+C_4X^4+ \frac{E}{T_o+\lambda X})(1-X) \quad (31)$$

where

$$b = \left(\frac{A_p}{A_t^{1/2}}\right)(2\phi_s I_{as})$$

$$C_1 = a_{11} + a_{12}T_o$$
$$C_2 = a_{12}\lambda + a_{21} + a_{22}T_o$$
$$C_3 = a_{22}\lambda + a_{31} + a_{32}T_o$$
$$C_4 = a_{32}\lambda$$

Now let

$$Q_s(X) = \frac{X}{\theta} \tag{14}$$

$$Q_c(X) = b\ (1-X)\ \mathrm{Exp}[f(X)] \tag{32}$$

where

$$f(X) = C_1X + C_2X^2 + C_3X^3 + C_4X^4 + \frac{E}{T_o + \lambda X} \tag{33}$$

the derivatives of $Q_c(X)$ are

$$Q_c'(X) = b\ [f'(X) - Xf'(X) - 1]\ \mathrm{Exp}[f(X)] \tag{34}$$

$$Q_c''(X) = b\ [\mathrm{Exp}(f(X))][(1-X)f''(X)+(1-X)f'^2-2f'(X)] \tag{35}$$

Case 1. <u>With no gel effect</u>

For the special situation, $A_1=A_2=A_3=0$, equations (32), (34), and (35) become,

$$Q_c(X) = b\ (1-X)\ \mathrm{Exp}\left(\frac{E}{T_o + \lambda X}\right) \tag{36}$$

$$Q_c'(X) = b\ \mathrm{Exp}\left(\frac{E}{T_o + \lambda X}\right)\left(\frac{H(X)}{(T_o + \lambda X)^2}\right) \tag{37}$$

$$Q_c''(0) = b\ \mathrm{Exp}\left(\frac{E}{\lambda}\right)\left(\frac{2\lambda^2E}{T_o^3} + \frac{\lambda^2E^2}{T_o^4} + \frac{2\lambda E}{T_o^2}\right) \tag{38}$$

where

$$-H(X) = (T_o + \lambda X)^2 + (1-X)\ \lambda E \tag{39}$$

Equation $H(X) = 0$ has two roots:

$$\begin{matrix} X_a \\ X_b \end{matrix} = \frac{(E-2T_o) \pm \sqrt{(E-2T_o)^2-(T_o^2 + \lambda E)}}{2\ \lambda} \tag{40}$$

It is apparent that there are two possible cases of multiplicity (Cases 5 and 6 in Figure 3). The necessary and sufficient conditions are given in Table 2. Q_{s1} and Q_{s2} are two tangents to Q_c with slopes of $1/\theta_1$ and $1/\theta_2$ respectively, where

$$\theta_1 = \frac{X_1}{b(1-X_1)\ \mathrm{Exp}\left(\frac{E}{T_o + \lambda X_1}\right)}$$

$$\theta_2 = \frac{X_2}{b(1-X_2)\ \mathrm{Exp}\left(\frac{E}{T_o + \lambda X_2}\right)} \qquad (41)$$

For adiabatic polymerizations, the system must have multiple steady states if necessary and sufficient conditions shown in Table 2 are satisfied. However, violation of these conditions will not guarantee the uniqueness of the system because these conditions are based on the assumption that gel effect is not significant.

Case 2. With gel effect

By setting $Q_s = Q_c$, one may obtain the steady state conversions as,

$$G(X) = Q_c(X) - Q_s(X) = b\ (1-X)\ \mathrm{Exp}[f(X)] - \frac{X}{\theta} = 0 \qquad (42)$$

The number of reactor steady states can be found by determining the number of real roots of the equation. However, experimental results indicate that the existence in a real

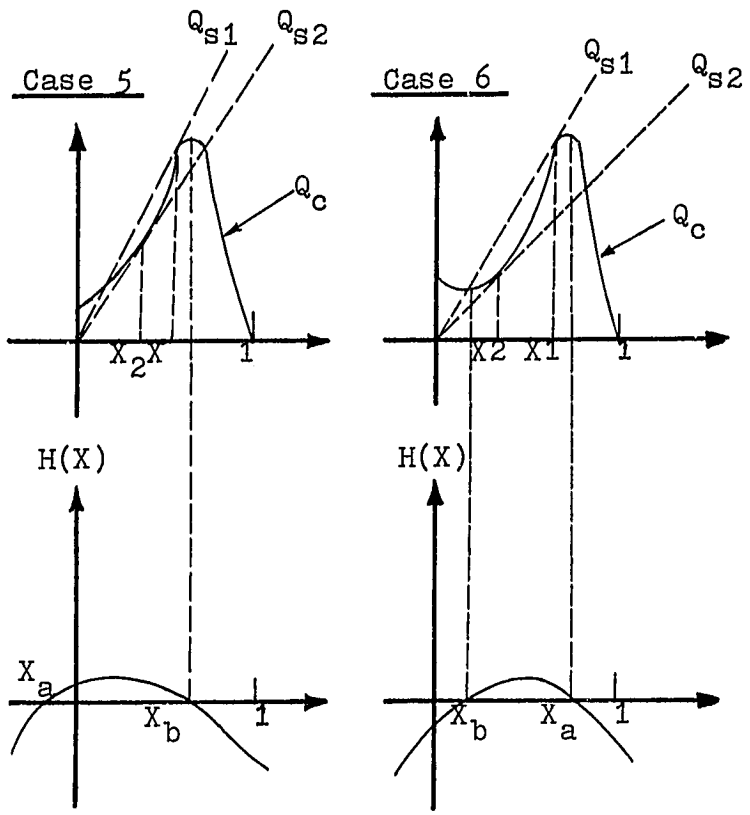

$H(0) = -E-T_o^2 > 0$ $\quad$ $H(0) = -E-T_o^2 < 0$

$H(1) = -(T_o+\lambda)^2 < 0$ $\quad$ $H(1) = -(T_o+\lambda)^2 < 0$

$H(+\infty) = -\infty$ $\quad$ $H(+\infty) = -\infty$

$H(-\infty) = -\infty$ $\quad$ $H(-\infty) = -\infty$

Figure 3. Schematic Plots of Q_c and Q_s vs. X - Adiabatic Conditions

TABLE 2

MULTIPLICITY CRITERIA FOR ADIABATIC CONDITIONS

	Case 5	Case 6
Necessary Conditions	X_a and X_b must be real and either one must be between 0 and 1. $Q_c''(0) > 0$	X_a and X_b must be real and between 0 and 1. $X_a \neq X_b$
Cufficient Condition	$\theta_1 < \theta < \theta_2$	$\theta_1 < \theta < \theta_2$

system with more than three steady states is questionable. More likely is the occurance of one or three steady states. When three steady states are found, there are two tangent points, X_1 and X_2, and the slopes of the two curves $Q_c(X)$ and $Q_s(X)$ at X_1 and X_2 should be equal:

$$\begin{aligned} \ell(X_1) &= X_1^2\, f'(X_1) - X_1\, f'(X_1) + 1 = 0 \\ \ell(X_2) &= X_2^2\, f'(X_2) - X_2\, f'(X_2) + 1 = 0 \end{aligned} \tag{43}$$

where f(X) is defined by equation (33). The exact multiplicity criteria are:

Necessary Condition

The equation $\ell(X) = 0$ has two distinct real roots between 0 and 1, i.e., $1 > X_1 > X_2 > 0$.

Sufficient Condition

$$\theta_1 < \theta < \theta_2$$

where

$$\theta_1 = \frac{X_1}{b\,(1-X_1)\,\mathrm{Exp}[f(X_1)]} \qquad \theta_2 = \frac{X_2}{b\,(1-X_2)\,\mathrm{Exp}[f(X_2)]} \tag{44}$$

A sample calculation based on the above derivation of an adiabatic CSTR is given in Appendix B.

Above is a simple steady state analysis on reactor multiplicity. A successful operation of a photo chemical reactor near the metastable state requires a better understanding of the reaction kinetics and a detailed analysis of the process dynamics. The reactor stability and the characteristics of photopolymerization will be discussed in the following chapters.

CHAPTER 3

EXPERIMENTAL APPARATUS AND PROCEDURE

Experimental investigation of photopolymerization of styrene initiated by photodissociation of sensitizer (Benzoin Methyl Ether, BME) accompanied by thermal decomposition of monomer are carried out in a stirred baffled stainless steel reactor. Experimental apparatus and procedure are described as follows:

3-1. Experimental Apparatus

(A) Adiabatic CSTR

The experimental apparatus is shown schematically in Figure 4. The reactor is a stirred baffled stainless steel vessel (7 cm ID and 6 cm height). The reactor volume is partially illuminated with a light beam through the bottom of the reactor. The reaction temperature is used to activate the controller which opens or close the shutter. The controller has upper and lower set points, thereby providing a temperature dead band which may be varied. The reactor is also provided with a preheat coil and insulated with 40 mm fiber glass insulation covered by a polished aluminum jacket. The outside jacket is covered by an electric heating tape which permits the jacket temperature to be maintained at approximately the same temperature as the reactor, thereby assuring

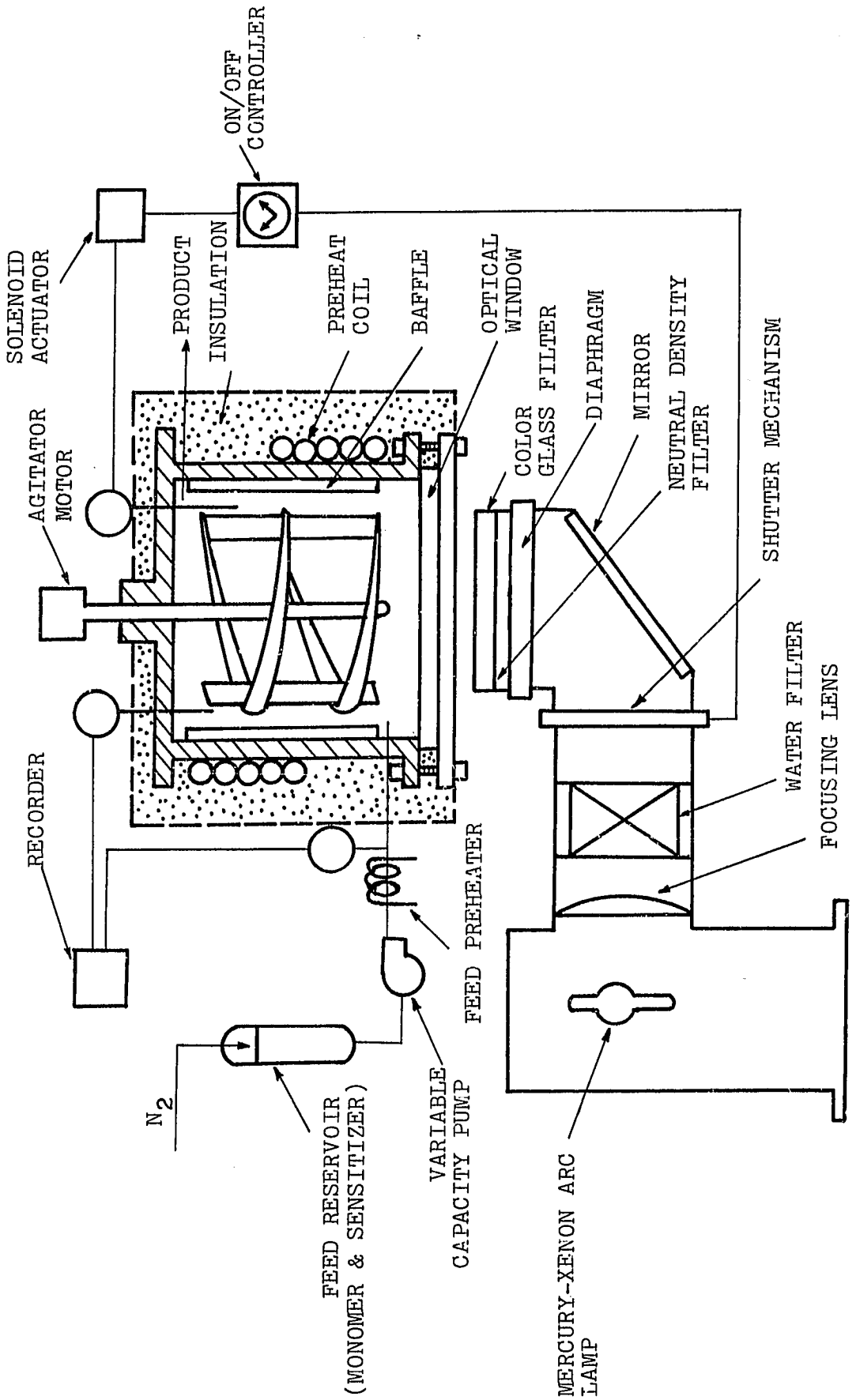

Figure 4. Arrangement of Experimental Apparatus of Adiabatic CSTR

adiabatic operation.

The optical system provides a parallel ultraviolet beam. A 1000 Watt mercury Xenon arc lamp is housed in an air cooled lamp housing and supplied with power by regulating a DC power supply (manufactured by Oriel Optical Co.). The housing contains a mirror which increases the effective intensity of the lamp. A focusing lens mounted in the housing collects the light and produces a collimated beam which passes through a water filter. The filtered beam is reflected upward by a mirror and passes through neutral density fiters to improve its cross sectional uniformity and then through a color glass filter which transmits light with a wavelength of 310-420 nm. An iris diaphragm located under the neutral density filter is used to provide nonuniform irradiation.

(B) Isothermal CSTR

Isothermal experimental apparatus similar to that used in the adiabatic operation which is shown in Figure 5. However, the reaction vessel (7cm ID and 6 cm height) is maintained at a constant temperature by the use of a constant temperature bath which circulates water in the jacket. For the control system, instead of a temperature controller, an UV spectrophotometer is used to monitor the reaction conversion. By providing an upper and lower limits of conversion, shutter

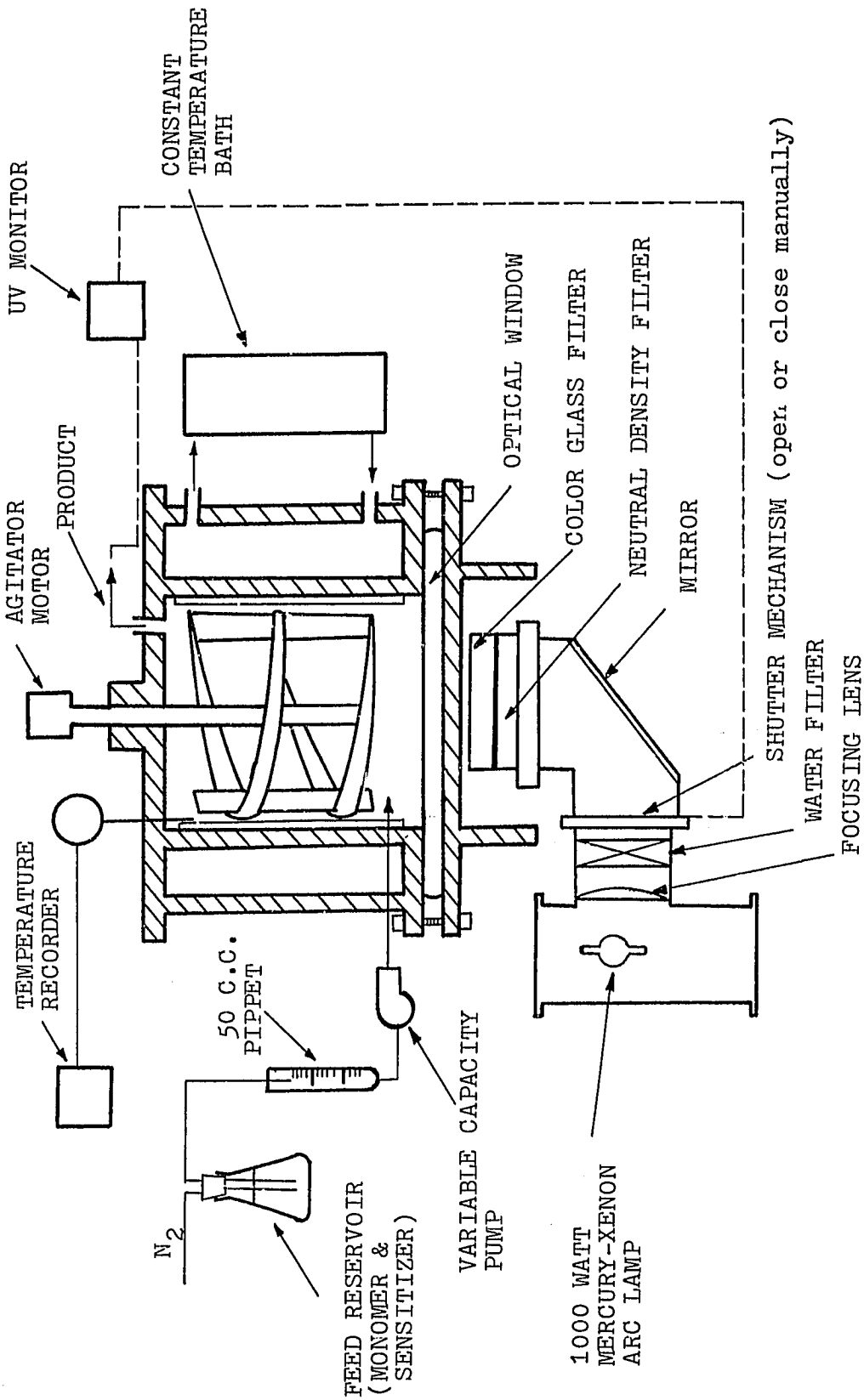

Figure 5. Arrangement of Experimental Apparatus of Isothermal CSTR

mechanism can be open or closed manually. Agitation speed is measured by a tachometer.

It should be pointed out that in this experimental investigation, both adiabatic and isothermal batch operations are also included. The reactor used for above batch systems is the one in isothermal CSTR except the inlet and outlet are stopped. Insulation for adiabatic batch system is installed in the same manner as described in adiabatic CSTR.

3-2. Analytical Procedures

(1) Purification of Styrene Monomer

The styrene monomer used for this study is from Aldrich Chemical Co. of purity 99% purity inhibited with 10-15 ppm of p-tertbutylcatechol. Inhibitor is removed by passing the monomer through a column (5 cm ID and 60 cm length) packed with activated alumina, followed by passage through a same size column packed with silica gel to remove moisture. The inhibited monomer is allowed at a flow rate about 1 cc/min through these two columns. The collection vessel is nitrogen blanked and nitrogen is bubbled through the monomer to remove oxygen. The sensitizer, benzoin methyl ether (manufactured by Aldrich Chemical Co.) is added to the monomer immediately before start-of run. The experimental work also involves styrene polymerization by using benzene as solvent. Purifi-

cation of benzene (99.9% purity manufactured by J.T. Baker Co.) is the same as styrene purifying procedure.

(2) Measurement of Polymer Conversion

The determination of polymer fractional conversion is by means of gravimetric technique presented by Boundy and Boyer [10]. About two to three grams of reaction mixture is collected from the reactor, the mixture is then added to 100 cc methyl alcohol (99.9% purity by Aldrich Chemical Co.) to precipitate the product polymer. For the mixture having more than 30% conversion, 5 cc of p-dioxane is needed to add to the solution before precipitation. The polymer is then dried in a vaccum oven at 70 C for at least 12 hours to remove traces of monomer and the conversion can thus be determined.

Gravimetric method gives satisfactory results, but the time involved is lengthy. At on-off regulation of an isothermal CSTR (concentration stability), which needs to know the reaction concentration instantaneously. A rapid spectrophotometric procedure by Newell [34] and McGovern et al. [33] is used. The concentration of styrene monomer dissolved in tetrahydrofuran (THF) at the order of 0.001 wt%, monomer absorbance at wave length 250 mμ varies linearly with its concentration. Thus, the fraction of styrene monomer in the reaction mixture can be expressed as,

$$g = \frac{\text{absorbance of unknown sample}}{\text{absorbance of pure styrene}} \qquad (45)$$

and the conversion can be determined as,

$$X = 1 - g \qquad (46)$$

A bausch and Lamb Spectronic 710 spectrophotometer is used for conversion measurement.

(3) Measurement of Incident Light Intensity

Measurement of incident light intensity is made by means of the potassium ferrioxlate actinometer as described by Parker [35] and Hatch and Parker [36]. The experiment is carried out in an acrylic reactor (3.8 cm ID and 5 cm height). All the measurements are made in the dark room. The following procedure is used for the determination of photolysis products:

1. Solution A: Dissolve 0.006 molar of $K_3Fe(C_2O_4)\cdot 3H_2O$ (2.947 g) into 100 cc of 1N H_2SO_4 and then diluted to 1000 cc.
2. Solution B: Dissolve 0.1 g of 1,10 phenathroline into 100 cc of H_2O (0.1 wt%).
3. Solution C: 600 cc of 1N sodium acetate is added to 360 cc of 1N H_2SO_4 and then diluted to 1000 cc.
4. 25 cc of A is added into the reactor under exposure of ultraviolet light. Exposing time ranges from 3 to 20 seconds for each run.

5. 1 cc of solution A from the reactor is transferred to a 25 cc calibrated flask. 2 cc of solution B is added followed by 0.5 cc of buffer solution C, and then diluted to 25 cc.
6. After making up and mixing, the liquid is allowed to stand at least one hour for complete reaction. The measurement is then made at 5100 Å and 9 C through the use of a spectrophotometer.

Note that incident light intensity can be varied by either changing the number of neutral density filters or the opening of an iris diaphragm. Experimental measurements of light intensity are summaried in Figure 6. Detailed calculations can be found elsewhere [19,37].

(4) Measurement of Molecular Weight Distribution

The molecular weight distribution of product polymer is determined via gel permeation chromatography manufactured by Water Associates model 6000A. The chromatograph is equipped with five μstyrgel columns. The columns are packed in series having permeability limits of 10^6, 10^5, 10^4, 10^3 and 500 A's respectively. There are six standard polystyrene samples (supplied by Water Associates) used to calibrate the columns having molecular weights $4x10^3$, $9x10^3$, $5x10^4$, $2.4x10^5$, $4.7x10^5$ and $2.7x10^6$ respectively. Calibration curve can be expressed as a semilogarithmic relation of molecular weight with elution

TABLE 3

SUMMARY OF INCIDENT LIGHT INTENSITY MEASUREMENTS

RUN No.	No. of N.D. Filters	Reactant Volume (c.c.)	Time (sec)	Absorbance	$I_o \times 10^{-8}$ ($\frac{Eins}{sec\text{-}cm^2}$)
1	0	25	3	0.135	15.75
2	0	24	6	0.278	15.57
3	0	23	9	0.415	14.85
4	0	22	12	0.563	14.45
5	0	21	15	0.712	13.96
6	1	25	3	0.100	11.67
7	1	24	6	0.212	11.87
8	1	23	9	0.339	12.13
9	1	22	12	0.441	11.32
10	1	20	18	0.738	11.48
11	2	25	5	0.103	7.24
12	2	24	10	0.207	6.99
13	2	23	15	0.284	6.12
14	2	22	20	0.403	6.23
15	3	25	5	0.074	5.20
16	3	24	10	0.143	4.83
17	3	23	15	0.234	4.83
18	3	22	20	0.331	4.89

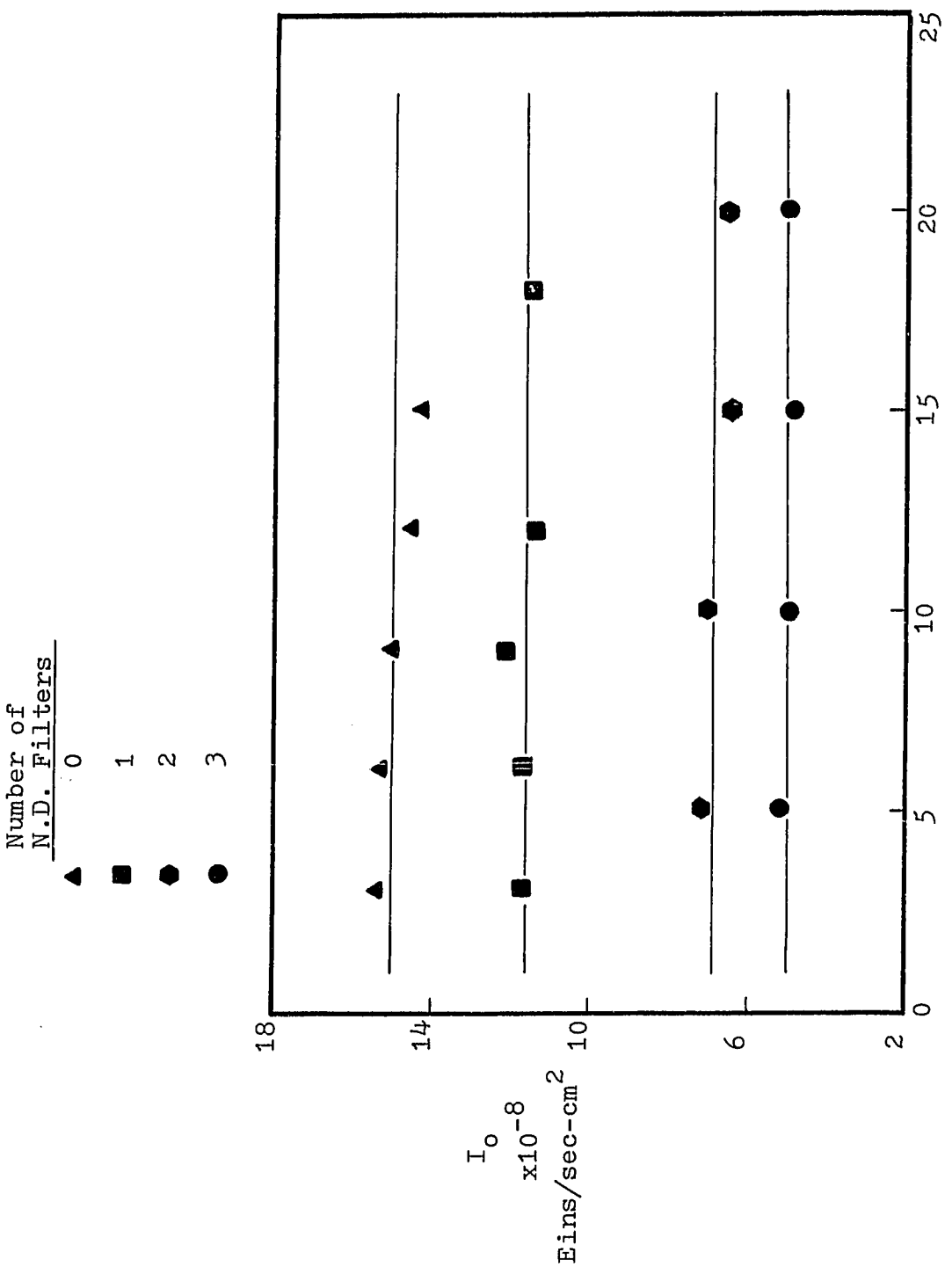

Figure 6. Experimental Measurements of Incident Light Intensity

volume, a typical one is shown in Figure 7. The polymer sample is prepared at a concentration of 0.025 wt% dissolved in toluene prior to the injection. The solvent, toluene is allowed at a flow rate of 2.5 cc/min through the columns. Number average and weight average molecular weights are determined from the GPC elution curves by numerical quadrature using Simpson's rule.

3-3. Preliminary Batch Tests

Some preliminary tests are made in an isothermal batch reactor in order to check the conformity with published results [2]. The experimental procedure for these batch tests can be described as follows:

The reactor is filled with 200 cc of purified styrene monomer well mixed with sensitizer. Nitrogen is then pumped to the reactor to remove oxygen and moisture. UV light initiation and circulation of constant temperature bath are started at the same time. A constant agitation speed is applied throughout the reaction. Normally, it takes about five to ten minutes for the system to reach to the desired reaction temperature. Samples are collected in the middle of the reactor and product polymer is precipitated from the mixture immediately using gravimetric method. The reaction is usually stopped at 60% conversion due to high viscosity.

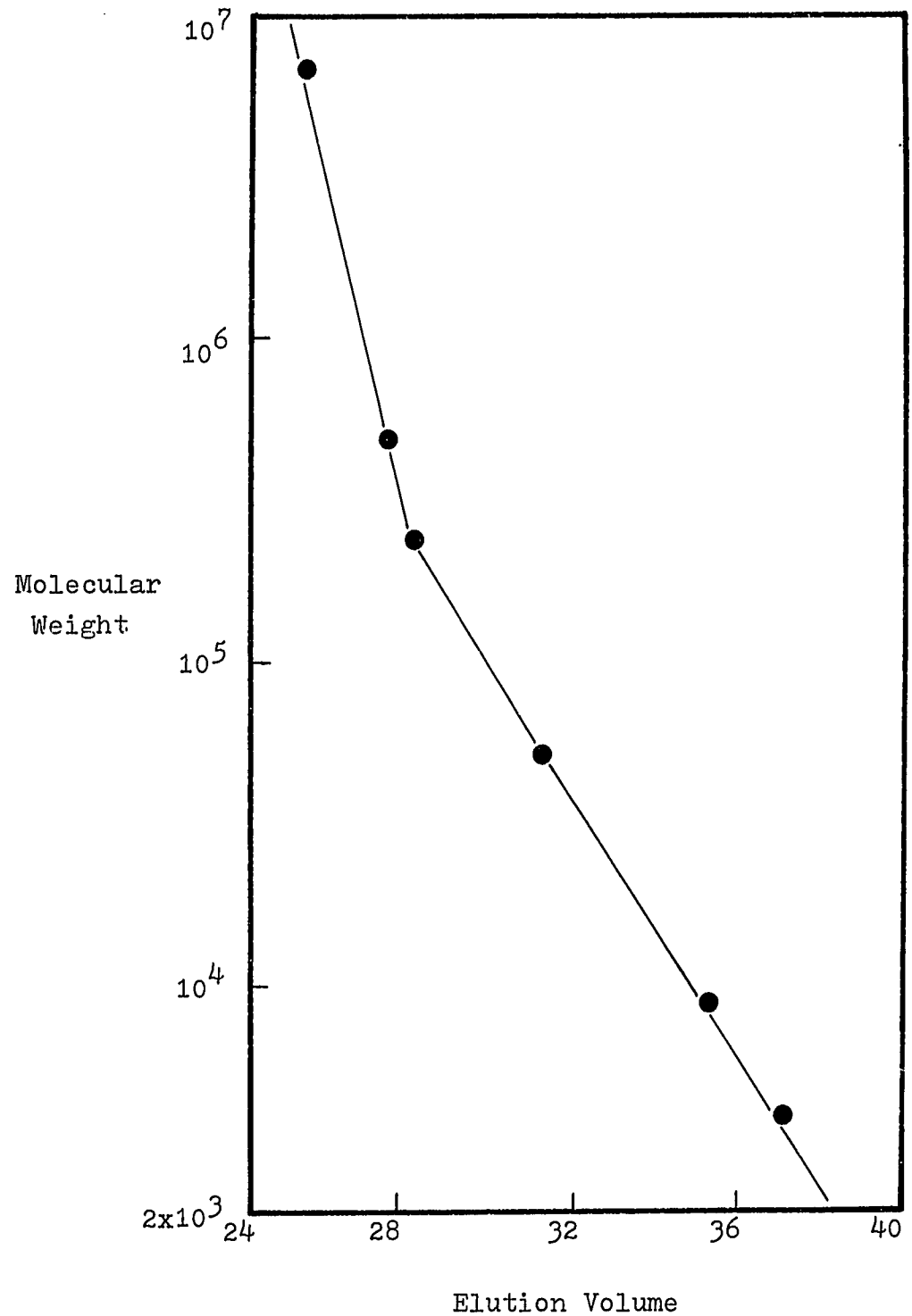

Figure 7. Molecular Weight vs. Elution Volume for GPC Calibration

Figure 8 presents some experimental results carried out at 383 K. For a thermal polymerization run (case 1), the experimental conversion data show good agreement with the 3rd order monomer initiation model [2]. Experimental batch data are basically reproducible. Some repeated runs indicated that the conversion and product molecular weight distribution (number and weight average chain lengths) are within the range of 5%. However, in comparing the molecular number and weight average chain lengths with the published results [2], a large difference is observed. As shown in Table 34, the measured number average chain lengths are about more than 50% less than the 3rd order model predicted and the polydispersity values obtained in this study are higher. To deal with a larger reactor unit such as the one used in this work, it is expected some mixing effects occured during polymerization, in which the reaction temperature will not be homogeneous throughout the reactor. This nonuniform temperature in the reactor system does not affect observed conversion as shown in Figure 8, but will strongly affect the product molecular weight distribution. In some preliminary test runs which showed that even when the agitation speed was raised to as high as 1500 rpm, only little improvement was observed on the molecular number and weigh average chain lengths. The reasons responsible for lower number average chain lengths and higher polydispersity values will be discussed in chapter 7. It is believed that all experimental results obtained in this

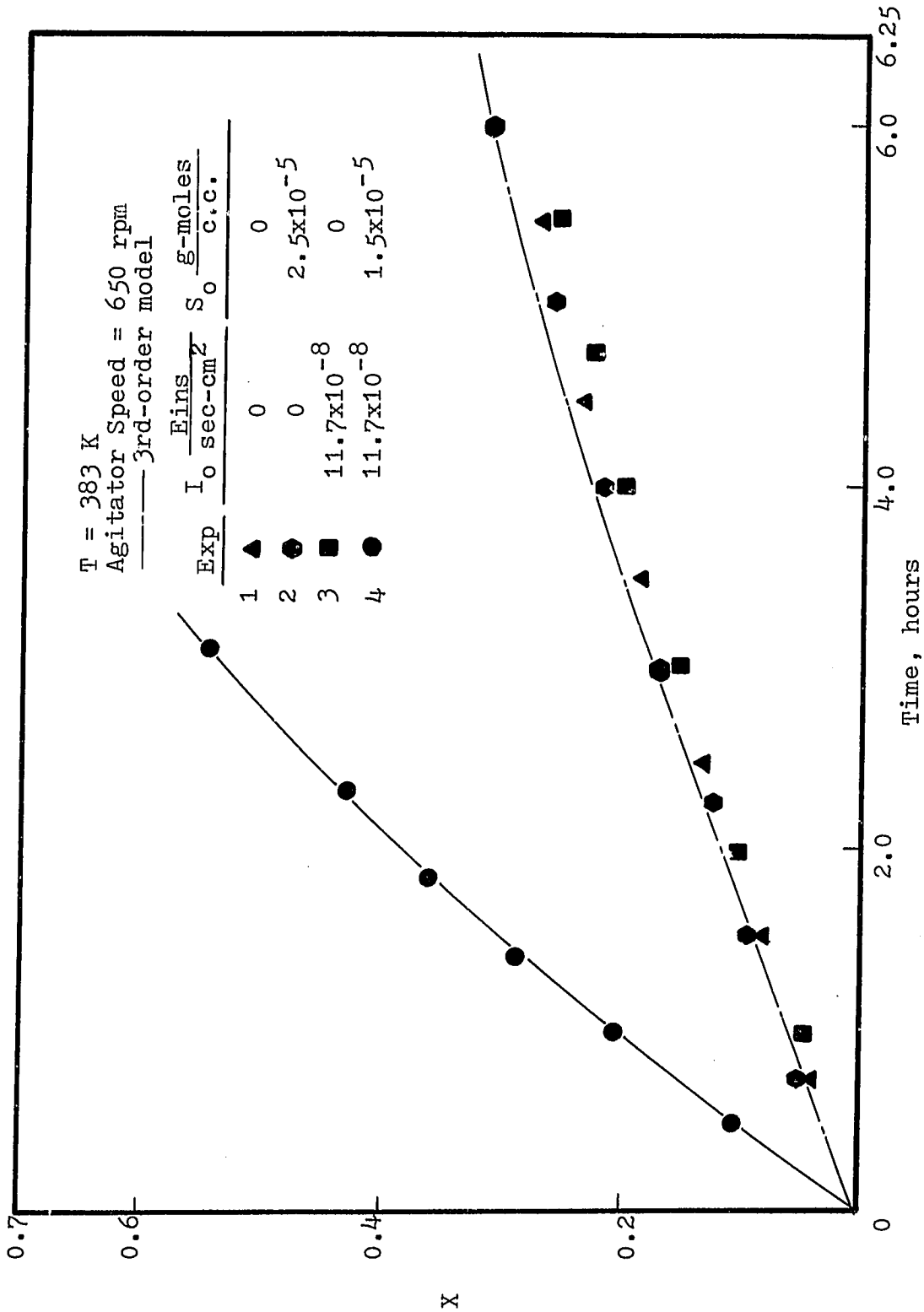

Figure 8. X vs. time for Bulk Polymerization of Styrene at 383 K

work will have relatively lower molecular number average chain lengths depending on the reaction temperatures. This thermal effect becomes less pronounced as reaction temperature decreases which can be seen from the experimental batch results. This is one limitation of the experimental apparatus. In Figure 8, the experimental results also show that the initiation rates due to thermal decomposition of sensitizer (case 2) or photodecomposition of monomer (case 3) are almost negligible. In the following model development work, only thermal decomposition of monomer and photodecomposition of sensitizer are considered as the initiation modes.

The effect of thermal initiation on photopolymerization can be seen in Figure 9. Contribution of thermal initiation at temperature 358 K is small, and then becomes significant at 393 K. This shows that styrene polymerization is strongly temperature dependent. The same figure also indicates that the molecular number average chain length increases as temperature increases. In Figure 10, the experimental results were obtained at a very low agitation speed (350 rpm). Samples were collected from both top and bottom of the reactor. Both conversion and number average chain length do not vary with position appreciably. This implies that both monomer and polymer concentrations are uniform in the reactor even at a very low stirring speed. The above experimental results will be supporting the assumption that monomer and polymer concen-

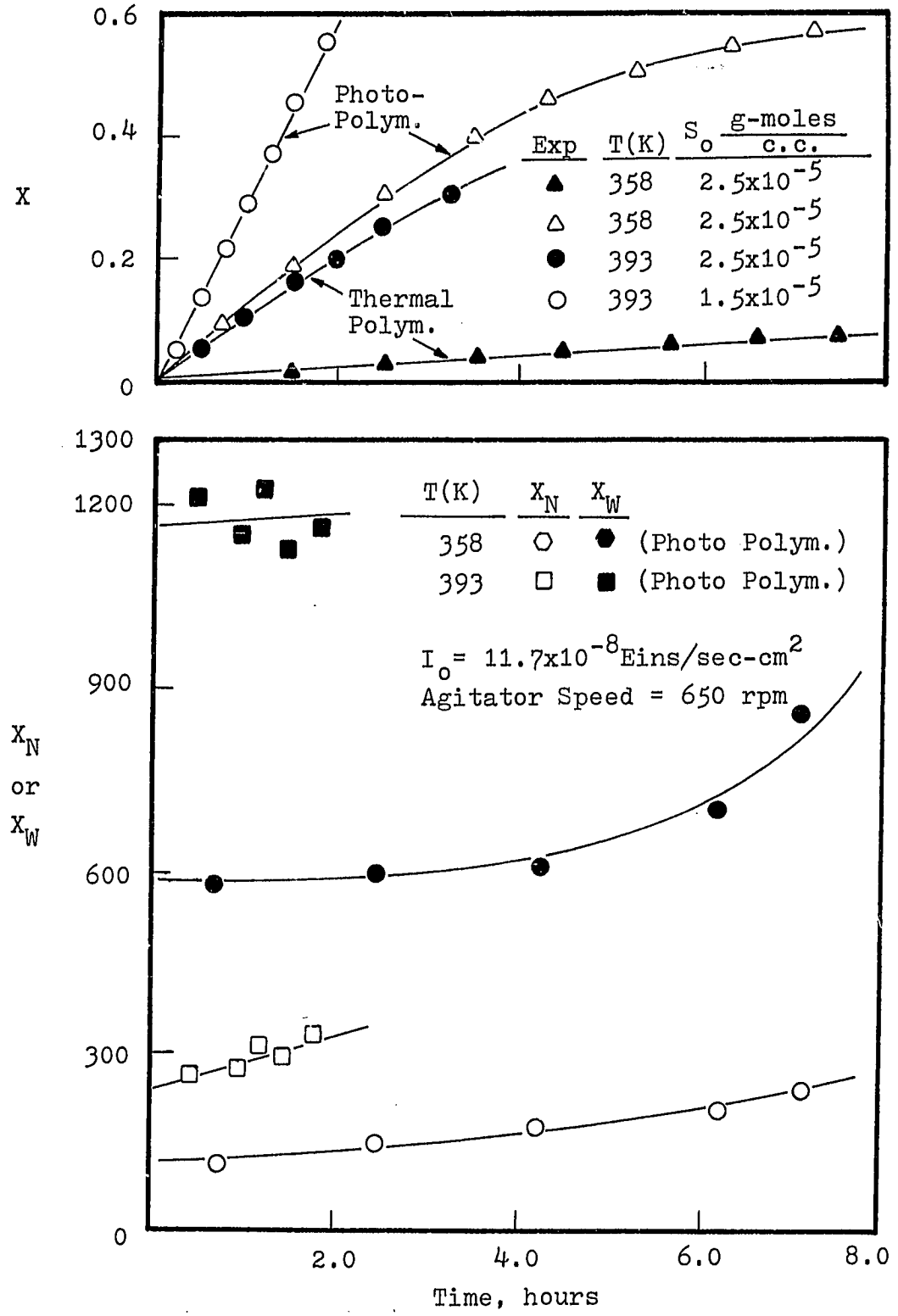

Figure 9. Effect of Thermal Initiation on Photopolymerization in a BR

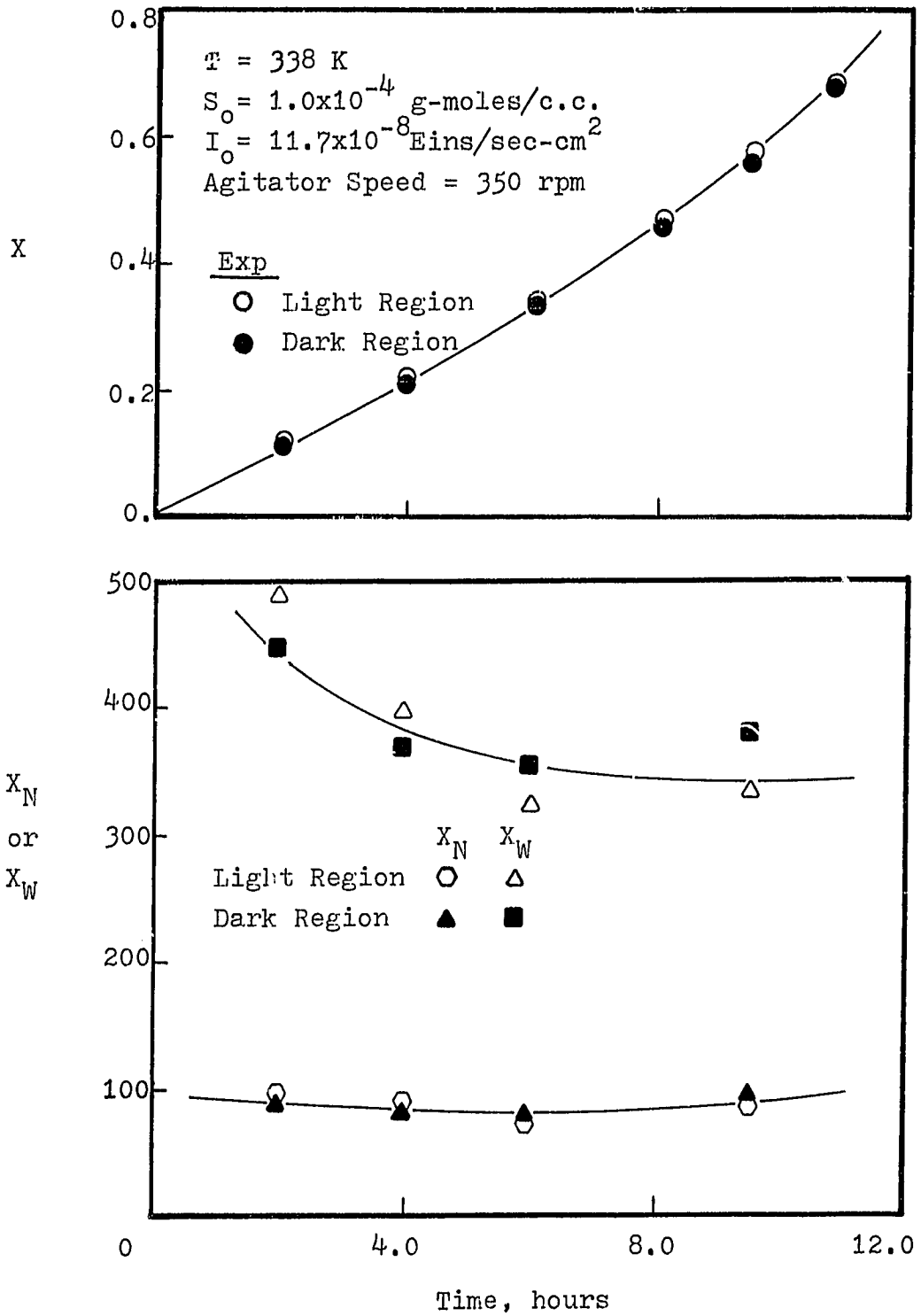

Figure 10. Mixing Effect of Photopolmerization at low Agitation Speed

trations are in the perfect mixing conditions.

There are eighteen isothermal batch runs carried out in this study. Detailed discussion on the experimental results and the comparison with proposed mathematical model will be given in chapter 7.

CHAPTER 4

PHOTOPOLYMERIZATION IN AN ISOTHERMAL AND CONTINUOUS STIRRED TANK REACTOR: CONCENTRATION STABILITY

4-1. Introduction

Photopolymerization of styrene in an isothermal and continuous stirred tank reactor is investigated. Conversion, molecular weight averages and molecular weight distribution at 338 K and 358 K and conversion up to 65% are measured. Three steady states are found to exist if the gel effect becomes pronounced.

The reactor performance characteristics in terms of fractional conversion and number average chain lengths are presented in this chapter. There are three possible regions of operation: low stable, metastable and high stable states. Operation in high stable region may be discounted for bulk polymerization because of very high viscosity. With regard to the other two regions, the obvious advantage of operation in the metastable one is the significantly higher conversion and molecular weight attainable for the same residence time. In addition, photo chemical initiation has a positive temperature coefficient of the degree of polymerization, which is in contrast with the results found for the thermal chemical initiation. In this chapter, emphasis is placed on steady

state multiplicity, stability and controllability of an isothermal and continuous stirred tank reactor.

4-2. Reactor Equations

The initiation mechanism considered are photochemical decomposition of sensitizer by ultraviolet light accompanied by thermal decomposition of monomer. For thermal initiation, a third order initiation model is used [2].

$$M \xrightarrow{k_{im}} R_1 \qquad \Omega_{im} = 2\, k_{im} m^3$$

the total initiation rate Ω_i is then,

$$\Omega_i = \Omega_{is} + \Omega_{im} \tag{47}$$

At present time, it is assumed that the fraction of light absorbed by the monomer and polymer is constant, i.e., $\epsilon_m m_o = \epsilon_m m + \Sigma \epsilon_{pi} P_i$, equation (3) becomes,

$$I_{as} = I_o \frac{\epsilon_s S}{\epsilon_m m_o + \epsilon_s S} \frac{1 - \mathrm{Exp}[-(\epsilon_s S + \epsilon_m m_o)L]}{L} \tag{48}$$

For styrene polymerization, a considerable volume change is involved. A linear relationship of volume versus monomer conversion is used [2], i.e.,

Volumetric flow rate for the inlet stream = Q

Volumetric flow rate for the outlet stream = $Q(1+\epsilon X)$

The material balance equations for the reactor are:

for sensitizer,

$$\frac{dS}{dt} = - \phi_s I_{as} + \frac{S_o - S(1+\epsilon X)}{\theta} \qquad (49)$$

for monomer,

$$\frac{dm}{dt} = \frac{m_o - m(1+\epsilon X)}{\theta} - \Omega_i^{1/2} m \left(\frac{k_p}{k_t^{1/2}}\right)_o \mathrm{Exp}(A_1 X + A_2 X^2 + A_3 X^3) \qquad (50)$$

the number and weight average chain lengths of the polymer are defined as,

$$X_N = \frac{\Sigma i P_i}{\Sigma P_i} \qquad (51)$$

$$X_W = \frac{\Sigma i^2 P_i}{\Sigma i P_i} \qquad (52)$$

where ΣP_i, $\Sigma i P_i$, and $\Sigma i^2 P_i$ are, respectively, the zero-th, first and second moments of the dead polymer size distribution in the outlet stream and can be expressed as [7],

$$\frac{d\ \Sigma P_i}{dt} = - \frac{\Sigma P_i (1+\epsilon X)}{\theta} + (k_{td} + \tfrac{1}{2} k_{tc})\left(\frac{\Omega_i}{k_t}\right) + \frac{k_{fm}}{k_p} m\, \Omega_i^{1/2} \left(\frac{k_p}{k_t^{1/2}}\right) \qquad (53)$$

$$\frac{d\ \Sigma i P_i}{dt} = - \frac{\Sigma i P_i (1+\epsilon X)}{\theta} + \left(\frac{k_p}{k_t^{1/2}}\right) m\, \Omega_i^{1/2} \qquad (54)$$

and

$$\frac{d\ \Sigma i^2 P_i}{dt} = -\frac{\Sigma i^2 P_i (1+\epsilon X)}{\theta} + \left(\frac{m\ \Omega_i^{1/2}}{\frac{k_t^{1/2}}{k_p}\Omega_i^{1/2} + \frac{k_{fm}}{k_p} m}\right)^2 \left(\frac{k_{tc}}{k_t}\right)$$

$$+ \frac{2\ m^2\ \Omega_i^{1/2} (k_p/k_t^{1/2})}{\frac{k_t^{1/2}}{k_p}\Omega_i^{1/2} + \frac{k_{fm}}{k_p} m} + \left(\frac{k_p}{k_t^{1/2}}\right) m\ \Omega_i^{1/2} \qquad (55)$$

where

$$\frac{k_{fm}}{k_p} = \left(\frac{k_{fm}}{k_p}\right)_o + B_1 X \qquad (56)$$

4-3. Multiple Steady States

By setting the left hand side of equation (50) equal to zero, one can determine the possible steady state points for the operation of the reactor. As described in Chapter 2, the general method is to separate equation (5) into two terms, mass supply rate (MSR) and mass consumption rate (MCR):

$$MSR = \frac{m_o - m(1+\epsilon X)}{\theta} = \frac{m_o X}{\theta} \qquad (57)$$

$$MCR = \Omega_i^{1/2} \frac{m_o (1-X)}{1+\epsilon X} \left(\frac{k_p}{k_t^{1/2}}\right)_o \mathrm{Exp}(A_1 X + A_2 X^2 + A_3 X^3) \qquad (58)$$

where the initiation rate, Ω_i can be calculated by equations

(47), (1), and (48) along with equation (49) (by setting $dS/dt = 0$).

Figure 11 shows typical solutions obtained for styrene polymerization. At steady state, MSR should be equal to MCR. MSR is essentially a linear function of conversion with a slope of m_o/θ. The existence of the two steady states shown in this figure requires the supply and consumption cueves be tangent at one point which is a physically unlikely situation. More likely is the occurance of one or three steady states. When three steady states (a,b,c) are found, the central one (b) is metastable state. At this state, a decrease in conversion results in less mass consumption, the monomer concentration increases (or conversion decreases) until it reaches the lower steady state (a). On the other hand, if conversion is increased (or monomer concentration is decreased) from the metastable state value, MCR > MSR, and the mass continues to fall (or conversion to increase) until the upper steady state (c) is reached.

It should be pointed out that a plot similar to Figure 11 was also obtained by Knorr and O'Driscoll [1]. However, they were concerned with thermal chemical initiation and the results here are based on photochemical initiation.

4-4. Reactor Performance Characteristics

TABLE 4

SUMMARY OF KINETIC MODEL PARAMETERS AND

THERMOPHYSICAL PROPERTY DATA

$(k_p)_o = 1.051 \times 10^7 \text{Exp}(-3557/T)$ Liter/g-mole-sec

$(k_t)_o = 1.255 \times 10^9 \text{Exp}(-844/T)$ Liter/g-mole-sec

$(k_{fm})_o = 2.31 \times 10^6 \text{Exp}(-6377/T)$ Liter/g-mole-sec

$\overline{k}_i = 2.19 \times 10^5 \text{Exp}(-13810/T)$ $\text{Liter}^2/\text{g-mole}^2\text{-sec}$

$A_1 = 2.57 - 5.05 \times 10^{-3} T$

$A_2 = 9.56 - 1.76 \times 10^{-2} T$

$A_3 = -3.03 + 7.85 \times 10^{-3} T$

$B_1 = -1.013 \times 10^{-3} \text{Log}_{10}((473.12-T)/202.5)$

$\epsilon_s = 0.0155$ Liter/g-mole-cm

$\epsilon_m = 88.5$ Liter/g-mole-cm

$\phi_s = 0.072$ g-moles/Eins

$\Delta H = -16683$ cal/g-mole

$C_r = 0.376$ $\text{cal/cm}^3\text{-K}$

$\rho_m = 924 - 0.918 \times (T-273.1)$ g/liter

$\rho_p = 1084.8 - 0.605 \times (T-273.1)$ g/liter

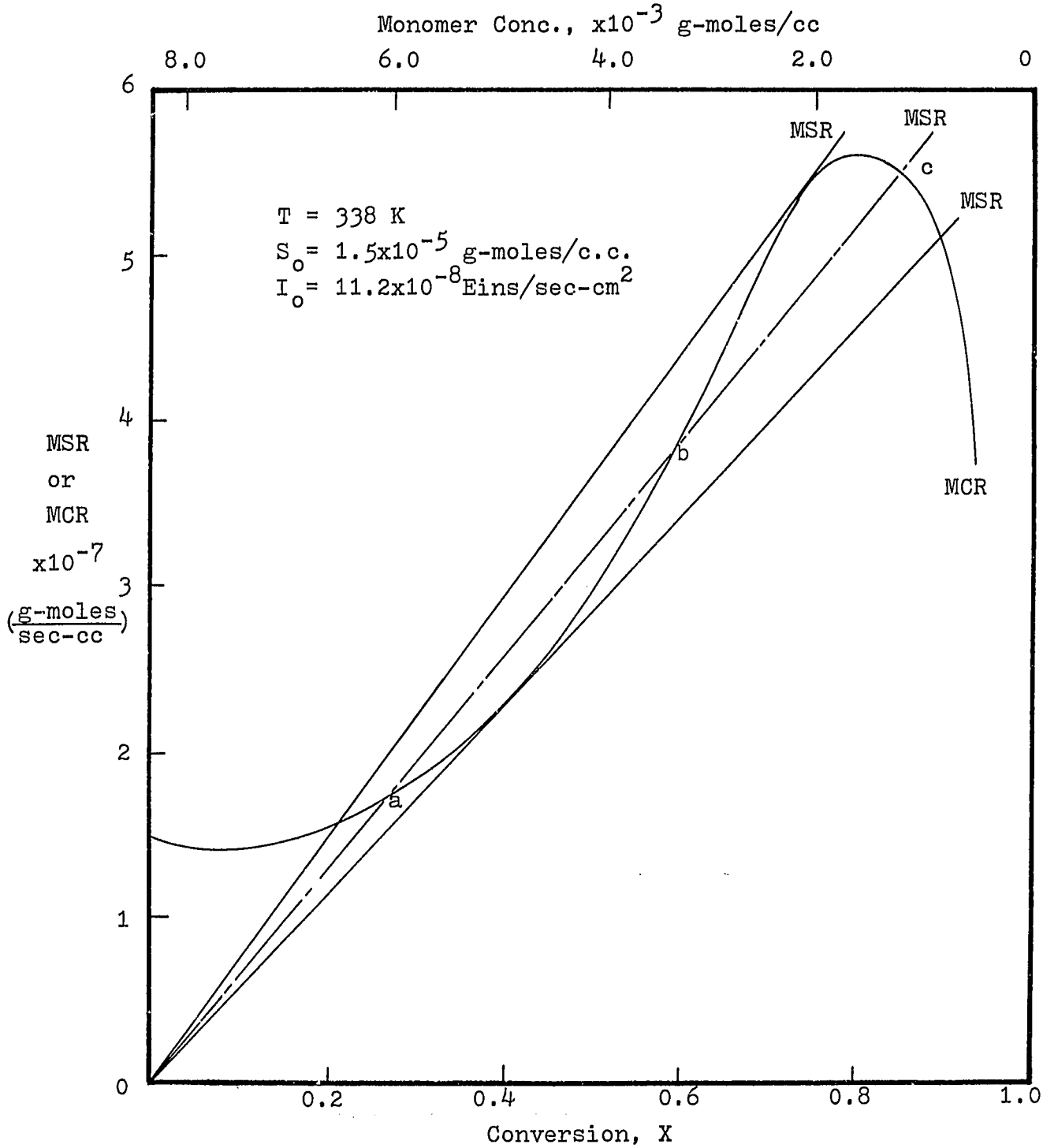

Figure 11. MSR and MCR vs. X or m

Figure 12 shows the calculated results representing the reactor performance characteristics in terms of fractional conversion X, and number average chain length, X_N. Note that while the reactor is operated in low stable state, an increase in residence time at a fixed light intensity I_o, will result in an increase for both X and X_N. The converse is true at metastable region. Also, an increase in I_o would shift the characteristic curve to lower residence time, however the sensitizer S_o, has no appreciable effect on the curve. Notice that all the metastable region operations are inherently unstable, the reactor only operates by forcing it to with appropriate control.

The striped bands shown in Figure 13 are metastable region. As shown in the figure, while I_o decreases, the band becomes larger. For a given I_o, when the couple of residence time and reaction temperature falls into the band, the reaction conditions have three steady states, two of which are stable and another unstable one. A decrease in temperature results in a greater possibility of existence of multiple steady states induced by gel effect.

4-5. Lower and Metastable Steady States

Conversion of metastable states have been obtained by observing the effect of perturbation from stable conversion.

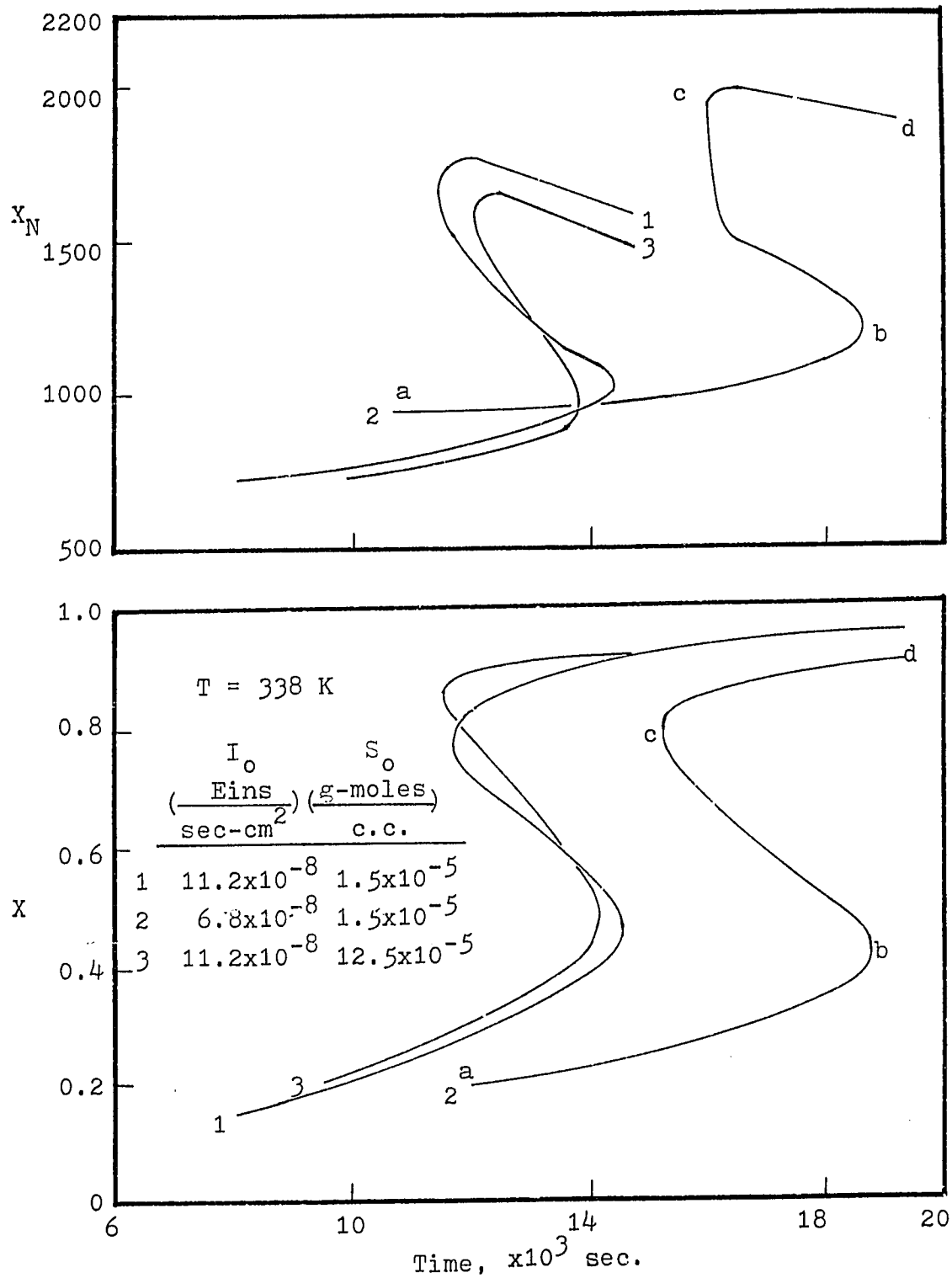

Figure 12. Isothermal Reactor Performance Characteristics - Calculated Results

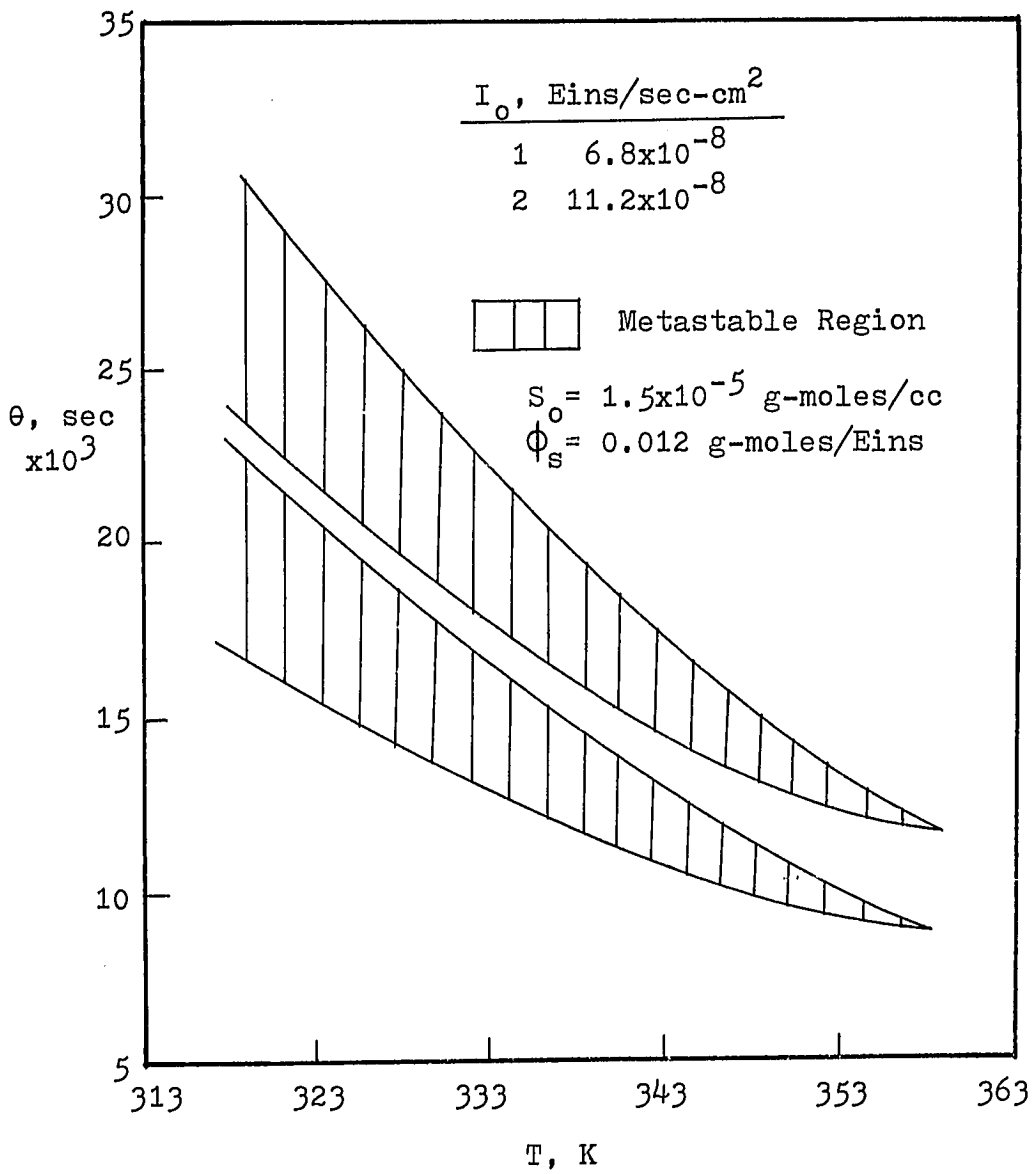

Figure 13. Metastable State Region for Isothermal CSTR

Figure 14 shows a typical approach. The conversion is raised to the predicted low stable steady state by means of the batch operation. The reactor is then operated continuously at a flow rate of 0.43 cc/min, the reaction is permitted to find its real steady state. Once at the steady state, reaction conditions are maintained for a time period of approximately one residence time. The conversion is then raised to the predicted metastable state by means of raising reaction temperature to 393 K. After the reaction is reached to certain conversion, temperature is then dropped to 338 K. Instant conversion can be observed through the use of spectrophotometric method as described in chapter 3. A decrease in conversion following the continuous operation indicates undershoot below the metastable point and the conversion is raised by the batch operation. Similarly, an increase in conversion indicates overshoot beyond the metastable point and the shutter is closed to lower the conversion. By means of this step-wise procedure, the metastable point is reached. Figure 15 shows the experimental results (low and metastable state regions).

4-6. The Control System

Experimental results has been carried out on the reactor control by on-off regulation of the light intensity. This is deemed most suitable for a UV lamp which for proper operation must be maintained at constant output. At a given time interval

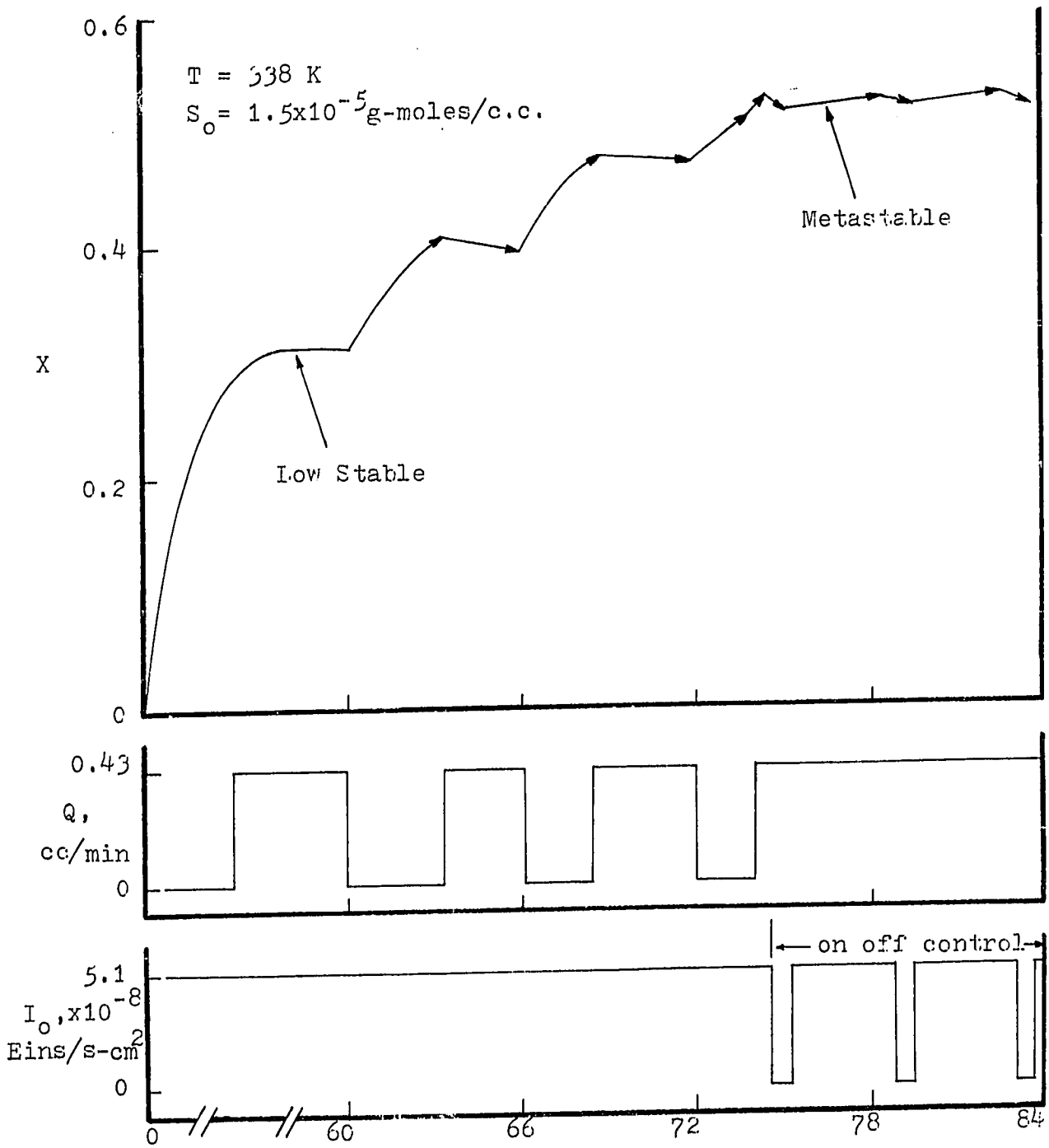

Figure 14. Transient Responses to Perturbation from Stable Conversion

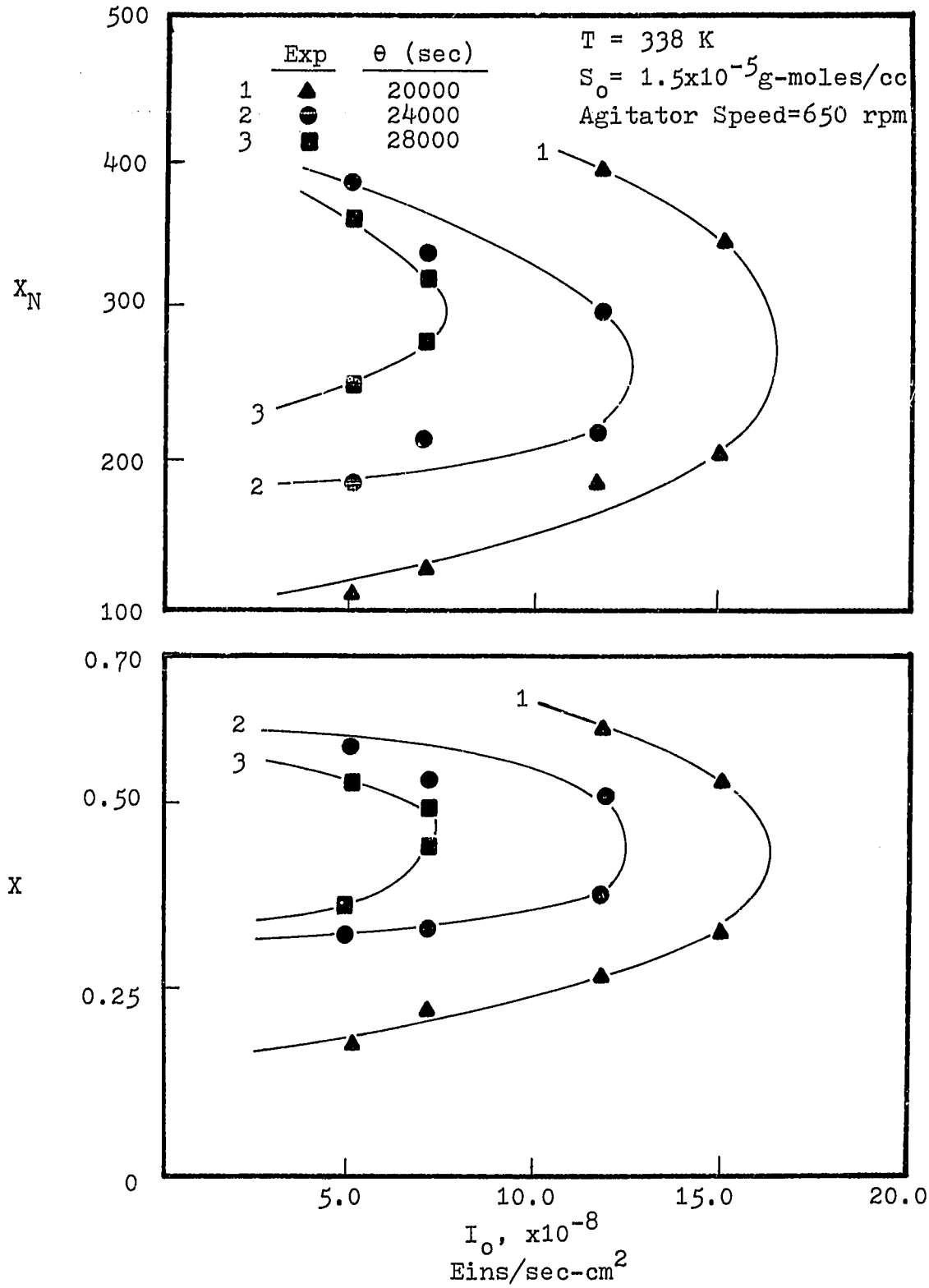

Figure 15. Isothermal Reactor Performance Characteristics - Experimental Results

(approximately 1200 sec.) samples were collected from the product stream and analyzed by UV spectrophotometry to determine the styrene concentration m. If $m > m_{sp} + db$ (m_{sp} = desired concentration, db = dead band), the shutter was closed manually, and vice versa. Conversion was readily controlled with 0.015 below or above the set point. The instantaneous number average chain lengths varied with the range from 313 to 400 as shown in Figure 16. Also, the polymer formed at the metastable state has a higher number average chain length than that obtained at the lower stable state (Figure 17). Figure 18 presents the results of dynamic simulation around the metastable point using on-off regulation of UV light. The control period is about 2.1 times of the reactor holding time which is depending on the control limits (db) and the degree of instability at the point to control.

The above is intended as an application to the concept of viscosity stability in styrene polymerization. The developed model is based on the assumption that the reactor is perfectly mixed. By comparing Figures 12, 15, and 18, one may notice that the calculated values of conversion and number average chain length are higher than those obtained experimentally. A detailed discussion on this, and the effect of mixing on the concentration stability will be given in the later chapters.

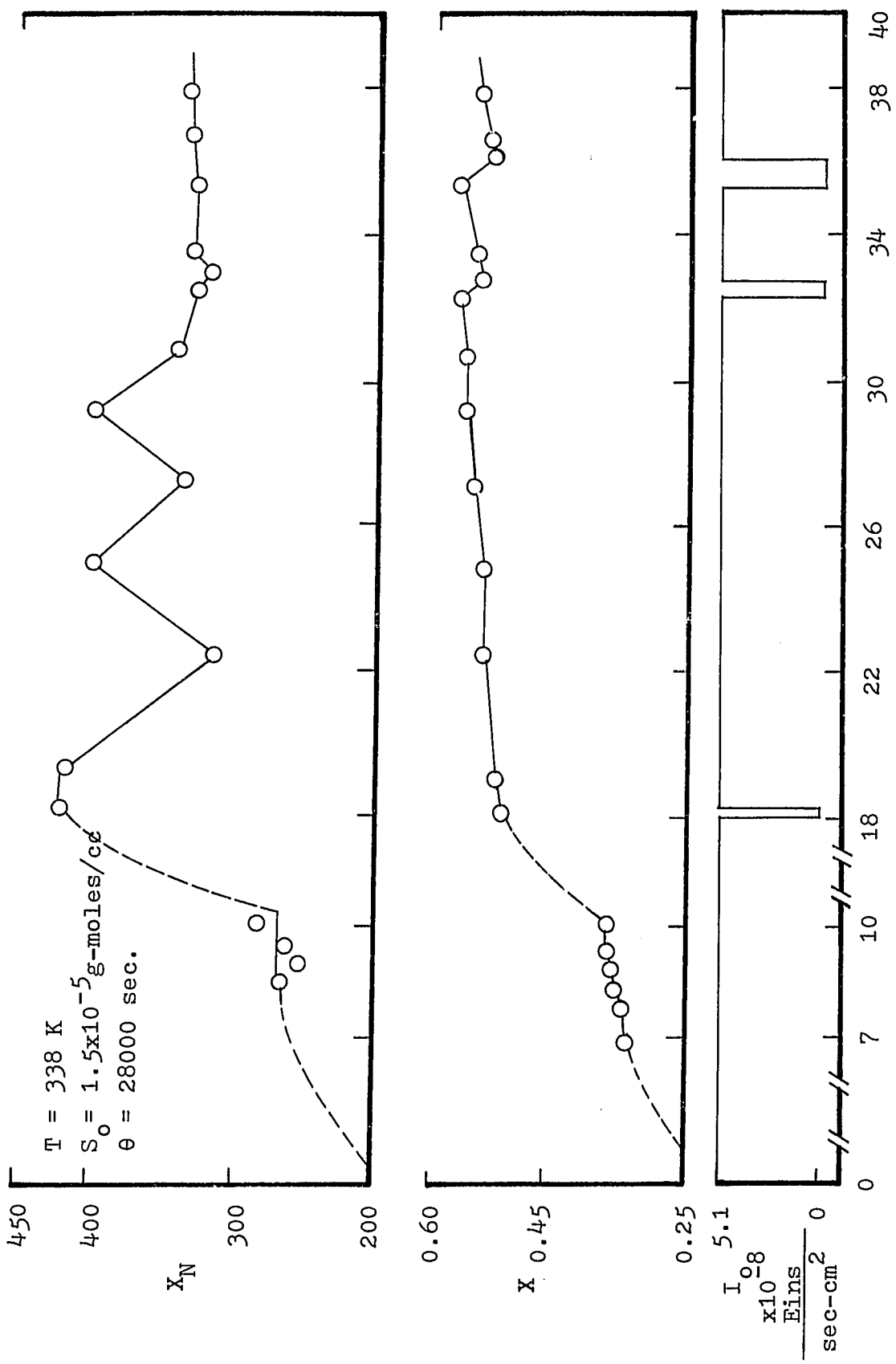

Figure 16. Experimental Results for Photosensitized Polymerization in the Controlled Isothermal CSTR

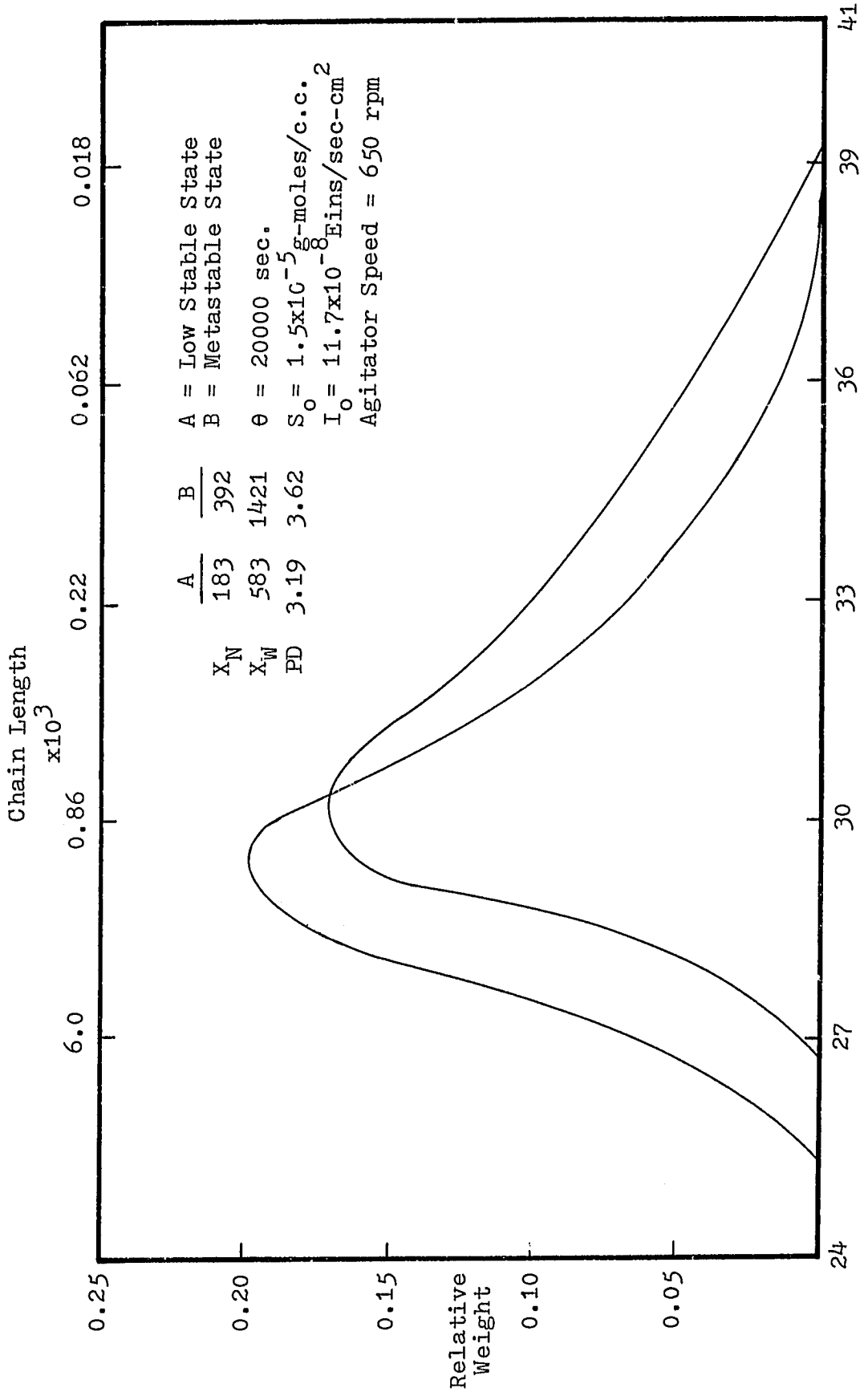

Figure 17. MWD by GPC at lower and Meta Stable States - Isothermal CSTR

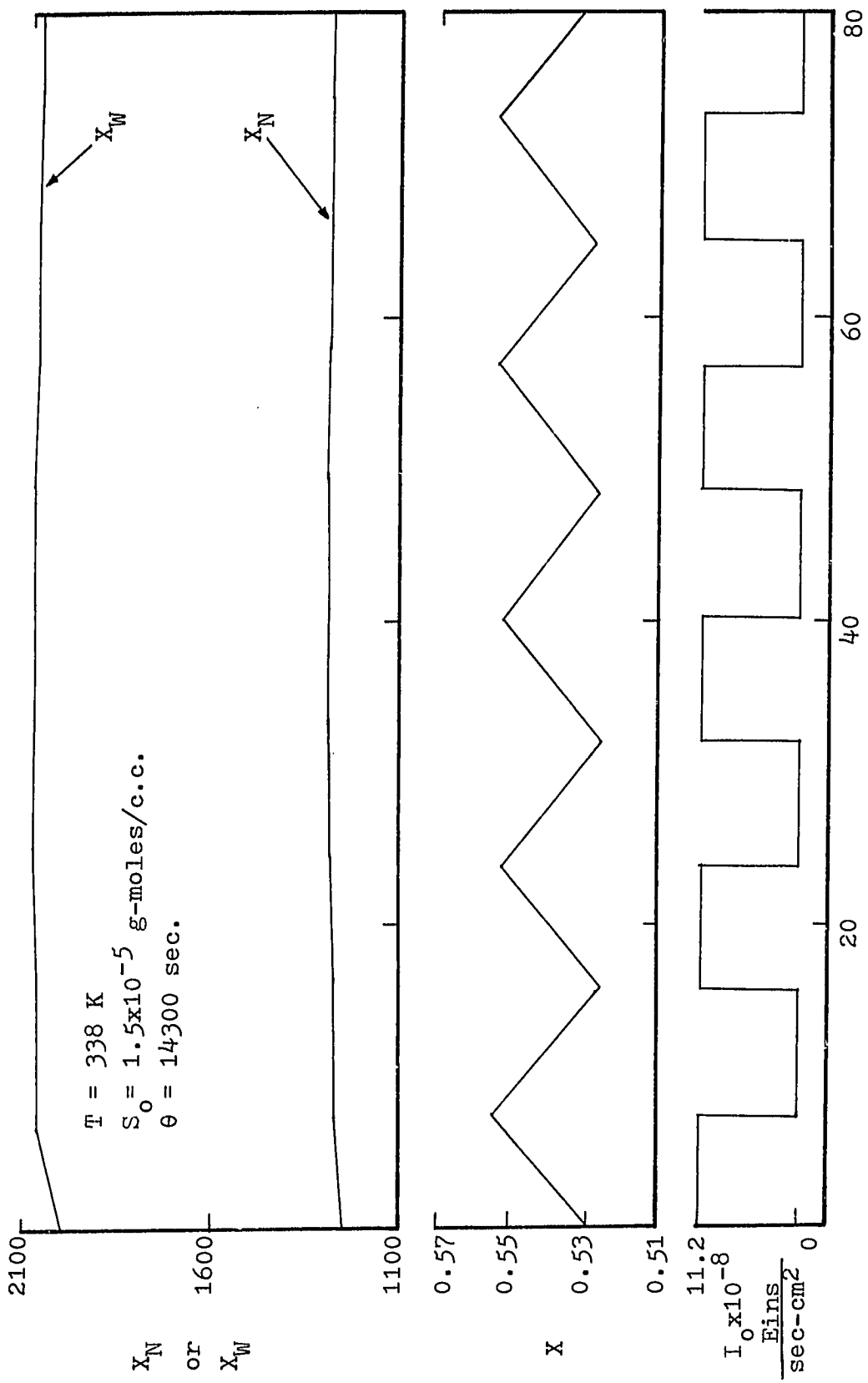

Figure 18. Computer Simulation of the Controlled Isothermal CSTR

CHAPTER 5

PHOTOPOLYMERIZATION IN AN ADIABATIC AND CONTINUOUS STIRRED TANK REACTOR: TEMPERATURE STABILITY

In this chapter, experimental and theoretical investigations of polymerization of styrene initiated by photodissociation of sensitizer were made in an adiabatic CSTR. The use of ultraviolet light as a generator of free radicals offers a significant improvement in the control of polymerization reactions and to determine the effect on molecular weight distribution of the polymer formed.

5-1. Multiple Steady State Analysis

At steady state, equations (8), (49) and (50) become,

$$-\phi_s I_{as} + \frac{S_o - S(1+\varepsilon X)}{\theta} = 0 \qquad (59)$$

$$-\Omega_m + \frac{m_o - m(1+\varepsilon X)}{\theta} = 0 \qquad (60)$$

$$Q \rho C_p (T_o - T) - (-\Delta H) V \Omega_m = 0 \qquad (10)$$

The first term of equation (10) is heat withdrawl rate (HWR) from the reactor system and the second one is heat produced rate (HPR) of the polymerization reaction. At steady state condition, these two terms should be equal. Traditionally in studies of the adiabatic CSTR, the character of the steady

state is typically illustrated graphically by plotting both HWR and HPR vs. temperature and by examining the intersections of the resulting curves. Due to the nonlinear nature of Arrhenius rate, three steady states may be obtained at certain conditions.

When three steady states are found, the middle one is metastable state. At this state, an increase in temperature results in more heat generation than the heat withdrawl rate, consequently, the temperature continues to rise until it reaches the upper steady state. On the other hand, if the temperature is decreased from the metastable state value, the heat produced rate becomes less than heat withdrawl rate and temperature will continue to fall until the lower steady state is reached. Notice that the steady state problem is reducible to a single equation involving only temperature if equations (59) and (60) are substituted into equation (10).

5-2. Experimental

Metastable state temperatures have been obtained by observing the effect of perturbation from stable temperatures. Figure 19 shows a typical approach. The reaction temperature is raised to the predicted low stable state temperature by means of the preheat coil. Flow through the preheat coil is then stopped, and the reaction is permitted to find its real

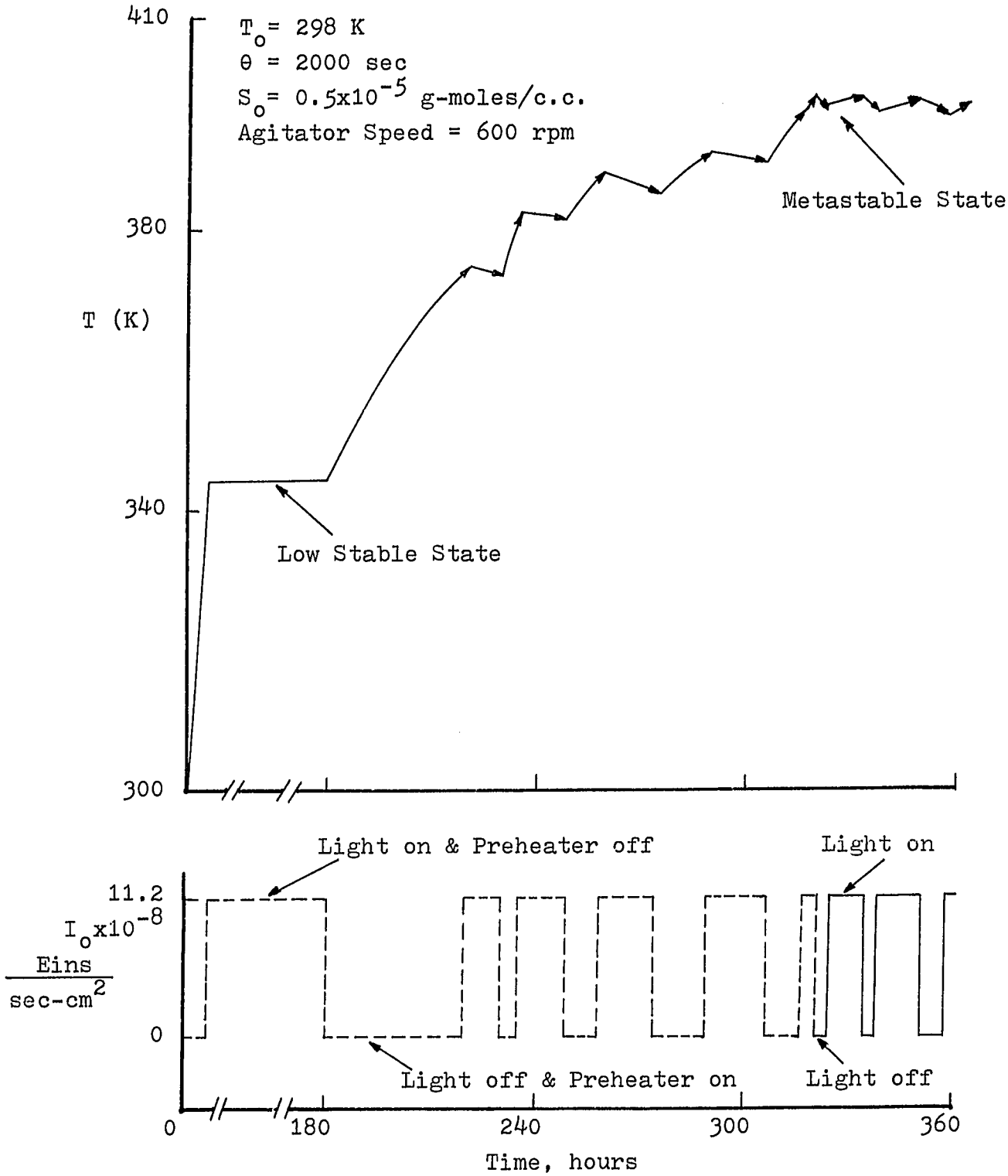

Figure 19. Transient Responses to Perturbation from Stable Temperature

steady state. Once at the steady state, reaction conditions are maintained for a time period of approximately one residence time. The reaction temperature is then raised to the predicted metastable stable state by means of the preheat coil. A decrease in temperature following the cessation of preheat indicates undershoot below the metastable point, and the temperature is raised via the preheat coil. Similarly, an increase in reaction temperature indicates overshoot beyond the metastable state, and the shutter is closed to lower the reaction temperature. By means of this step-wise procedure, the metastable point can be reached.

Figure 20 shows the experimental results representing the reactor performances in terms of fractional conversion and reaction temperature. Figure 21 are the experimental results of measured number and weight average chain lengths at various I_o. In both figures, the solid lines represent the predicted values based on the three equations (10),(59),(60). Note that there are three regions, the curves a-b (low stable state), and curve b-c (metastable state) and operation in region of high stable state (not shown) may be discounted for bulk polymerization because of very high temperature and low molecular weight. Operation at metastable state has the same advantage as that of an isothermal operation. Comparison of adiabatic and isothermal operations will be discussed in Chapter 7.

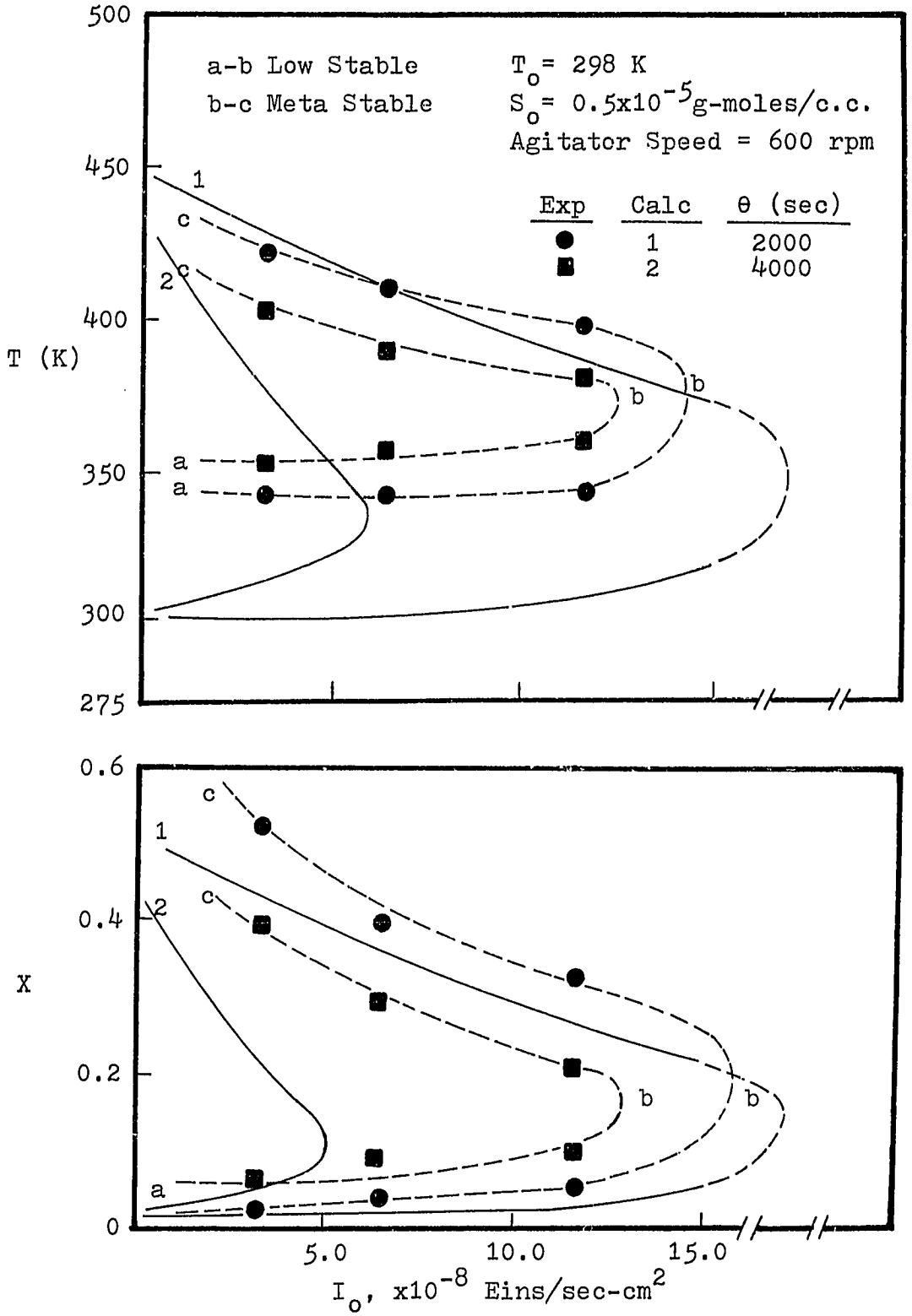

Figure 20. Steady State Conversion and Temperature for Adiabatic CSTR

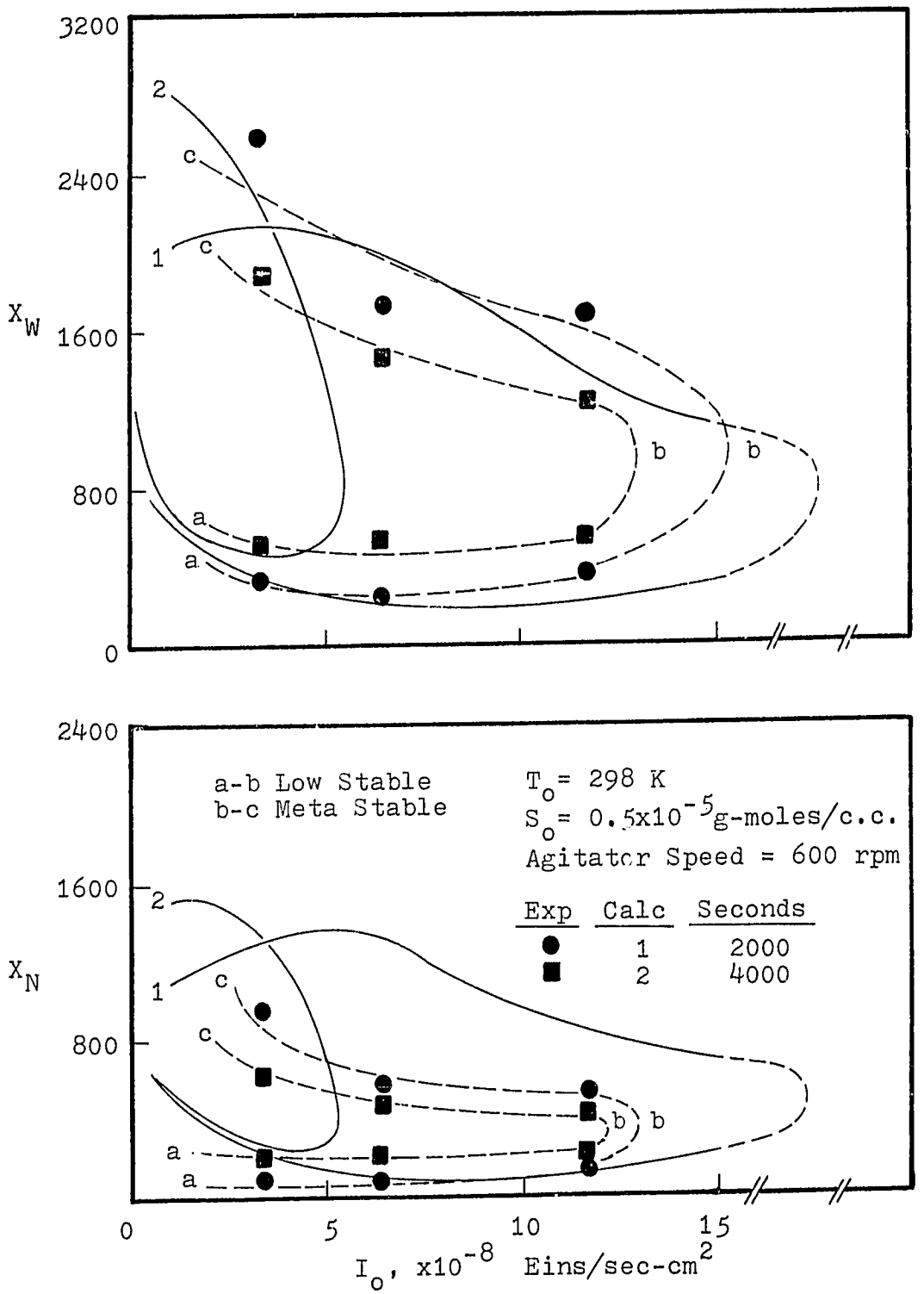

Figure 21. Steady State X_N and X_W for Adiabatic CSTR

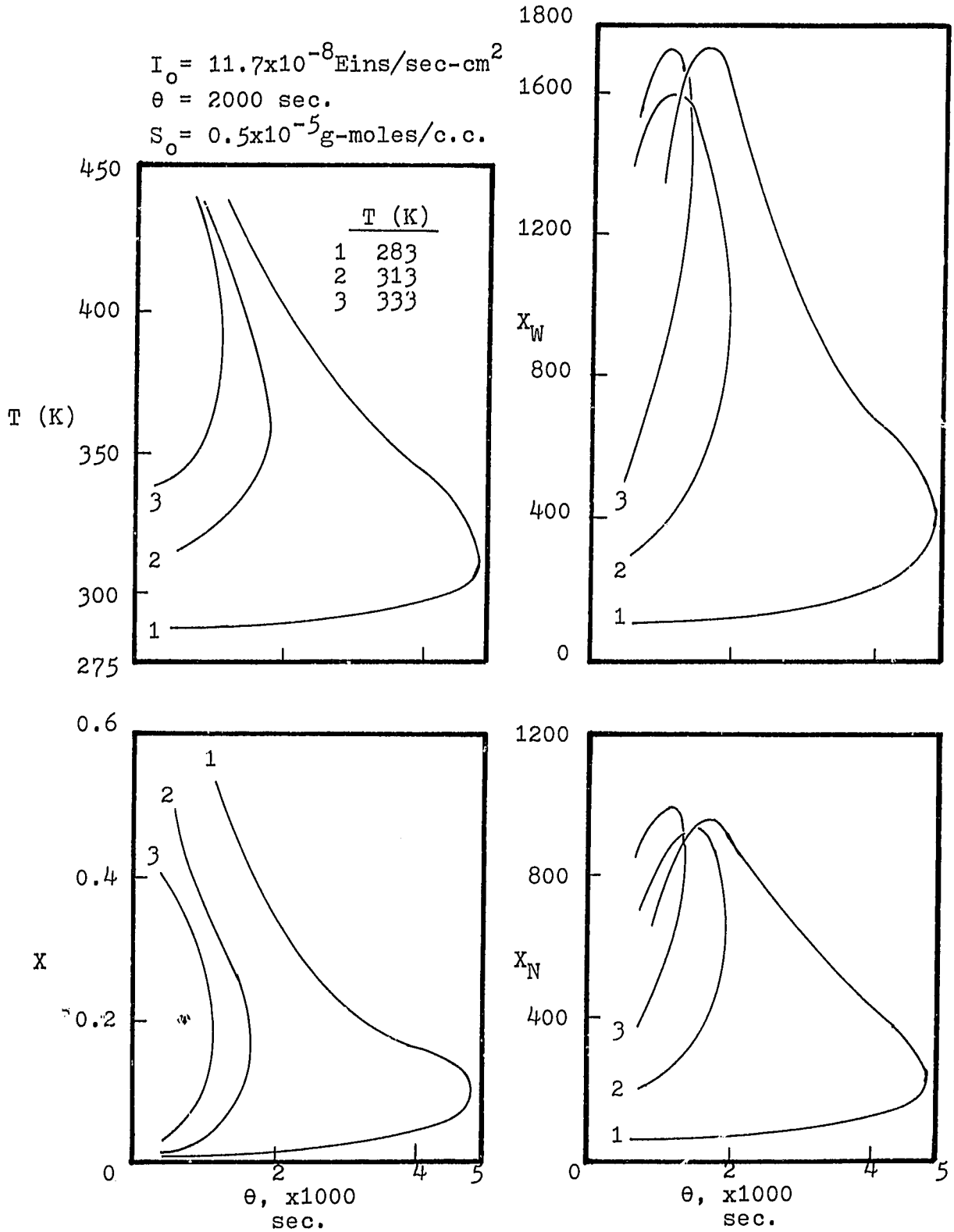

Figure 22. Effect of T_o on Multiple Steady States in an Adiabatic CSTR

As shown in Figure 20, the influence of increasing the residence time from 2000 to 4000 seconds is to shift the temperature (or conversion) curve towards the lower light intensity to obtain the same temperature (or conversion). Also, for higher residence time the possibility of multiple steady states is lower. Figure 22 shows the inlet temperature (T_o) effect on multiple steady states. The multiple steady state region will be reduced as T_o increases. Metastable state operation at a very low residence time, the molecular weight number and weight average chain lengths are usually very low due to thermal decomposition of polymer product at high temperature. Photochemical reactor operated at metastable region offers the advantage of high conversion without sacrifice of the product molecular weight. This is unique to the radiation initiation system.

The importance of setting the correct start-up conditions for the reactor operation can be deduced from Figure 20. An incident light intensity I_o approximately about 13×10^{-8} Eins/sec-cm^2 for θ = 4000 seconds would automatically bring the reactor to its higher steady state. The result is a substantial drop in the chain length.

5-3. The Contrcl System

Experimental investigation has been carried out on the reactor control by on-off regulation of the light intensity.

The on-off operation with a dead band is obtained through a shutter mechanism as shown in Figure 23. The reaction temperature is readily maintained with 2.5 K below or above the set point and responds quickly to the change in the light intensity. The polymer formed at metastable state has a higher number average chain length than that obtained at low stable state, typical molecular weight distributions of these two states are given in Figure 24.

Figure 25 shows the calculated results of the metastable state operation. The reactor response of an adiabatic CSTR is much quicker than that of an isothermal operation (Figure 18). At lower I_o or θ operation conditions, exothermic reaction requires to take place at elevated temperature levels for a normal operation, which the thermal initiation term is becoming to dominate the polymerization reaction. As a result, the reactor operation becomes less controllable. Figure 26 shows the ratio of photo initiation rate to the total initiation rate at two residence time levels.

5-4. Summary

On the basis of this study, it has been concluded that the photopolymerization reactor could be operated close to a metastable state operating point using suitable on-line control system. A control system such as the one used in this

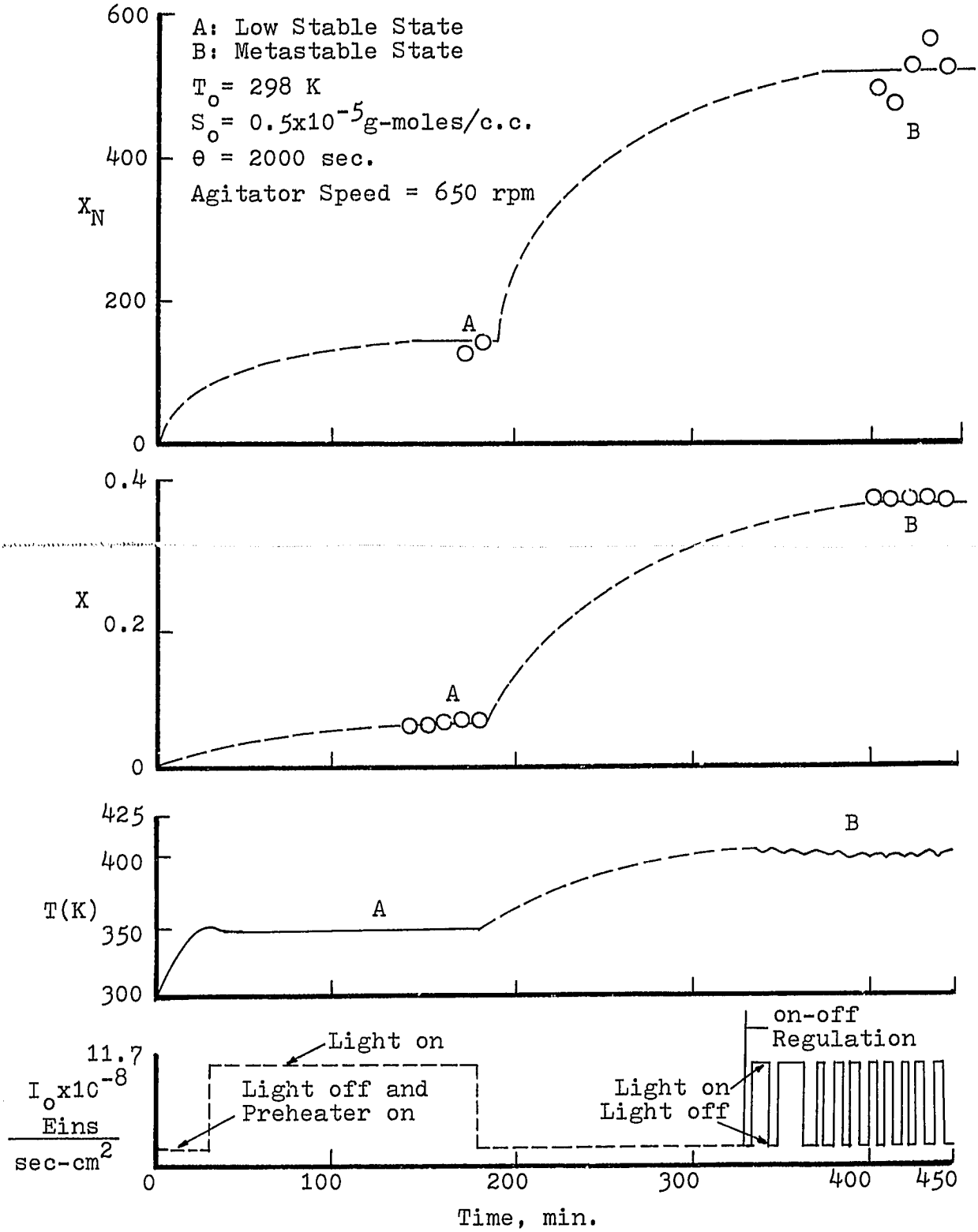

Figure 23. Experimental Results for Photosensitized Polymerization in the Controlled Adiabatic CSTR

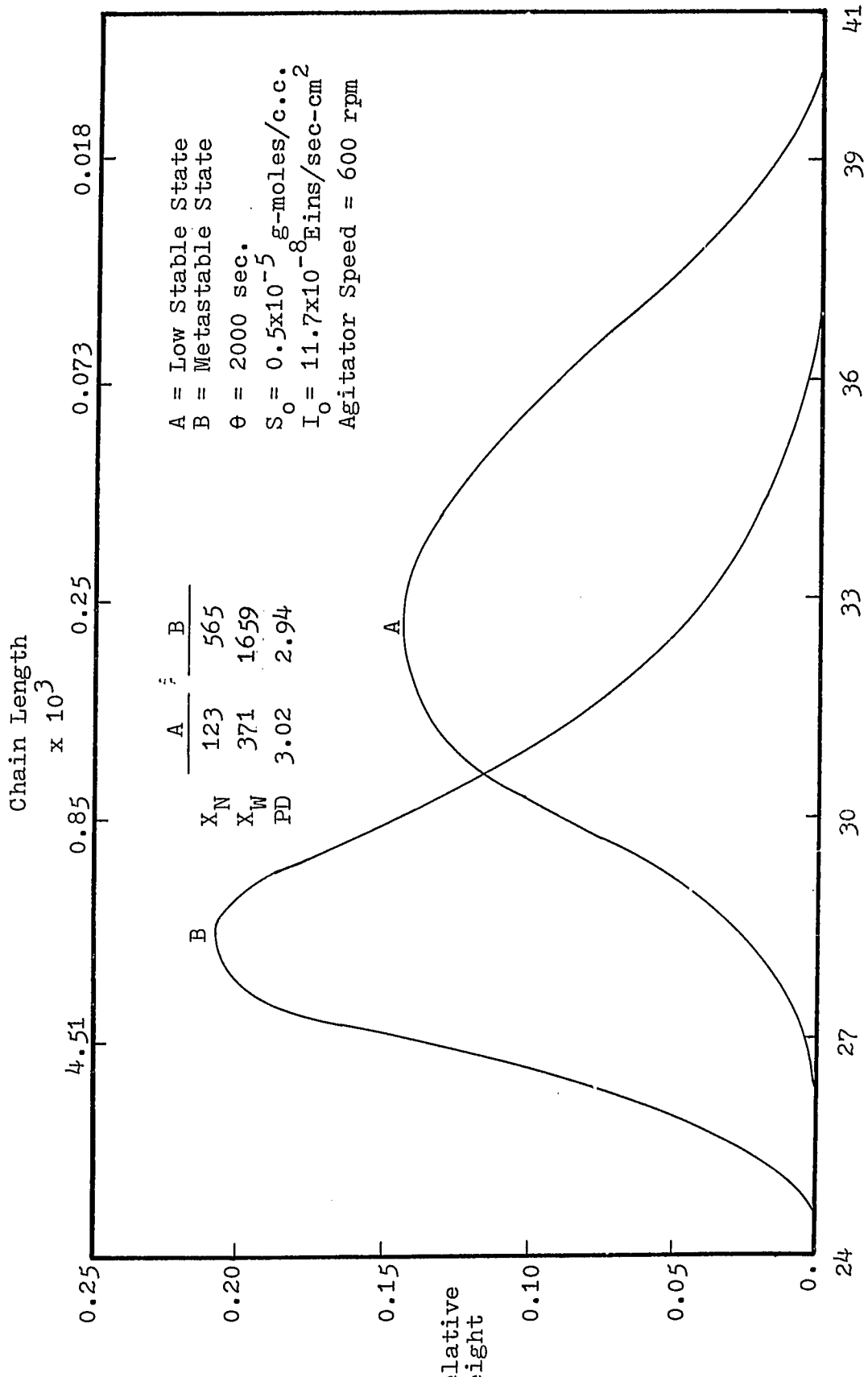

Figure 24. MWD by GPC at Lower and Meta Stable States - Adiabatic CSTR

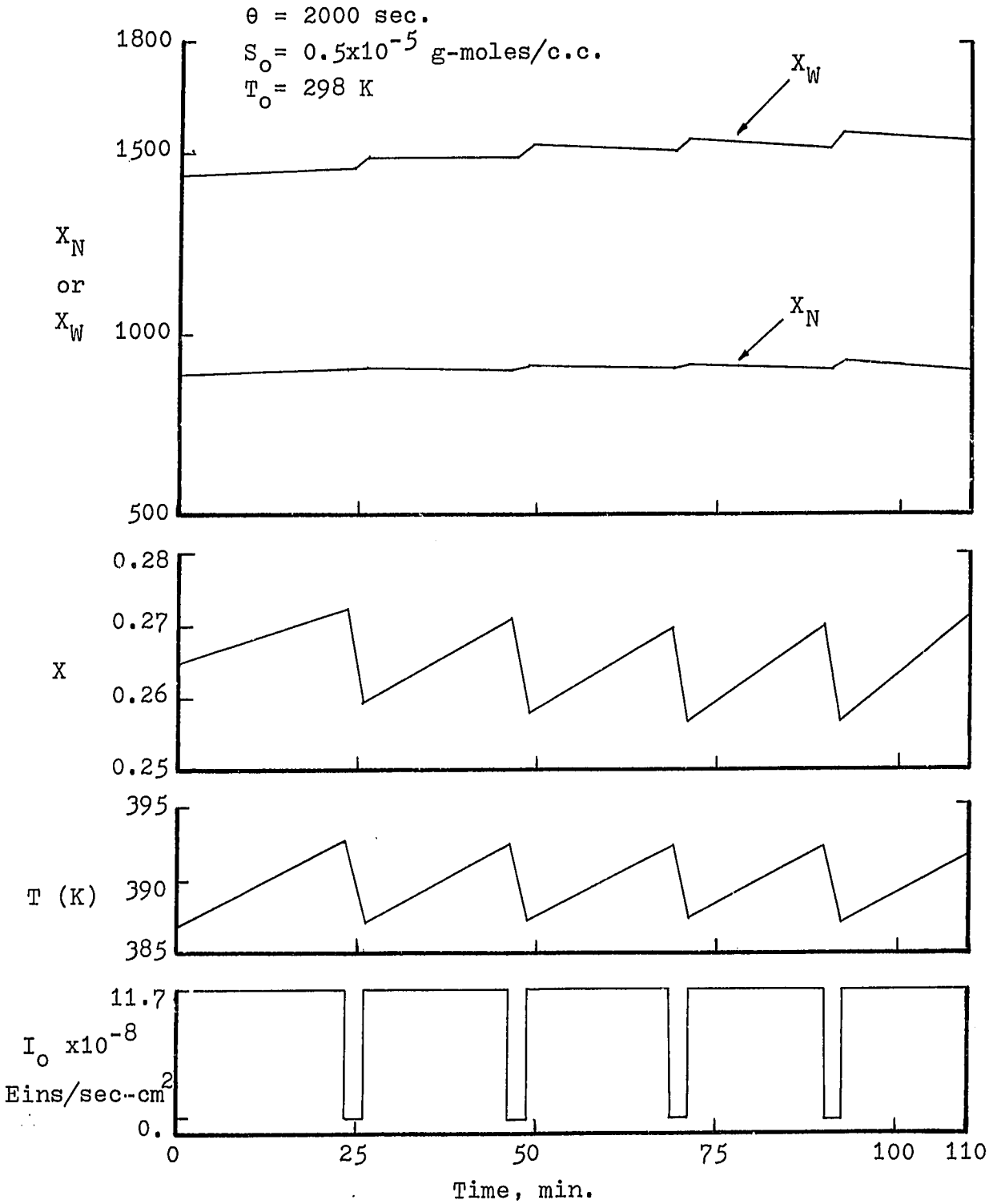

Figure 25. Computer Simulation of the Controlled Adiabatic CSTR

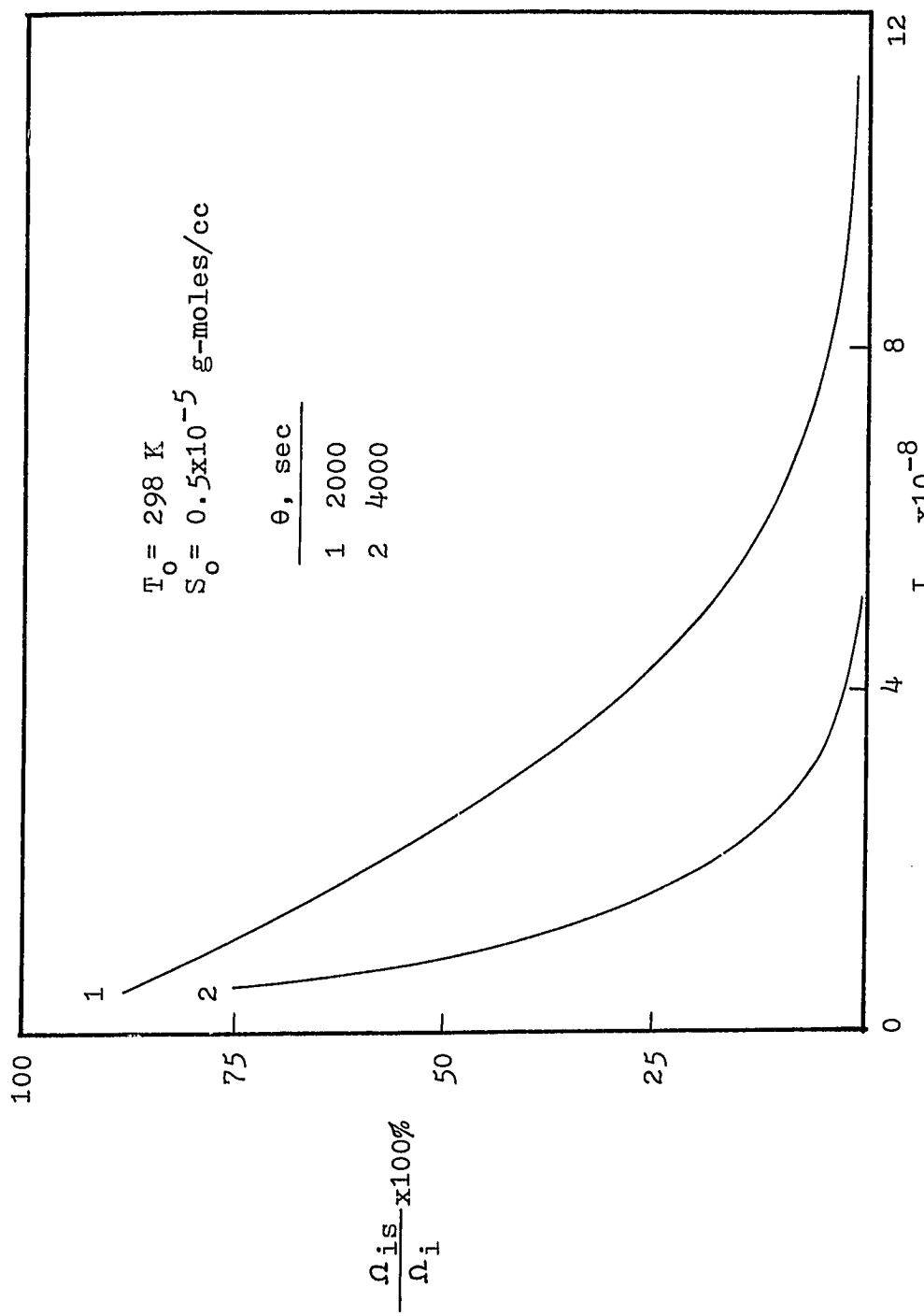

Figure 26. Effect of Thermal Initiation on Photopolymerization in an Adiabatic CSTR - Calculated Results

study could be designed for a photopolymerization reactor in such a way that any minor disturbances during the regular operation, such as feed flow rate, reactant concentration in the feed or reactor temperature will not cause a permanent change in the reactor operation.

The proposed simple on-off regulation of UV light to the reactor control has demonstrated to be a good approach if operating at metastable state is necessary. Some alternate means such as reactant or coolant flow rate control or the combination are also applicable by using a more sophisticated control scheme. One very important thing to note is that by applying the control procedure, such as the on-off regulation, the reactor should be brought to the unstable steady state point. This will usually require some special startup procedures. Such procedures could be developed using a suitable model for simulating the dynamic behavior of the reactor.

Experimental results have indicated the possibilities that more than one steady states are obtainable in the exothermic polymerization reaction. There are some limitations of the experimental results which have to be considered. The reactor size in this study is relatively small in which a considerable amount of heat loss to ambient is inevitable. Also, the amount of heat generated by mechanical work due to agitation in the viscous reaction mixture may be large.

Contributions of the above two terms are difficult to correlate experimentally. To avoid heat loss, a heating tape is surrounded to the outside of the insulation fiber glass where the temperature is adjusted manually close to the reactor temperature. If heat generation due to agitation is not significant, it is expected a higher reaction temperature will be obtained near the metastable state point.

CHAPTER 6

MATHEMATICAL MODEL

A mathematical model is developed to correlate the mixing effect in photopolymerization, in which a nonuniform distribution of absorbed light intensity occurs. The kinetic scheme used in this study is essentially that of Bamford and Dewar [20] as extended by Pryor and Coco [21] and Hui and Hamielec [2]. To the mixing effect on radiation-induced polymerization, up to this time, two different calculation methods have been reported. One is based on a diffusion model in which the free radicals produced in the higher dose rate area are assumed to be dispersed throughout the reaction by diffusion [22,23]. The other one is a circulation model, in which fluid elements are assumed to be irradiation periodically by going around in the reactor [3,15]. In this work, a circulation flow model will be extended.

6-1. Kinetic Model

There are many theories which have been proposed to account the unusually high thermal initiation of styrene polymerization. Pryor and Coco [21] have reviewed the chronologic development of these theories and have outlined an acceptable mechanism for the thermal polymerization of styrene, as follows:

Initiation:

$$M + M \underset{k_{-1}}{\overset{k_1}{\rightleftharpoons}} \text{(AH)}$$

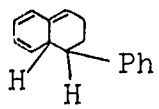

$$M + M \underset{k_{-2}}{\overset{k_2}{\rightleftharpoons}} \text{PhĊHCH}_2\text{CH}_2\text{ĊHPh}$$

$$\text{PhĊHCH}_2\text{CH}_2\text{ĊHPh} \xrightarrow{k_{cyc}} \text{1,2-diphenylcyclobutanes}$$

$$AH + RS \xrightarrow{k_s} \text{non-radical products}$$

$$M + AH \xrightarrow{k_i} \text{PhCHCH}_3 + \text{(Ȧ)}$$

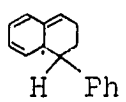

$$M + AH \xrightarrow{k_c} \text{trimer}$$

$$A \xrightarrow{\text{aromatization}}$$

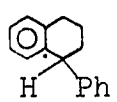

(Ȧ)

$$\dot{A} + M \xrightarrow{k_A} R_1$$

$$\dot{M} + M \xrightarrow{k_B} R_1$$

Propagation:

$$R_i + M \xrightarrow{k_p} R_{i+1}$$

Termination by combination:

$$R_i + R_j \xrightarrow{k_t} P_{i+j}$$

Chain transfer:

$$R_i + M \xrightarrow{k_{fm}} P_i + R_1$$

$$R_i + AH \xrightarrow{k_{fAH}} P_i + R_1$$

In the above scheme, AH is a Diel-Alder adduct and RS is a radical scavenger. Let Ω_{im} be the initiation in g-moles/cc-sec;

$$\Omega_{im} = - \frac{d[R_1]}{dt} = (k_A [\dot{A}] + k_B [\dot{M}]) [M] \qquad (61)$$

for [M] and [AH],

$$\frac{d[\dot{A}]}{dt} = - k_A [\dot{A}] [M] + k_i [M] [AH] \qquad (62)$$

$$\frac{d[\dot{M}]}{dt} = k_i [M] [AH] - k_B [\dot{M}] [M] \qquad (63)$$

By applying the stationary state hypothesis to [A] and [M],

$$[\dot{A}] = \frac{k_i}{k_A} [AH] \qquad (64)$$

$$[\dot{M}] = \frac{k_i}{k_B} [AH] \qquad (65)$$

By substituting equations (64) and (65) inti (61),

$$\Omega_{im} = 2 k_i [AH] [M] \qquad (66)$$

Again, applying the stationary state hypothesis to [AH], and let [M] = m (g-moles/cc),

$$[AH] = \frac{k_1 m^2}{k_{-1} + (k_i + k_c) m + k_{fAH}(\frac{\Omega_{im}}{k_t})^{1/2}} \qquad (67)$$

The initiation rate can then be expressed as follows:

$$\Omega_{im} = \frac{2 k_i k_1 m^3}{k_{-1} + (k_t + k_c) m + k_{fAH}(\frac{\Omega_{im}}{k_t})^{1/2}} \qquad (68)$$

Hui and Hamielec concluded that the third order initiation in monomer shows a better correlation to their experimental results, that is,

$$\Omega_{im} = (\frac{2 k_i k_1}{k_{-1}}) m^3 = 2 \bar{k}_i m^3 \qquad (69)$$

A considerable volume change is involved in the styrene polymerization. Volume change is accounted for with the use of the variable volume equation,

$$\text{rate} = \frac{1}{V}\frac{dC}{dt} = \frac{dC}{dt} + \frac{C}{V}\frac{dV}{dt} \qquad (70)$$

Assuming that the volume of reaction mixture varies linearly with monomer concentration,

$$V = V_o (1 + \epsilon X) \qquad (71)$$

where ϵ is the volume expansion coefficient, defined as

$$\epsilon = \frac{V_{X=1} - V_{X=0}}{V_{X=0}} \qquad (72)$$

The conversion is defined as,

$$X = \frac{m_o V_o - mV}{m_o V_o} \tag{73}$$

or

$$X = \frac{m_o - m}{m_o + \epsilon m} \tag{74}$$

As mentioned previously, the termination rate becomes diffusion controlled as conversion increases. This is reflected by variation of the kinetic constants. An empirical expression for the variations of $(k_p/k_t^{1/2})$ and (k_{fm}/k_p) as follows:

$$(k_p/k_t^{1/2}) = (k_p/k_t^{1/2})_o \mathrm{Exp}(A_1X+A_2X^2+A_3X^3) \tag{6}$$

and

$$(k_{fm}/k_p) = (k_{fm}/k_p)_o + B_1X \tag{56}$$

where A_1, A_2, A_3 and B_1 values can be determined experimentally.

6-2. Perfect Mixing Model

The suggested kinetic model applied to photopolymerization, the material balance equations for sensitizer, monomer and dead polymer species are,

for sensitizer:

$$\frac{dS}{dt} = -\phi_s I_{as} - \frac{S}{V}\frac{dV}{dt} \tag{75}$$

for monomer:

$$\frac{dm}{dt} = -\left(\frac{k_p}{k_t^{1/2}}\right) m\, \Omega_i^{1/2} - \frac{m}{V}\frac{dV}{dt} \tag{76}$$

The zero-th, first and second moments of dead polymer can be expressed as:

$$\frac{d\ \Sigma P_i}{dt} = k_{fm} m\ \Sigma R_i + \frac{1}{2} k_t\ \Sigma R_i^2 - \frac{\Sigma P_i}{V} \frac{dV}{dt} \tag{77}$$

$$\frac{d\ \Sigma iP_i}{dt} = k_t\ \Sigma R_i\ \Sigma iR_i + k_{fm} m\ \Sigma iR_i - \frac{\Sigma iP_i}{V} \frac{dV}{dt} \tag{78}$$

$$\frac{d\ \Sigma i^2 P_i}{dt} = k_t\ \Sigma R_i\ \Sigma iR_i + k_t\ \Sigma iR_i^2 + k_{fm} m\ \Sigma i^2 R_i - \frac{\Sigma i^2 P_i}{V} \frac{dV}{dt} \tag{79}$$

where

$$\Sigma iR_i = \frac{\Omega_i + (k_p + k_{fm})\ m\ \Sigma R_i}{k_t\ \Sigma R_i + k_{fm} m} \tag{80}$$

$$\Sigma i^2 R_i = \frac{\Omega_i + k_p m(\ \Sigma R_i + 2\ \Sigma iR_i) + k_{fm} m\ \Sigma R_i}{k_t\ \Sigma R_i + k_{fm} m} \tag{81}$$

The above equations (75) to (79) simply have to be integrated to yield conversion and molecular weight, this is done using a Runge-Kutta-Gill numerical integration [16].

A comparison of experimental batch data with the calculated results is shown in Figure 27. Perfect mixing model predicts a higher polymerization rate and higher molecular number average chain length than those obtained experimentally. Following is an alalysis to correlate this difference.

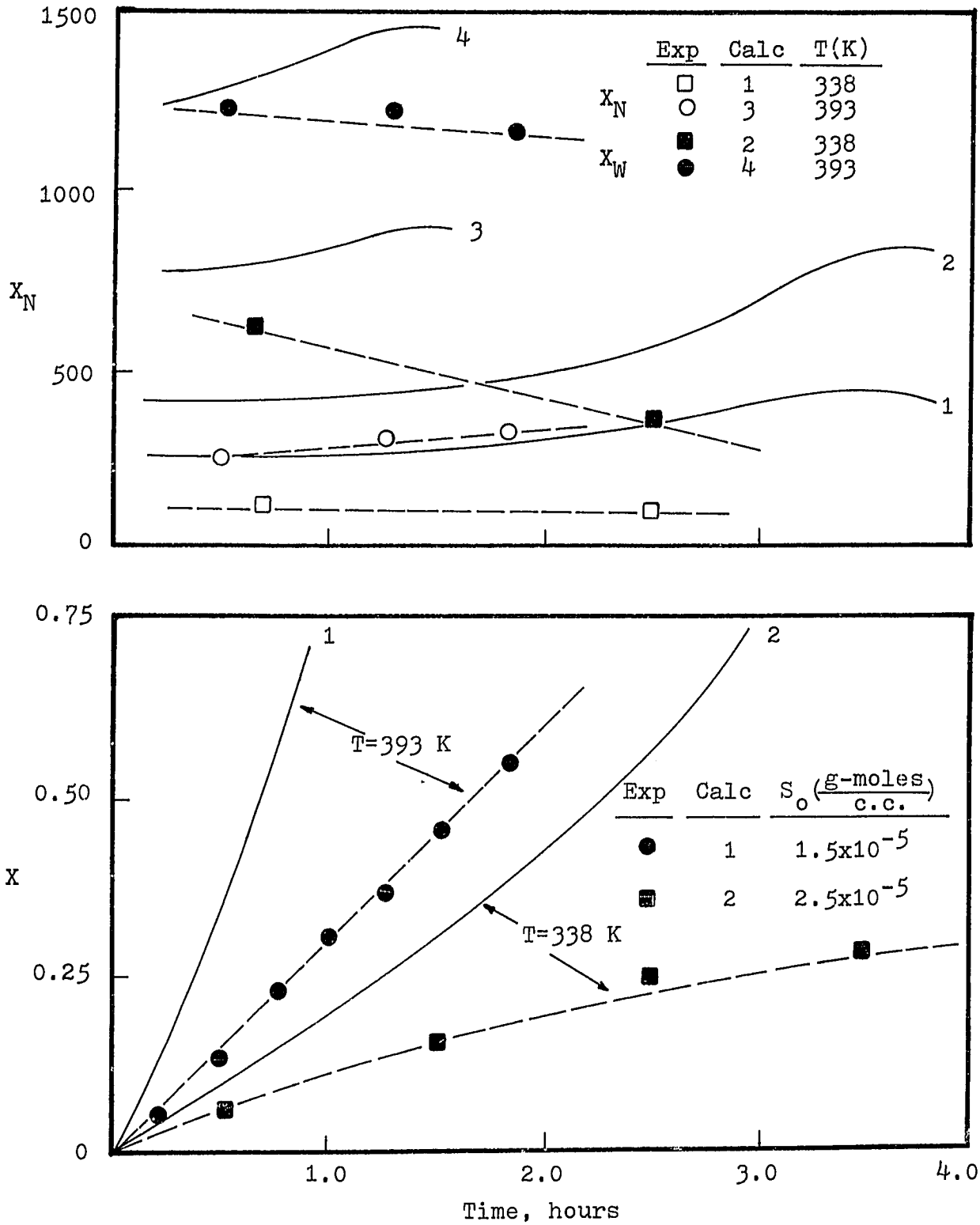

Figure 27. Experimental X and X_N vs. time and Prediction of Perfect Mixing Model

6-3. Model Development

The quantity I_{as} appearing in the preceeding discussion is the total rate of light absorption which is averaged over the path length of the light. If I_o is the flux of radiation incident upon the reactor, the light absorption by the sensitizer along the path length is,

$$I_{as} = I_o \epsilon_s S \, Exp[-(\epsilon_s S + \epsilon_m m)X] \qquad (82)$$

Averaging the absorbed light over the axial path length assumes that the effects of axial nonuniformities on the reaction rate are negligible, which in práctice, the above assumption is questionable. Figure 28 shows the calculated results based on equation (82) at different sensitizer concentration levels. With a highest sensitizer concentration (S_o= $1.0x10^{-4}$ g-moles/cc), light absorption by sensitizer only takes place at a very thin layer. As S_o decreases, I_{as} tends to be uniformly distributed throughout the reactor. Averaged absorption light assumption may produce significant errors especially at high sensitizer concentration calculations.

As an approximation of the light intensity distribution along the path length, the reactor is divided into a high dose rate region (I) and low dose rate region (II) as shown in Figure 29. If there is a flow pattern of circulation caused by the pumping action of impeller, the volumetric pumping rate

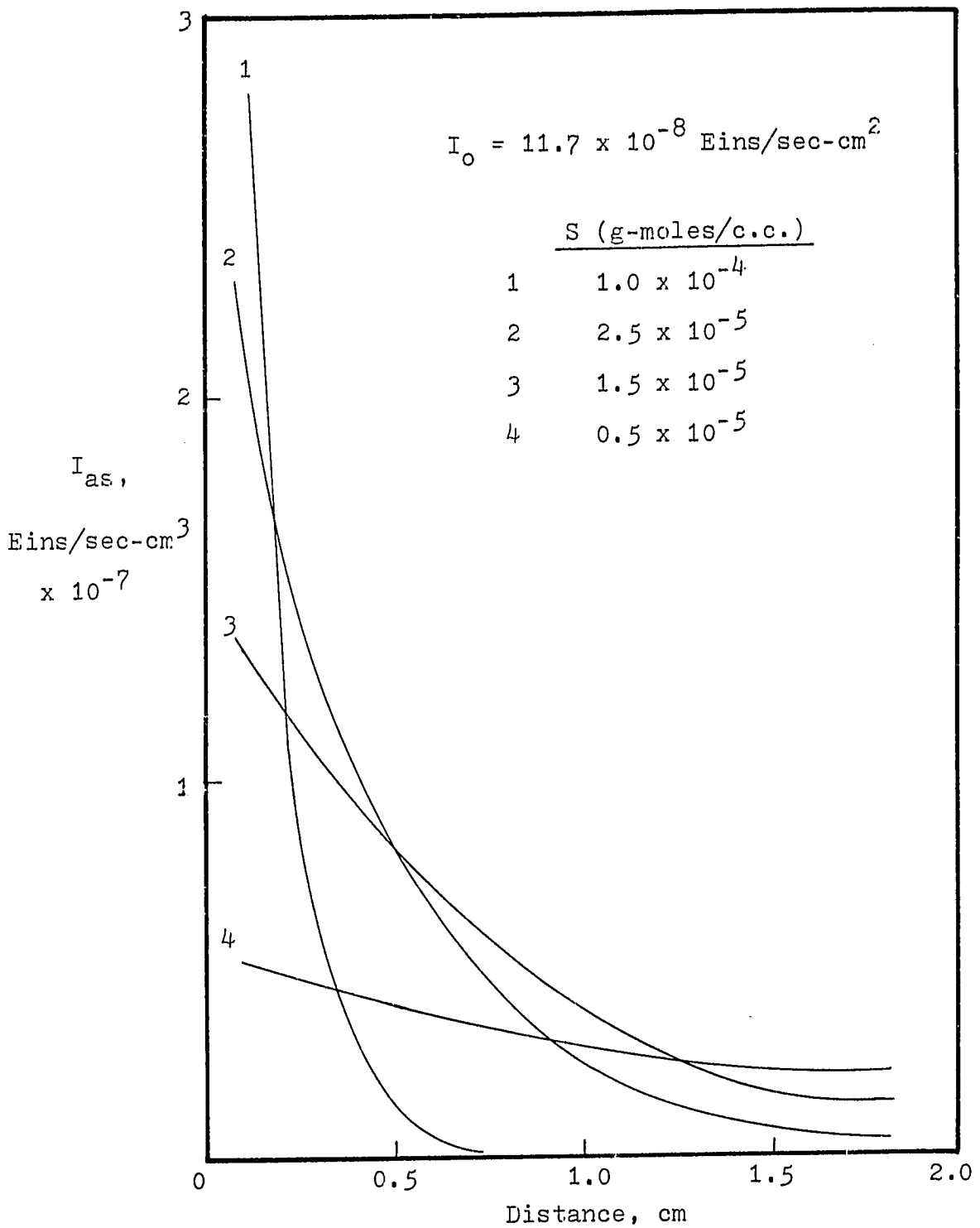

Figure 28. Absorbed Light Intensity Distribution in the Reactor

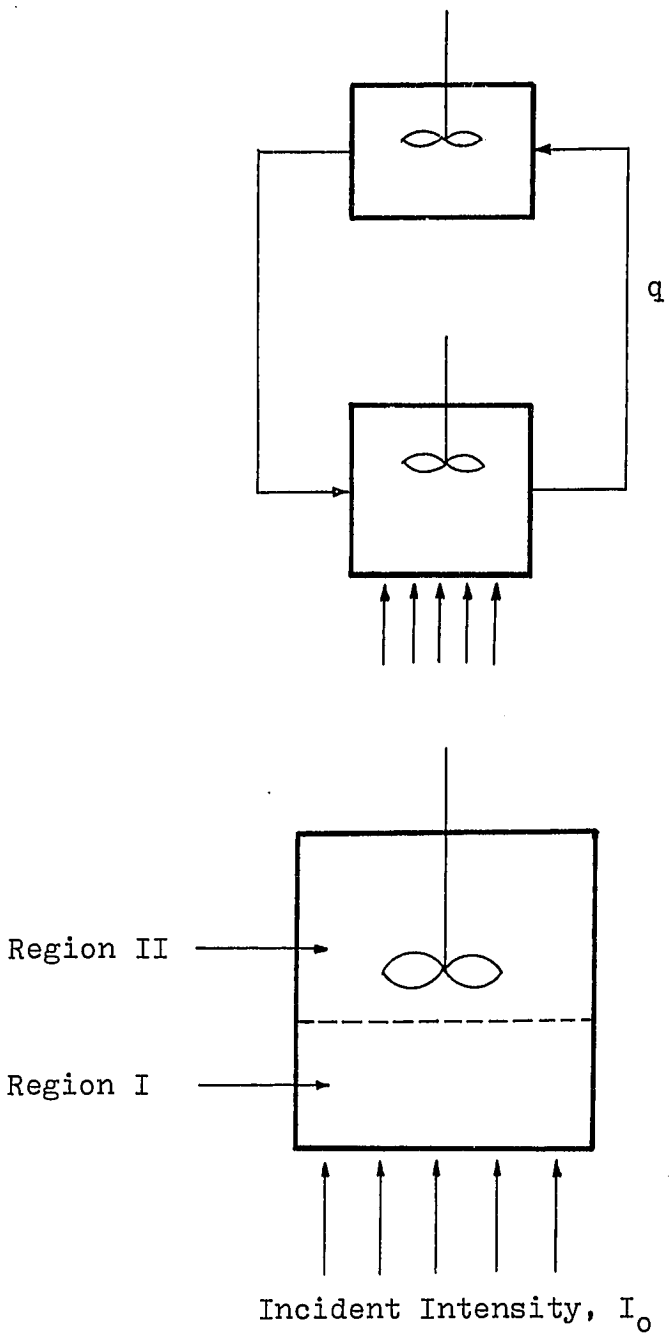

Figure 29. Schematic Diagram of a Flow Pattern Reactor

q is proportional to agitation speed [27]. Two region model can be described as follows:

for activated sensitizer S·, the material balance equations for both regions I and II are:

$$\frac{d\dot{S}_I}{dt} = \frac{(1+\epsilon X_{II})\dot{S}_{II} - (1+\epsilon X_I)\dot{S}_I}{\theta_I} + 2\,\phi_s{}^I a_{sI} - k_d \dot{S}_I m_I \qquad (83)$$

$$\frac{d\dot{S}_{II}}{dt} = \frac{(1+\epsilon X_I)\dot{S}_I - (1+\epsilon X_{II})\dot{S}_{II}}{\theta_{II}} + 2\,\phi_s{}^I a_{s_{II}} - k_d \dot{S}_{II} m_{II} \qquad (84)$$

If stationary state hypothesis is applied, and assume $k_d = k_p$, the above two equations become,

$$-(1+\epsilon X_{II})\dot{S}_{II} - (1+\epsilon X_I)\dot{S}_I + 2\,\theta_I\,\phi_s{}^I a_{s_I} - \theta_I k_p \dot{S}_I m_I = 0 \qquad (85)$$

$$-(1+\epsilon X_I)\dot{S}_I - (1+\epsilon X_{II})\dot{S}_{II} + 2\,\theta_{II}\,\phi_s{}^I a_{sII} - \theta_{II} k_p \dot{S}_{II} m_{II} = 0 \qquad (86)$$

After rearrangement of equations (85) and (86),

$$\dot{S}_I = \frac{(C_2/C_7 + C_5/C_3)}{(C_6/C_3 - C_1/C_7)} \qquad (87)$$

$$\dot{S}_{II} = \frac{(C_2/C_1 + C_5/C_6)}{(C_7/C_1 - C_3/C_6)} \qquad (88)$$

where

$$C_1 = (1+\epsilon X_I) + \theta_I k_p m_I$$

$$C_2 = 2\,\theta_I\,\phi_s{}^I a_{sI}$$

$$C_3 = (1+\epsilon X_{II}) + \theta_{II} k_p m_{II}$$

$$C_5 = 2\,\theta_{II}\,\phi s^{I}_{asII}$$

$$C_6 = 1 + \epsilon X_I$$

and $$C_7 = 1 + \epsilon X_{II}$$

The total initiation rate for each region can be expressed as,

$$\Omega_{iI} = 2\,\bar{k}_i m_I^3 + k_p \dot{S}_I m_I \qquad (89)$$

$$\Omega_{iII} = 2\,\bar{k}_i m_{II}^2 + k_p \dot{S}_{II} m_{II} \qquad (90)$$

The material balance of total active polymer concentration for each region is,

$$\frac{d\,\Sigma R_{iI}}{dt} = \frac{(1+\epsilon X_{II})\,\Sigma R_{iII} - (1+\epsilon X_I)\,\Sigma R_{iI}}{\theta_I} + \Omega_{iI} - k_{tI}\,\Sigma R_{iI}^2 \qquad (91)$$

$$\frac{d\,\Sigma R_{iII}}{dt} = \frac{(1+\epsilon X_I)\,\Sigma R_{iI} - (1+\epsilon X_{II})\,\Sigma R_{iII}}{\theta_{II}} + \Omega_{iII} - k_{tII}\,\Sigma R_{iII}^2 \qquad (92)$$

where

$$k_{tI} = k_{to}/\mathrm{Exp}(A_1 X_1 + A_2 X_1^2 + A_3 X_1^3) \qquad (93)$$

$$k_{tII} = k_{to}/\mathrm{Exp}(A_1 X_2 + A_2 X_2^2 + A_3 X_2^3) \qquad (94)$$

Again, by applying stationary state hypothesis, equations (91) and (92) become,

$$\theta_I k_{tI}\,\Sigma R_{iI}^2 + C_6\,\Sigma R_{iI} - (\theta_I\,\Omega_{iI} + C_7\,\Sigma R_{iII}) = 0 \qquad (95)$$

and

$$\theta_{II} k_{tII} \Sigma R_{iII}^2 + C_7 \Sigma R_{iII} - (\theta_{II} \Omega_{iII} + C_6 \Sigma R_{iI}) = 0 \qquad (96)$$

or,

$$\Sigma R_{iI} = \frac{-C_6 + \sqrt{C_6^2 + 4\theta_I k_{tI} (\theta_I \Omega_{iI} + C_7 \Sigma R_{iII})}}{2\theta_I k_{tI}} \qquad (97)$$

$$\Sigma R_{iII} = \frac{-C_7 + \sqrt{C_6^2 + 4\theta_{II} k_{tII} (\theta_{II} \Omega_{iII} + C_6 \Sigma R_{iI})}}{2\theta_{II} k_{tII}} \qquad (98)$$

The first and second moments of active polymers are,

$$\Sigma iR_{iI} = \frac{\frac{C_7}{\theta_I} \Sigma iR_{iII} + k_p m_I \Sigma R_{iI} + \Omega_{iI}}{\frac{C_6}{\theta_I} + k_{tI} \Sigma R_{iI}} \qquad (99)$$

$$\Sigma iR_{iII} = \frac{\frac{C_6}{\theta_{II}} \Sigma iR_{iI} + k_p m_{II} \Sigma R_{iII} + \Omega_{iII}}{\frac{C_7}{\theta_{II}} + k_{tII} \Sigma R_{iII}} \qquad (100)$$

$$\Sigma i^2 R_{iI} = \frac{\frac{C_7}{\theta_I} \Sigma i^2 R_{iII} + 2 k_p m_I \Sigma iR_{iI}}{\frac{C_6}{\theta_I} + k_{tI} \Sigma R_{iI} + k_{fm} m_I} \qquad (101)$$

and

$$\Sigma i^2 R_{iII} = \frac{\frac{C_6}{\theta_{II}} \Sigma i^2 R_{iI} + 2 k_p m_{II} \Sigma iR_{iII}}{\frac{C_7}{\theta_{II}} + k_{tII} \Sigma R_{iII} + k_{fm} m_{II}} \qquad (102)$$

for sensitizer,

$$\frac{dS_I}{dt} = -\phi_s{}^I a_{sI} + \frac{(1+\epsilon X_{II})S_{II} - (1+\epsilon X_I)S_I}{\theta_I} \qquad (103)$$

$$\frac{dS_{II}}{dt} = -\phi_s{}^I a_{sII} + \frac{(1+\epsilon X_I)S_I - (1+\epsilon X_{II})S_{II}}{\theta_{II}}$$

$$- \frac{S_{II}}{V_{II}} \frac{dV_{II}}{dt} \qquad (104)$$

for monomer,

$$\frac{dm_I}{dt} = k_p m_I \Sigma R_{iI} + \frac{(1+\epsilon X_{II})m_{II} - (1+\epsilon X_I)m_I}{\theta_I} \qquad (105)$$

$$\frac{dm_{II}}{dt} = k_p m_{II} \Sigma R_{iII} + \frac{(1+\epsilon X_I)m_I - (1+\epsilon X_{II})m_{II}}{\theta_{II}}$$

$$- \frac{m_{II}}{V_{II}} \frac{dV_{II}}{dt} \qquad (106)$$

For zero, first and second moments of the dead polymers,

$$\frac{d\,\Sigma P_{iI}}{dt} = k_{fmI} m_I \Sigma R_{iI} + \frac{1}{2} k_{tI} \Sigma R_{iI}^2 + \frac{(1+\epsilon X_{II})\,\Sigma P_{iII} - (1+\epsilon X_I)\,\Sigma P_{iI}}{\theta_I} \qquad (107)$$

$$\frac{d\,\Sigma P_{iII}}{dt} = k_{fmII} m_{II} \Sigma R_{iII} + \frac{(1+\epsilon X_I)\,\Sigma P_{iI} - (1+\epsilon X_{II})\,\Sigma P_{iII}}{\theta_{II}}$$

$$+ \frac{1}{2} k_{tII} \Sigma R_{iII}^2 - \frac{\Sigma P_{iII}}{V_{II}} \frac{dV_{II}}{dt} \qquad (108)$$

$$\frac{d\,\Sigma iP_{iI}}{dt} = k_{tI}\,\Sigma R_{iI}\,\Sigma iR_{iI} + k_{fmI}\,m_I\,\Sigma iR_{iI} + \frac{(1+\epsilon X_{II})\,\Sigma iP_{iII} - (1+\epsilon X_I)\,\Sigma iP_{iI}}{\theta_I} \qquad (109)$$

$$\frac{d\,\Sigma iP_{iII}}{dt} = k_{tII}\,\Sigma R_{iII}\,\Sigma iR_{iII} + k_{fmII}\,\Sigma iR_{iII} - \frac{\Sigma iP_{iII}}{V_{II}}\frac{dV_{II}}{dt} + \frac{(1+\epsilon X_I)\,\Sigma iP_{iI} - (1+\epsilon X_{II})\,\Sigma iP_{iII}}{\theta_{II}} \qquad (110)$$

$$\frac{d\,\Sigma i^2P_{iI}}{dt} = k_{tI}\,\Sigma R_{iI}\,\Sigma i^2R_{iI} + k_{tI}\,\Sigma iR_{iI}^2 + k_{fmI}m_I\,\Sigma i^2R_{iI} + \frac{(1+\epsilon X_{II})\,\Sigma i^2P_{iII} - (1+\epsilon X_I)\,\Sigma i^2P_{iI}}{\theta_I} \qquad (111)$$

and

$$\frac{d\,\Sigma i^2P_{iII}}{dt} = k_{tII}\,\Sigma R_{iII}\,\Sigma i^2R_{iII} + k_{tII}\,\Sigma iR_{iII}^2 - \frac{\Sigma i^2P_{iII}}{V_{II}}\frac{dV_{II}}{dt} + k_{fmII}m_{II}\,\Sigma i^2R_{iII} + \frac{(1+\epsilon X_I)\,\Sigma i^2P_{iI} - (1+\epsilon X_{II})\,\Sigma i^2P_{iII}}{\theta_{II}} \qquad (112)$$

Notice from the above equations ((103) to 112)), it is assumed that the volume of region I is constant, volume change due to polymerization reaction will be replenished by region II, this gives,

$$V_{II} = V_{oII}(1+\epsilon X_{II}) + V_{oI}\,\epsilon X_I \qquad (113)$$

where V_{oI} and V_{oII} are the volumes for regions I and II at initial conditions. To differentiate V_{II} with respect to time, this gives,

$$\frac{dV_{II}}{dt} = \frac{-\epsilon}{m_o + \epsilon m_{II}} \left(V_{II} \frac{dm_{II}}{dt} + V_I \frac{dm_I}{dt}\right) \qquad (114)$$

6-4. Data Analysis

The experimental batch results were analyzed by the proposed two region model. There are two unknown parameters, the circulating flow rate q, and the volume ratio of light and dark regions. some study indicates that the volumetric pumping rate is proportional to the agitation speed and implller diameter [38]. The experimental observations from this study show that both monomer and polymer concentrations in both regions are likely the same (Figure 10). Since q value can not be measured experimentally, the following steps were used to calculate the volumetric flow rate:

First, to choose an arbitrary volume ratio and assume a q value. Upon numerical integration of equations (103) to (112), time independent values of conversion, number and weight average chain lengths can be obtained. As shown in Figure 30, at a flow rate equals to 5.0×10^{-2} cc/sec, the calculated conversion is about 10 to 15% different from these two regions. By adjusting q equals to 1.0 cc/sec, the difference of conversion can be made as small as less than 0.3%.

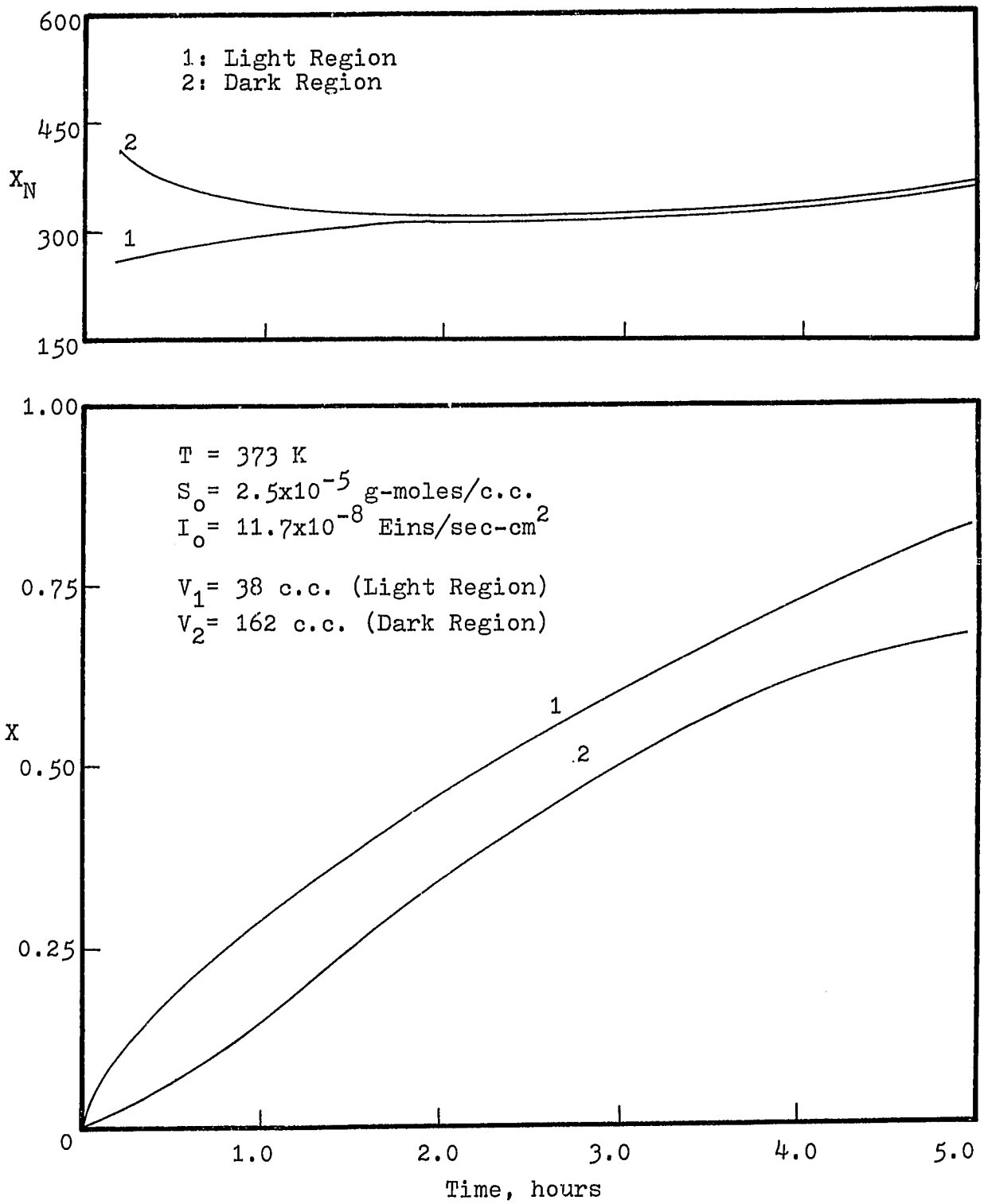

Figure 30. Effect of Volumetric Pumping Rate on X and X_N in Regions I and II

The second step involves fitting the experimental conversion data by varying volume ratio. This was done according to the light intensity profile along the reactor path length as shown in Figure 28. For a high sensitizer concentration, the light intensity distribution is sharp and light and dark regions are obvious. For low concentration, the profile is somewhat flattened and is very difficult to determine individual regions. In this experiment, the agitator is located at the center of the reactor which is about 1.5 cm above the optical glass window, region below agitator was assumed to be light illuminated. Figure 31 shows the results calculated at various volume ratios. By comparing with the experimental data, this ratio can then be determined.

During the calculations, it was found that using equation (3) can not accurately predicts experimental conversion at those low sensitizer concentration runs. This is due to the exponential expression of the equation is insensitive to sensitizer consumption rate. The following light intensity equation shows a better agreement with experimental results:

$$I_{as} = \frac{I_o}{L}\left[1-\text{Exp}\ (-\epsilon_s L)\right] \qquad (115)$$

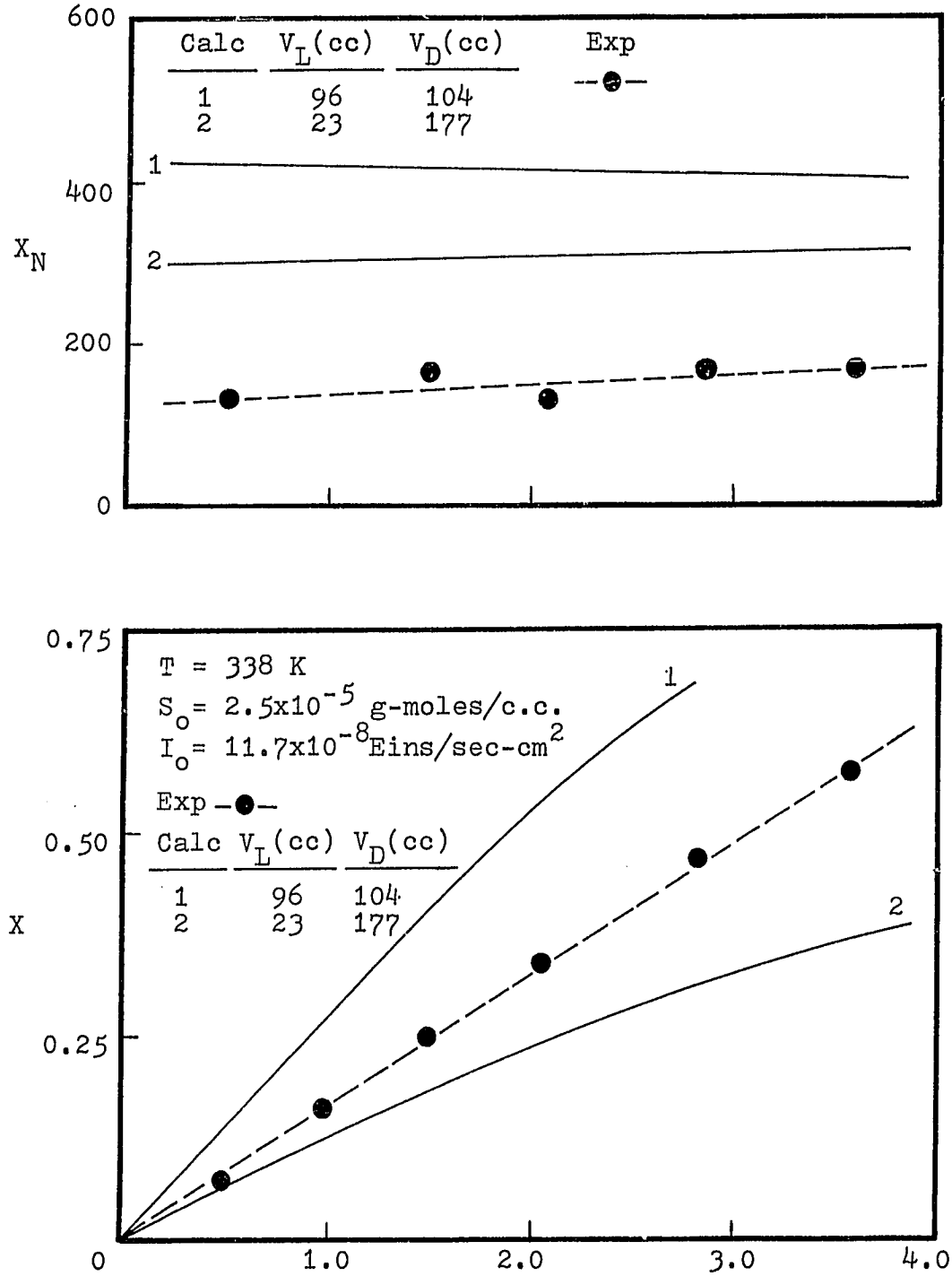

Figure 31. Effect of Volume Ratio Between Regions I and II on X and X_N

CHAPTER 7

DISCUSSION OF THE EXPERIMENTAL RESULTS

The experimental results from this study are presented and discussed in the following sections:

7-1. Exact Multiplicity and Uniqueness

Figure 32 shows the experimental results in an isothermal batch reactor at 338 K. Two levels of solvent (benzene) in the feed were considered: Run 1: 20 wt% of solvent; run 2: 0 % of solvent. For run 1, the gel effects were essentially insignificant. As the theory in Chapter 2 predicts (Figure 2), the conversion increases monotonically with time, while the rate of conversion decreases with increase in X and approaches zero as $X \rightarrow 1$. On the other hand, the gel effects are very pronounced in run 2. When $X > 0.3$, X increases very rapidly. This is due to a decrease in the rate at which the polymer molecules diffuse through the viscous medium, thus lowering the ability of two long chain radicals to come together and terminate. The decrease in termination rate leads to an increase in dX/dt. At very high conversion (80-90 %), dX/dt suddenly drops and falls to a very low value. Figure 33 shows the experimental results for an adiabatic batch polymerization. Two runs were made respectively with 13 wt% (run 3) and 0 % (run 4) of benzene in the feed. For run 4, dX/dt increases drastically from 0.12 1/hr at about 40% conversion to a peak (0.38 1/hr). Beyond

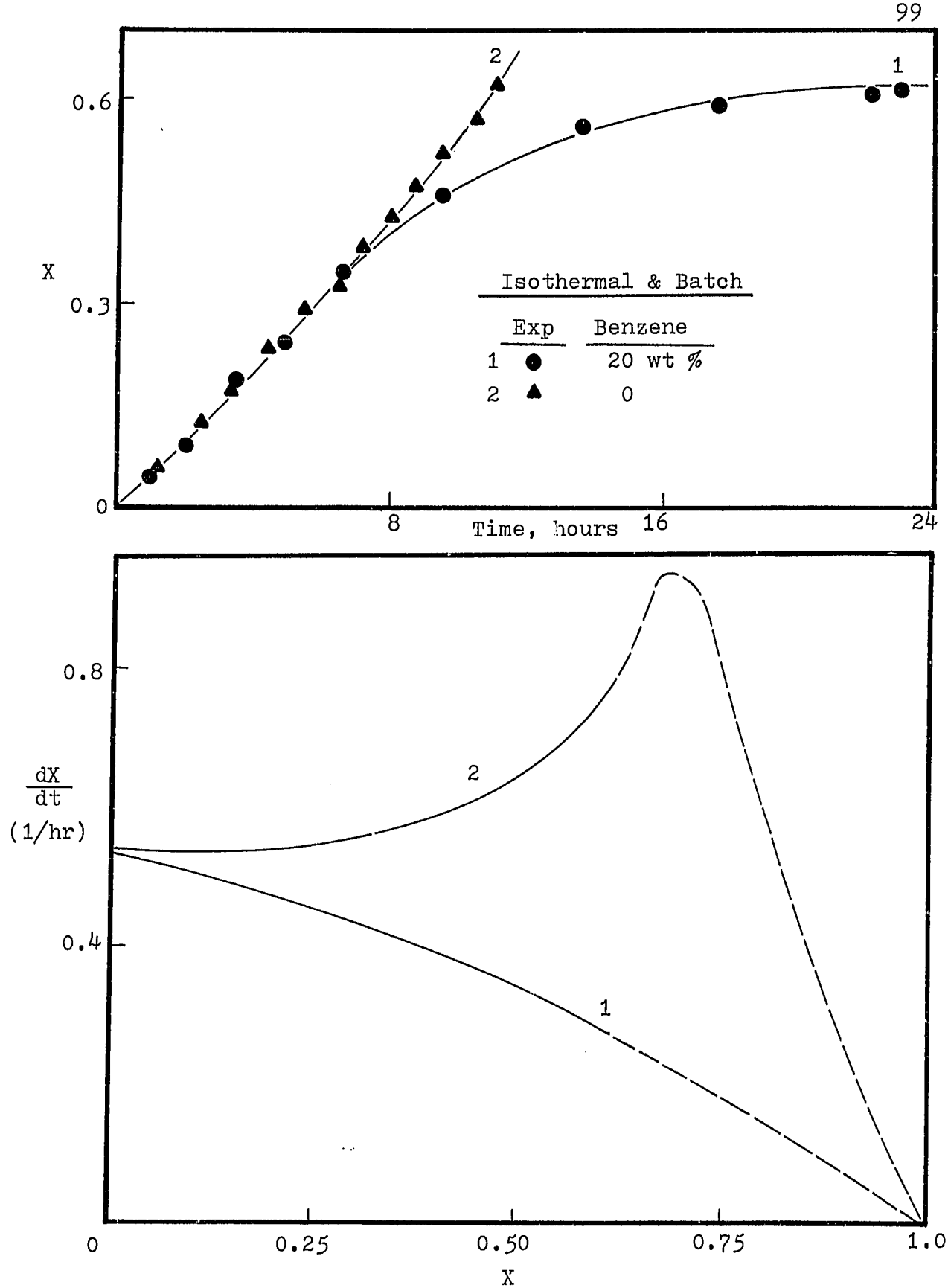

Figure 32. Experimental Results from an Isothermal Batch Reactor

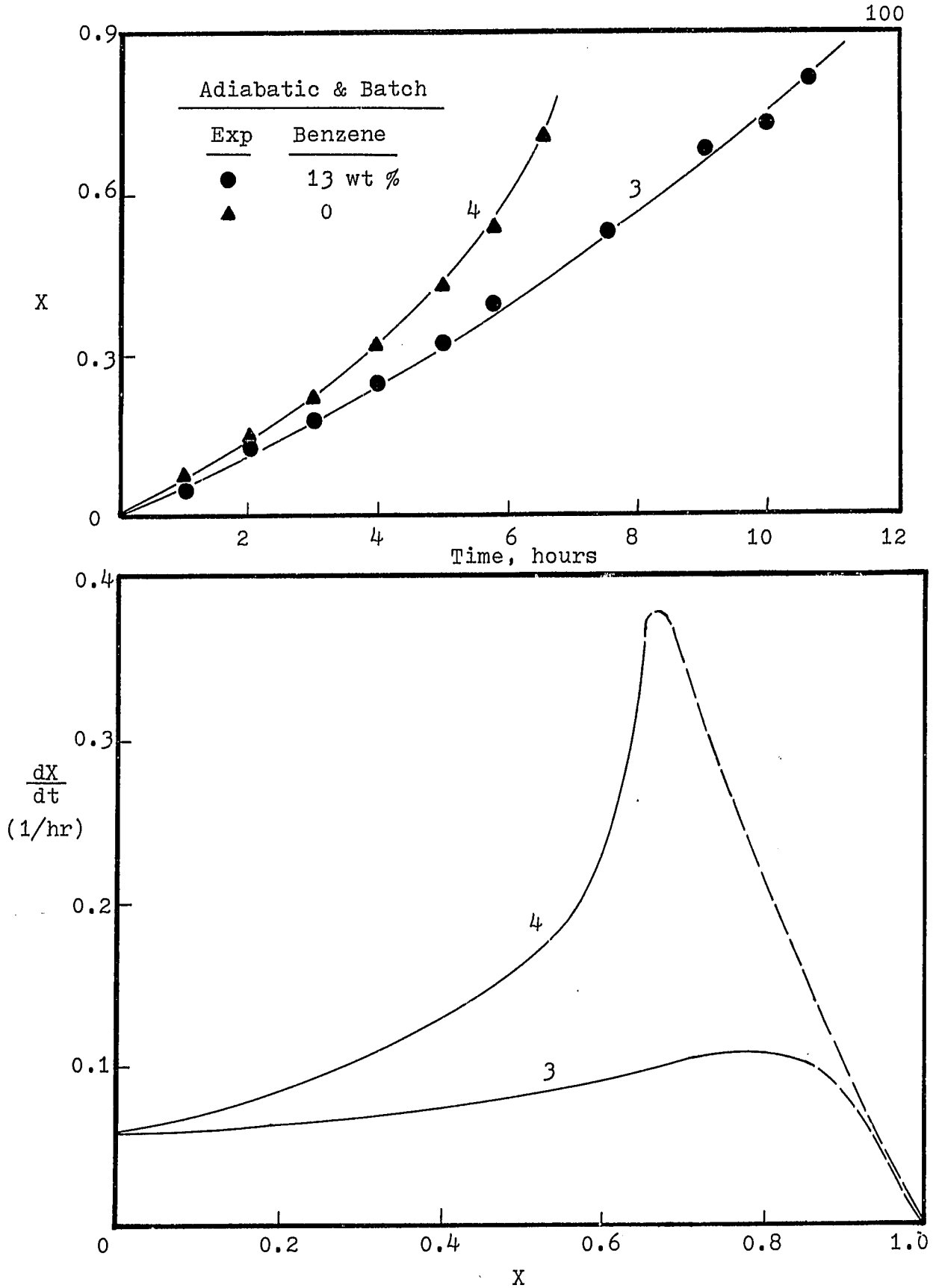

Figure 33. Experimental Results from an Adiabatic Batch Reactor

the maximum rate, dX/dt falls rapidly. Note that for the above four cases, the initial sensitizer concentration was high (S_o= $1.0x10^{-4}$g-moles/cc) and the rate of initiation was essentially independent of time. Thus the rate of conversion (dX/dt vs. X) obtained via batch operation may be adapted for the corresponding CSTR operation, although there are some differences on molecular weight distributions between batch and CSTR operations. It is apparent that the rate curves for runs 2 and 4 meet the necessary conditions for multiplicity. By comparing these two curves, one may see that $\Delta\theta$ ($=\theta_2-\theta_1$) for the adiabatic process is much greater than that for an isothermal CSTR.

Figures 34 and 35 show comparison between continuous and batch systems on fraction conversion and number average chain length. For both systems, the reaction time or holding time (to reach a given conversion level) for a continuous reactor is much less than that for the equivalent batch reactor, so that the reactor size for the continuous process can be made smaller for the same production rate. In addition, for a given holding time, conversion in the metastable region is much greater than that in the lower region. With respect to X_N, in the metastable region, the continuous reactor is clearly superior to the equivalent batch reactor. In the low stable region, the continuous and batch systems give nearly identical results.

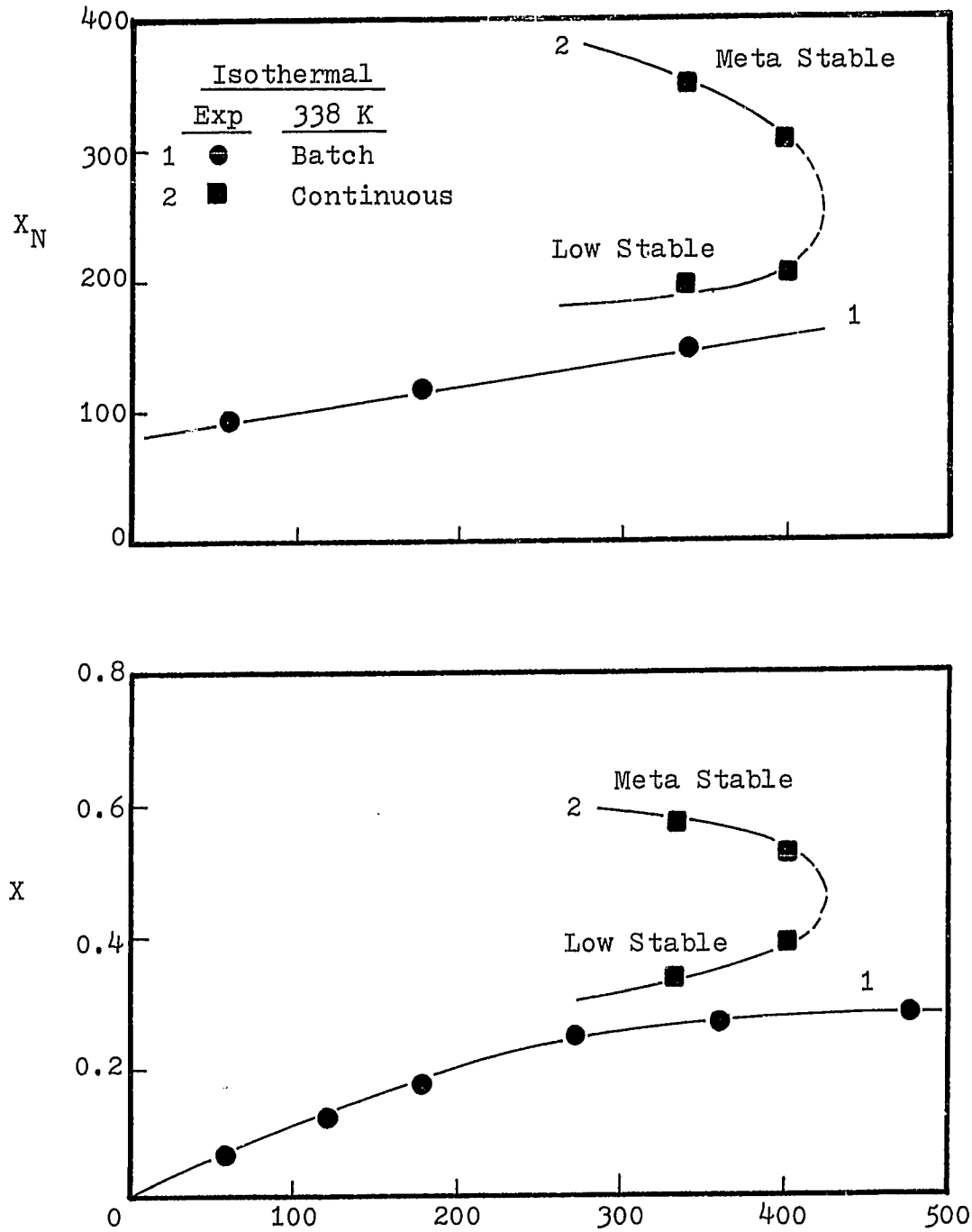

Figure 34. Comparison of X and X_N Between BR and CSTR Operations - Isothermal Conditions

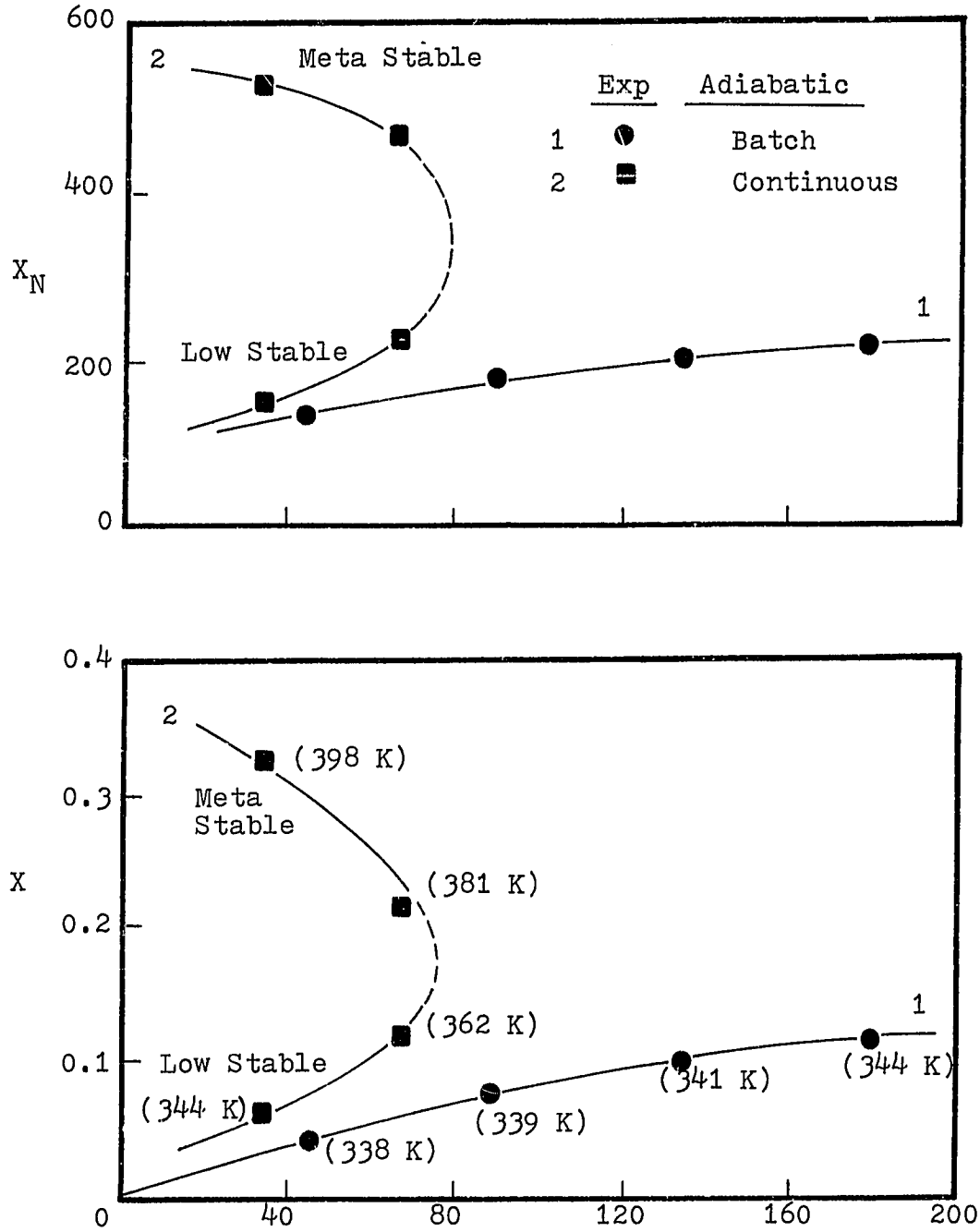

Figure 35. Comparison of X and X_N Between BR and CSTR Operations - Adiabatic Conditions

Figure 36 shows the experimental results for isothermal polymerization at differene temperature and sensitizer concentration levels. The influence of increasing the reactor temperature from 338 K to 358 K is to shift the fractional conversion (or number average chain length) curve towards to the lower holding time to obtain the same conversion (or chain length). Also for the reactor temperature, the possibility of existence of multiple steady states is lower. To increase sensitizer concentration from $1.5x10^{-5}$ to $2.5x10^{-5}$ g-moles/cc also shifts the fractional conversion to the lower residence time, while the corresponding number average chain length is lower as sensitizer concentration increases. This is due to a higher initiation rate at higher sensitizer concentration (at same temperature) results in lower molecular weight product. For higher sensitizer concentration used, the possibility of existence of multiple steady states is lower too. This is because of that as the MCR increases (Figure 11), multiple steady states region becomes narrower.

As an overall comparisons of adiabatic and isothermal CSTR with batch operation, the experimental results are shown in Figures 37 and 38. For the region of multiple steady states, the reactor holding time for an adiabatic operation is much less than that of an isothermal CSTR. This shows styrene polymerization is strongly temperature dependent and multiple steady states are obtainable evevn at low residence time. For

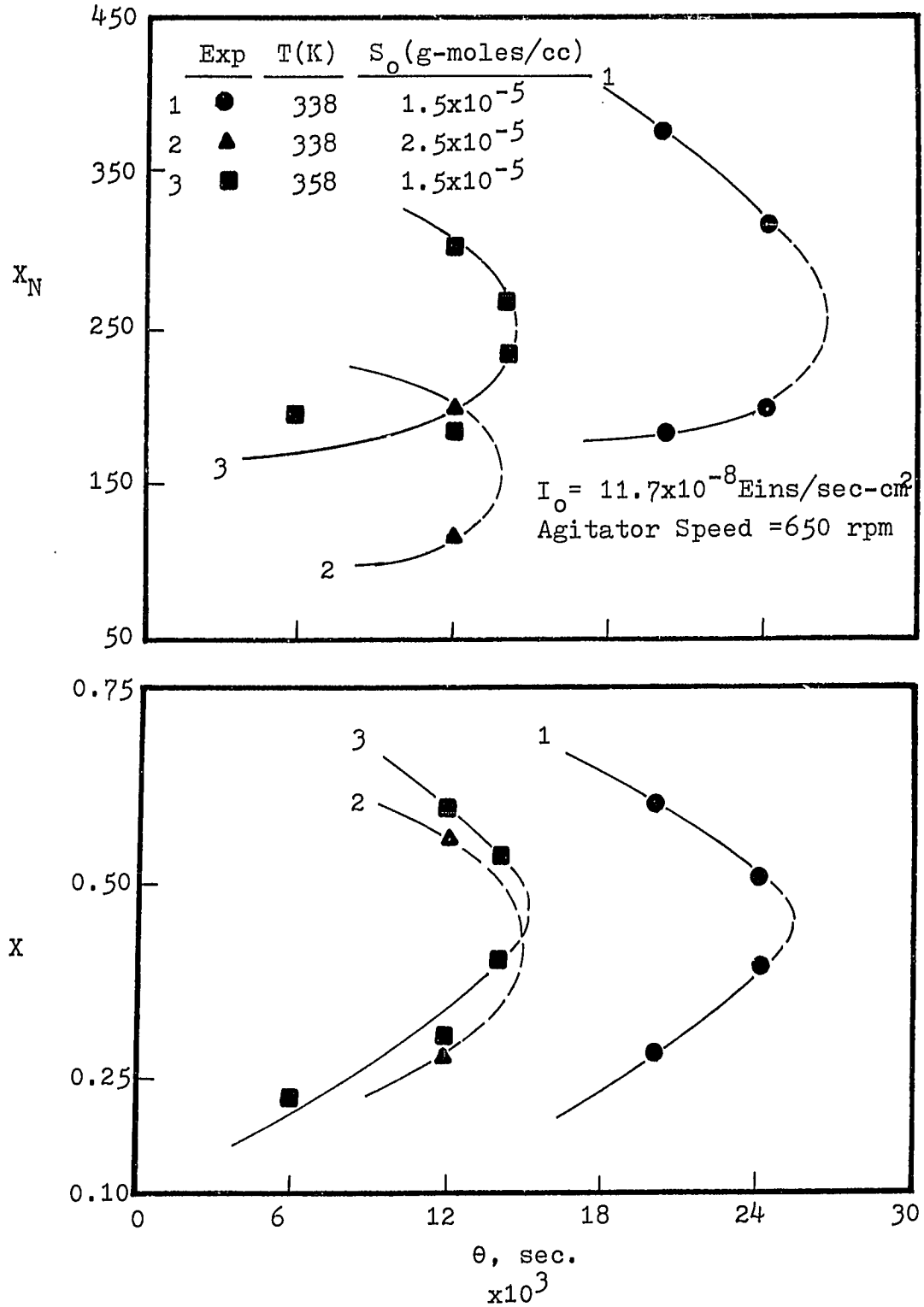

Figure 36. Effects of T and S_o on Multiple Steady States in an Isothermal CSTR

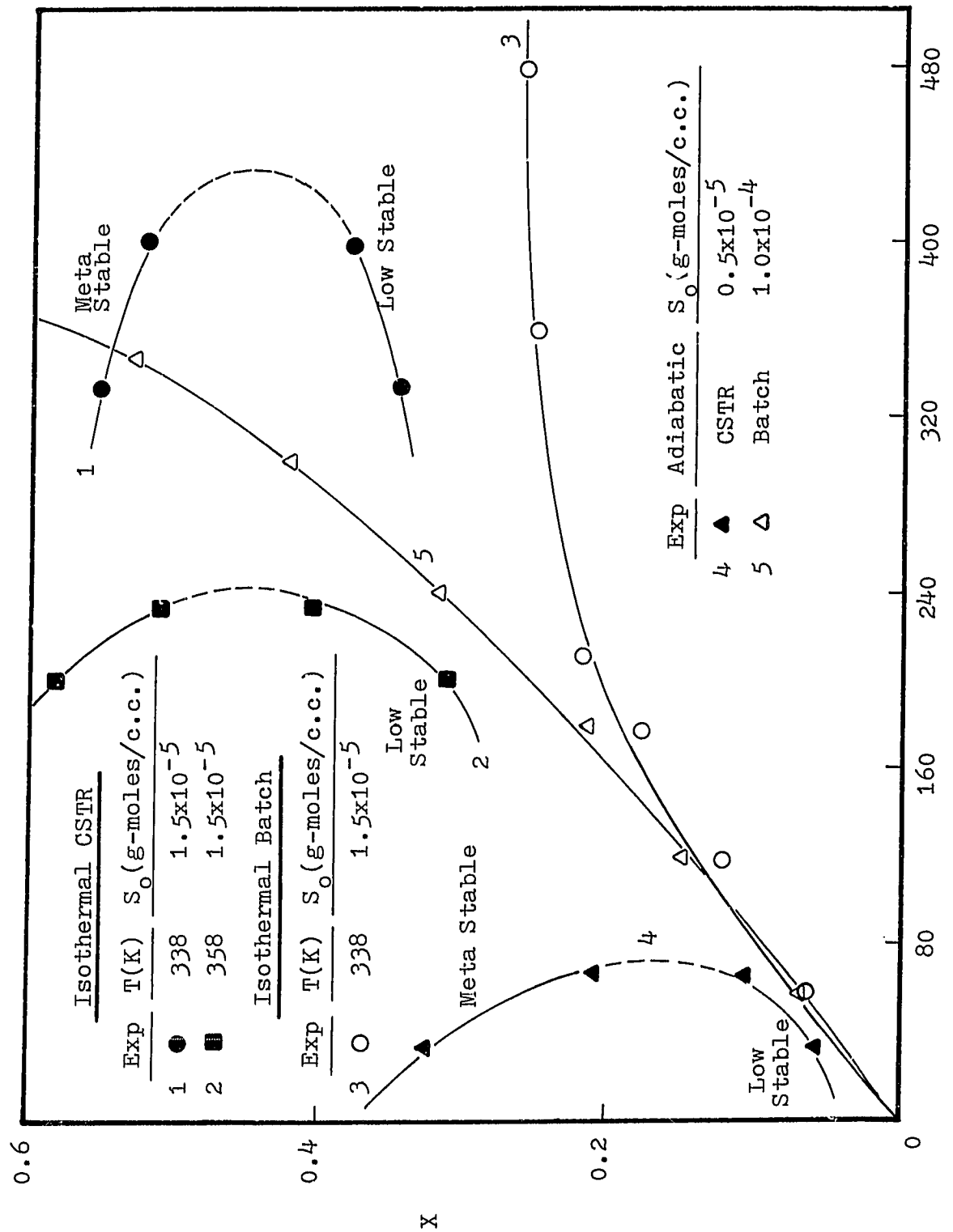

Figure 37. Comparison of X between BR and CSTR Operations

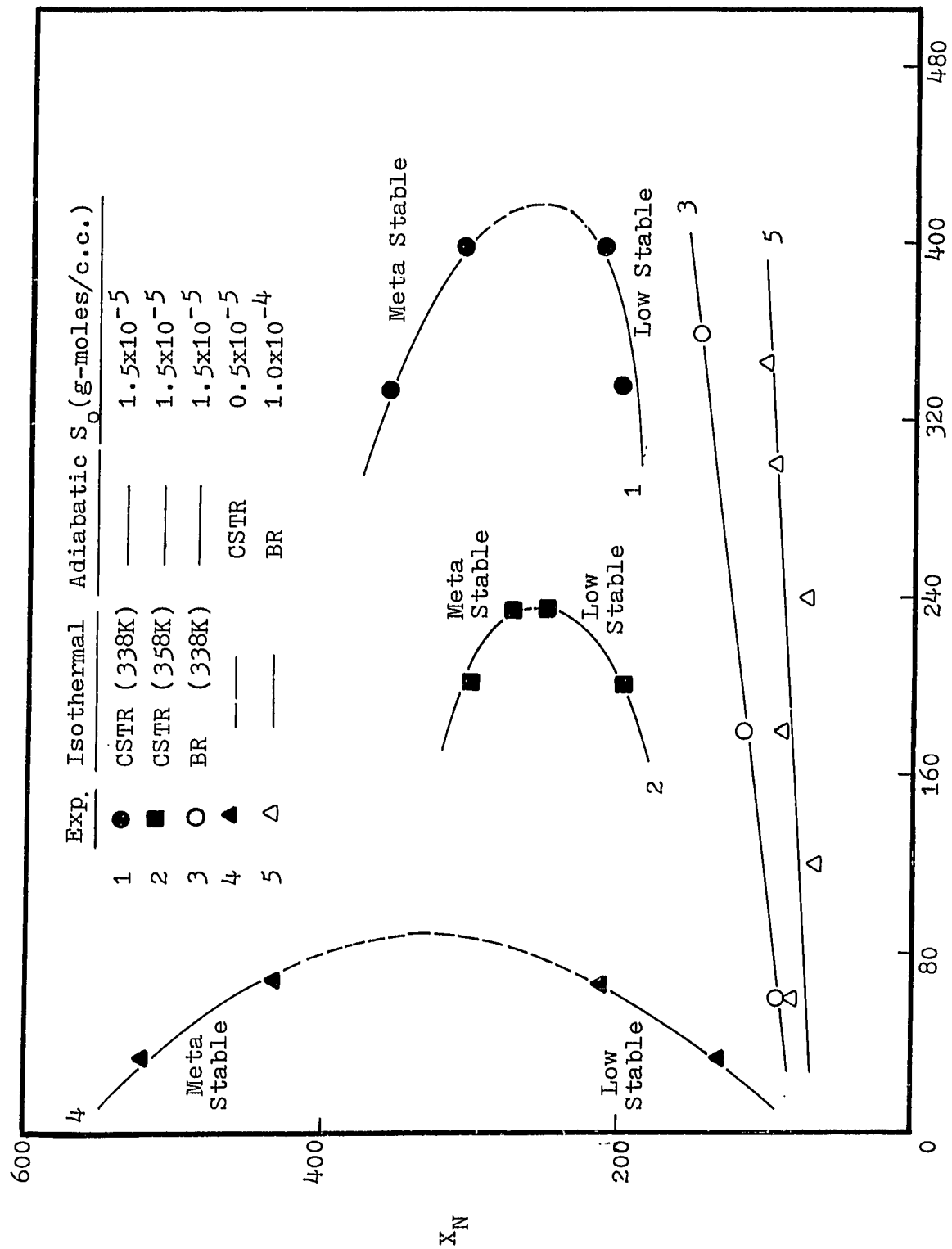

Figure 38. Comparison of X_N between BR and CSTR Operations

lower steady states, the fractional conversion is very low for adiabatic operation, while for number average chain length is about the same as isothermal CSTR. Conversion at metastable state, isothermal CSTR also shows higher yields than that of adiabatic operation. As to the number average chain lengths, adiabatic CSTR always shows better results (higher X_N values). Operation of an isothermal batch reactor shows very low degree of polymerization and number average chain length. An adiabatic batch operation can achieve to the same level of conversion at a given reaction time as that of isothermal operations (Figure 37), but the molecular weight chain lengths are lower as shown in Figure 38.

7-2. Characteristics of Batch Reactions

Figure 39 shows temperature effect on photopolymerization. At 337 K, a linear relationship of conversion versus time is observed. This is to say that the reaction rate is constant throughout the reaction time. As the monomer concentration decreases during polymerization, the reaction rate decreases. But at the same time, gel effect becomes pronounced as conversion increases which enhances polymerization rate and the observed rate is constant. For the two runs carried out at 338 K and 358 K, at the initial stage, the observed polymerization rates are constant (constant initiation rate). After this stage, reaction rate decreases as sensitizer in the mixture bas been consumed. Figure 40 shows the measured number and weight

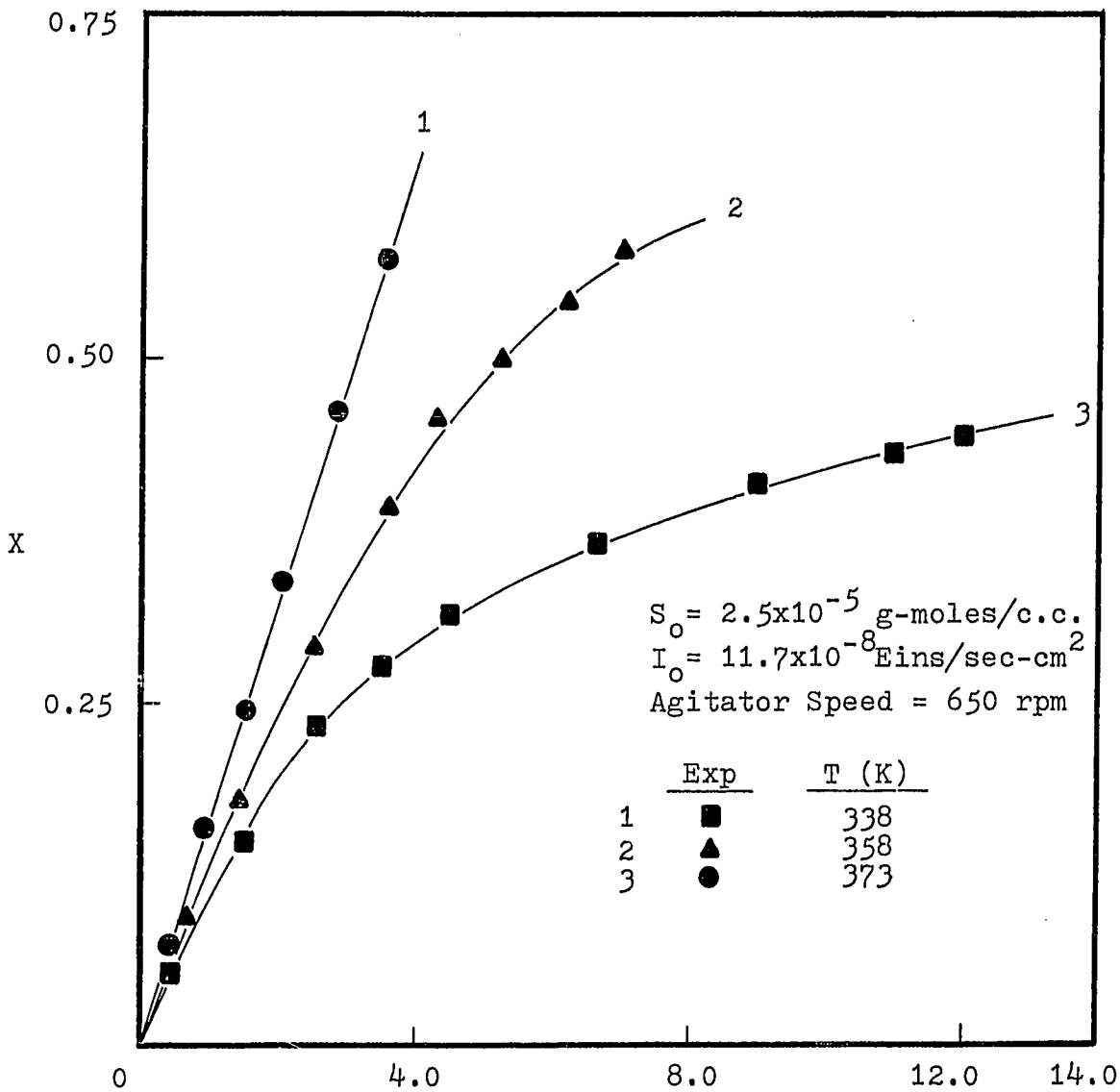

Figure 39. Effect of T on Photopolymerization in a Batch Reactor

average chain lengths for the above three runs. Note that the number average chain lengths obtained at low temperature runs (338 K and 358 K) are slightly higher than those at 373 K. At higher temperature, monomer decomposes quite rapidly which forms a large number of low molecular weight polymer molecules. number average molecular weight decreases rapidly because of it is sensitive to the number of low molecular weight molecules. Weight average molecular weight is virtually unchanged because it is sensitive to the amount of high molecular weight polymer.

The effect of light intensity on photopolymerization is shown in Figure 41. Reduction of optical paths (this can be done either by increasing the number of neutral density filters (run 3), or reducing the illuminated volume (run 2)), will reduce the polymerization rate. However, variation of light intensities do not effect number and weight average chain lengths appreciably which can be seen in Figure 42. A very interesting result was observed by varying sensitiser concentrations as shown in Figure 43. For the two low S_o runs 1 and 2 (S_o= 1.5×10^{-5} and 2.5×10^{-5}g-moles/cc, respectively.), the observed polymerization rates at the initial stage are higher than that of the high sensitizer concentration run 3 (S_o= 1.0×10^{4}g-moles/cc). Higher sensitizer concentration polymerization will be restricted at smaller illuminated reactor volume (Figure 28) and the overall reaction will be reduced. Figure 44 shows the experimental number and weight average

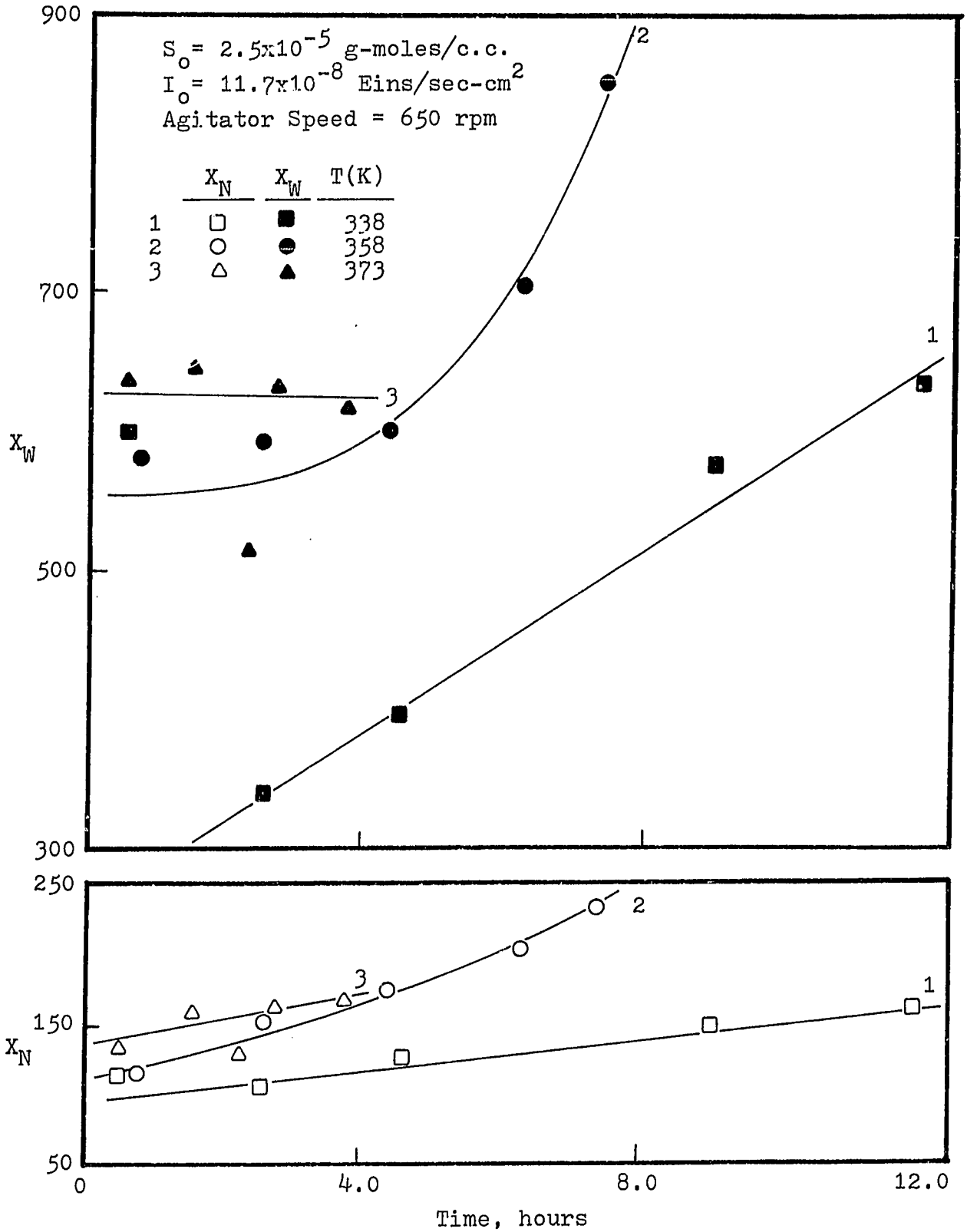

Figure 40. Effect of T on X_N and X_W for Photopolymerization in a Batch Reactor

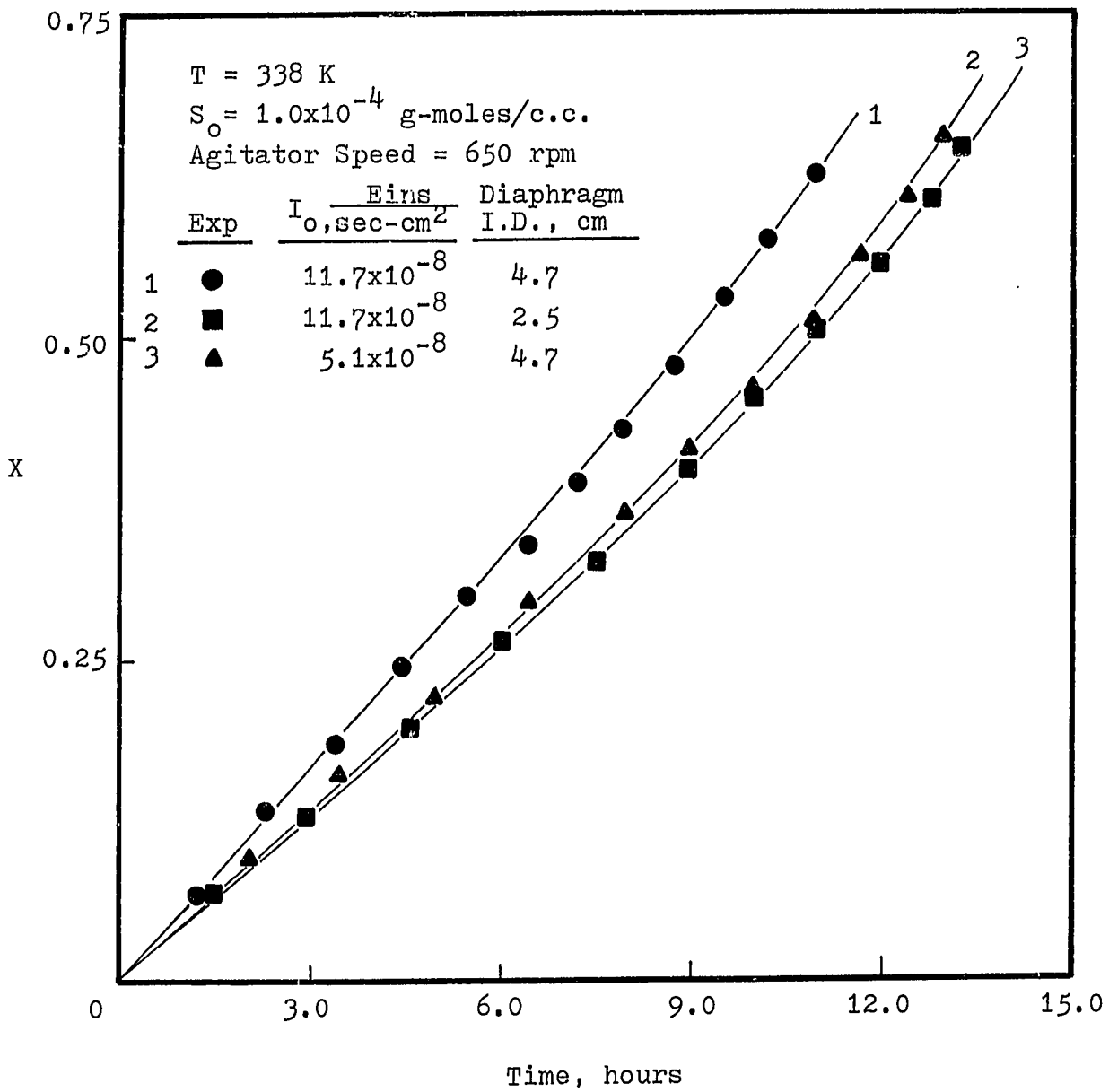

Figure 41. Effect of I_o on X for Photopolymerization in a Batch Reactor

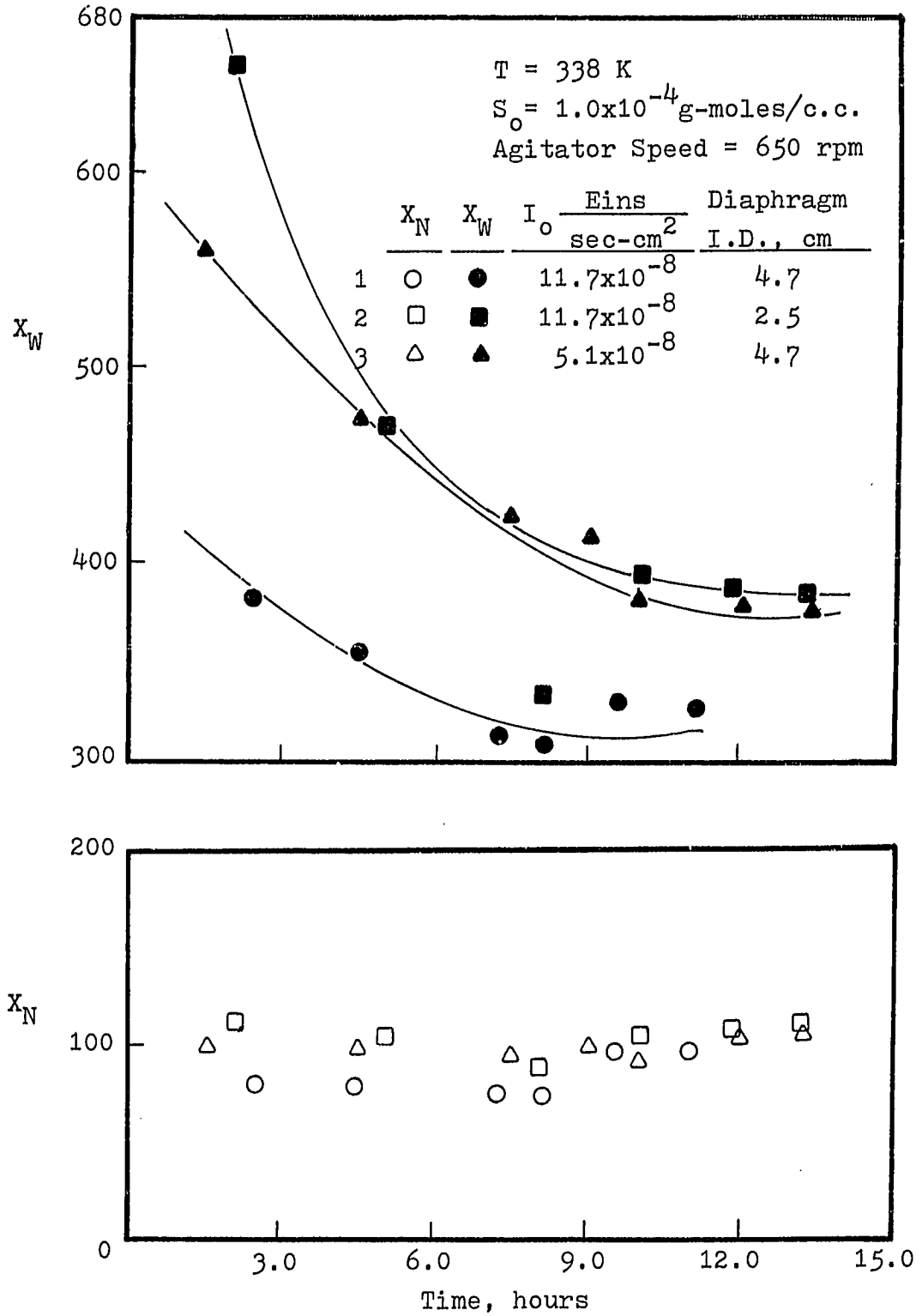

Figure 42. Effect of I_o on X_N and X_W for Photopolymerization in a Batch Reactor

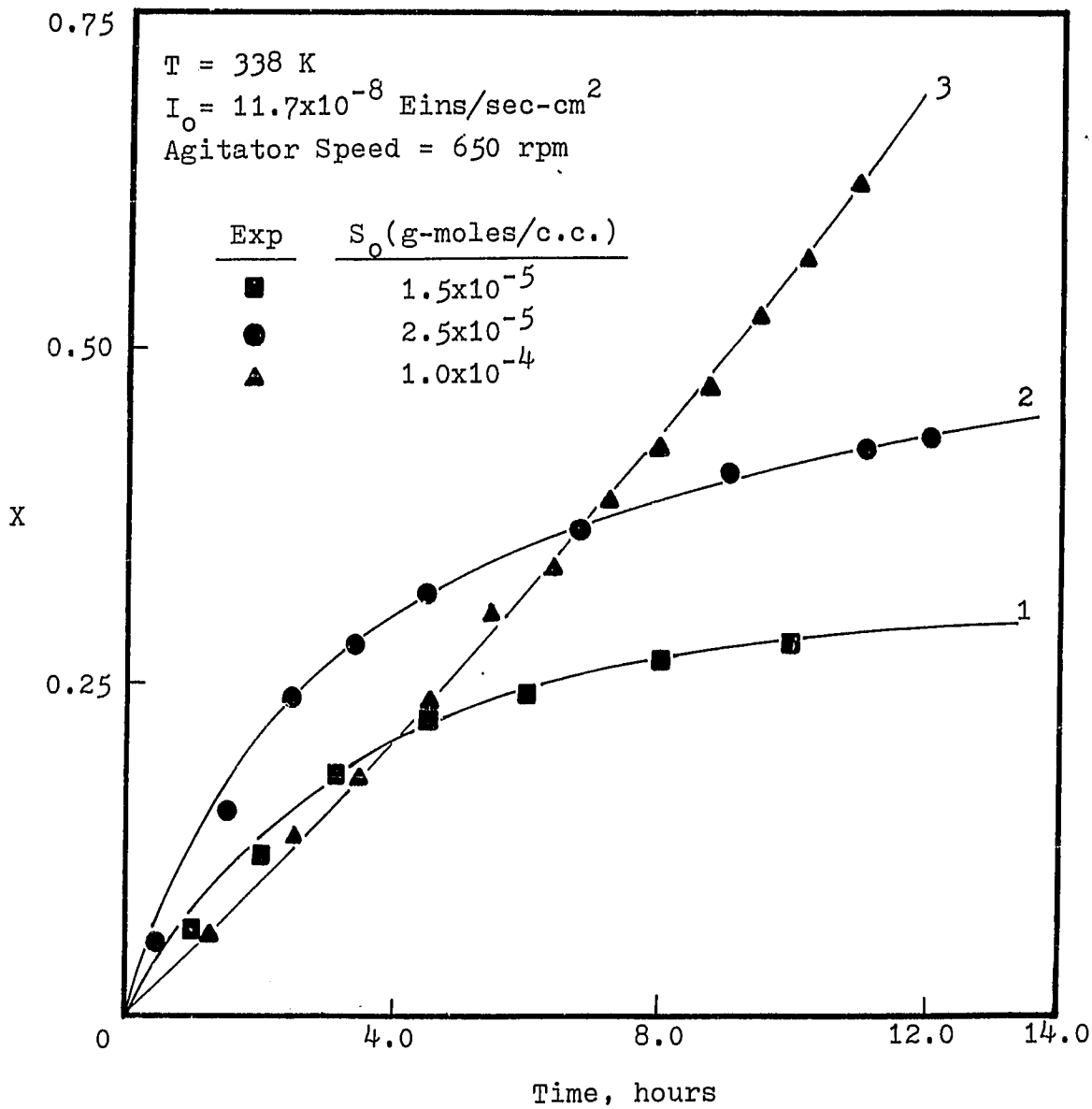

Figure 43. Effect of S_o on X for Photopolymerization in a Batch Reactor

chain lengths. For run 3 (high initiation rate), the values of number and weight average chain lengths are 25 to 50% higher than those of runs 1 and 2 (low initiation rates).

From Figures 45 to 55, conversion and number average chain lengths are plotted against time. The solid lines represent the predicted values using two region model. In Figure 45, the predicted conversion curve (V_I/V_{II}= 22/178) is in good agreement with experimental result, while the number average values are underestimated. In Figure 46 (T=323 K), both experimental conversion and number average chain lengths show good agreement with the predicted ones. For all the experimental runs using sensitizer concentration of 1.0×10^{-4}g-moles/cc (Figures 46, 49, 50 and 51), the predicted values at a volume ratio (V_I/V_{II}) equals 25/175 indicate the best results. The predictions have not been successful for low sensitizer concentration runs. Figures 47 and 48, V_I values were adjusted to be 48 cc and 38 cc at S_o= 1.5×10^{-5} and 2.5×10^{-5}g-moles/cc respectively. The predicted conversion curves overestimate the experimental values at the final stage of these two runs. This is probably because of the expression of light intensity (equation 115) is inadequate as the sensitizer concentration has been consumed to a very low value. Figure 50 shows the predicted conversion and number average chain length are lower than the experimental results at a low light intensity run (I_o= 5.1×10^{-8} Eins/sec-cm^2). The measured number average chain lengths for

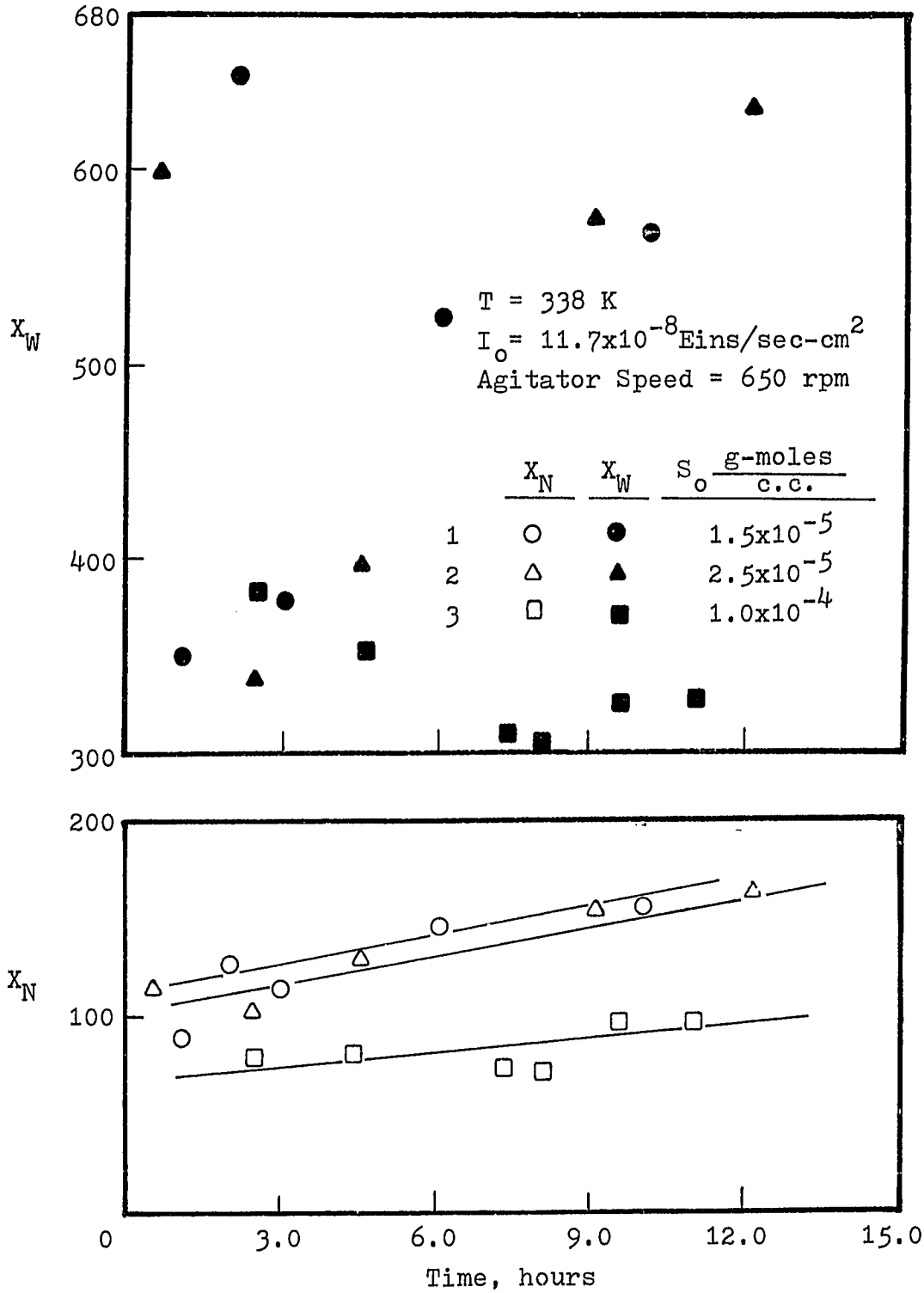

Figure 44. Effect of S_o on X_N and X_W for Photopolymerization in a Batch Reactor

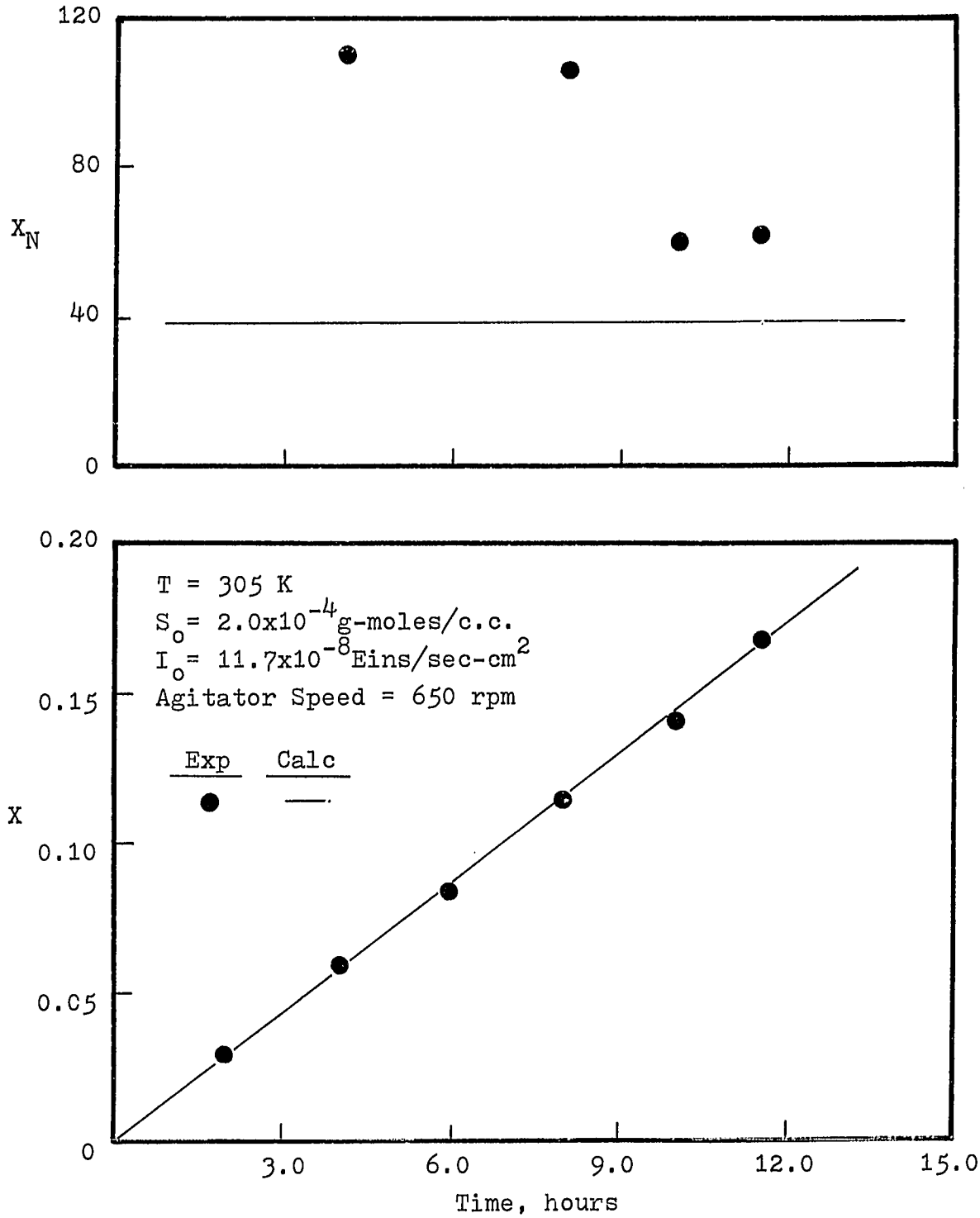

Figure 45. Experimental X and X_N vs. time Data and Prediction of Two Region Model at T = 305 K

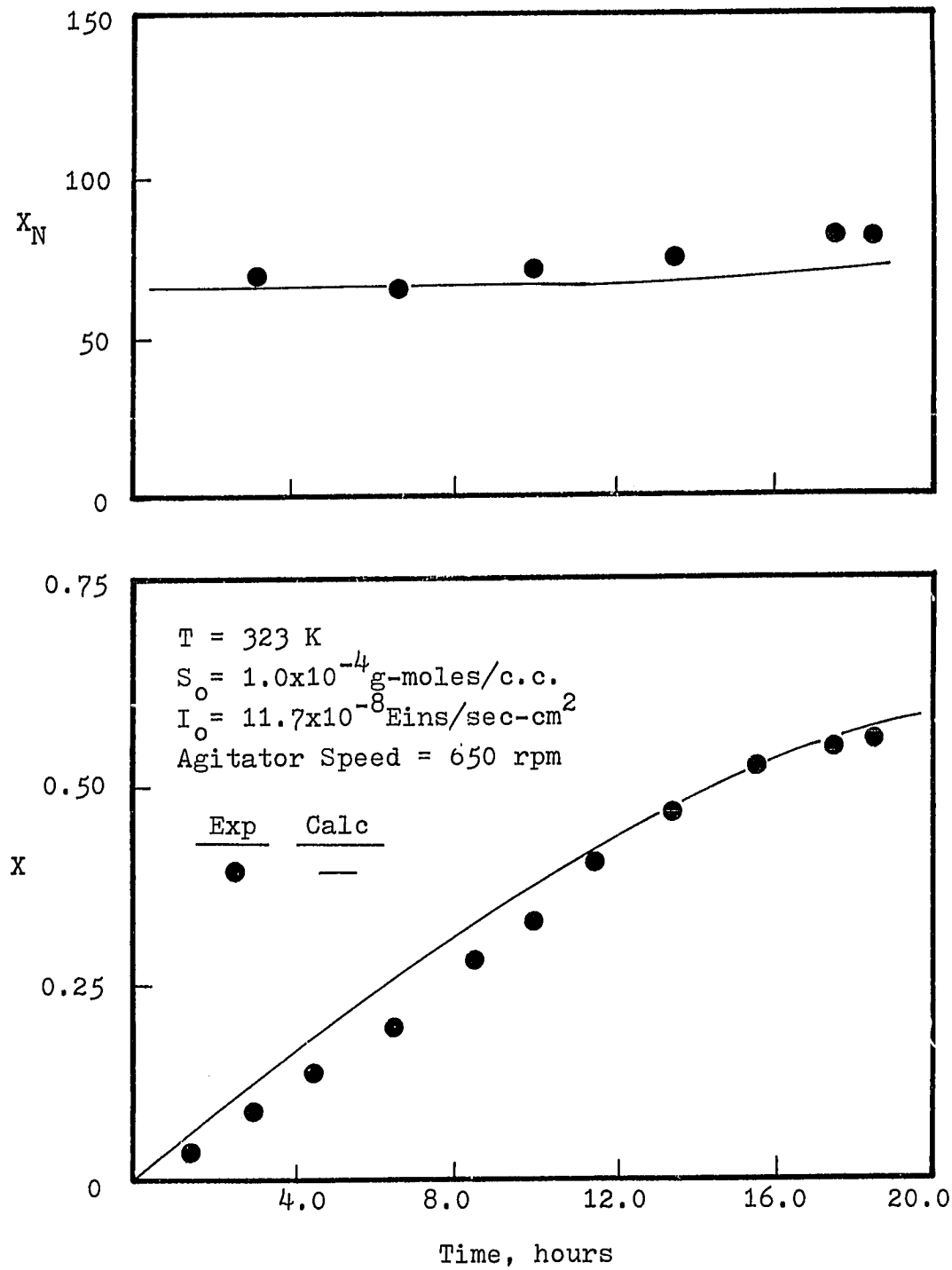

Figure 46. Experimental X and X_N vs. time Data and Prediction of Two Region Model at T = 323 K

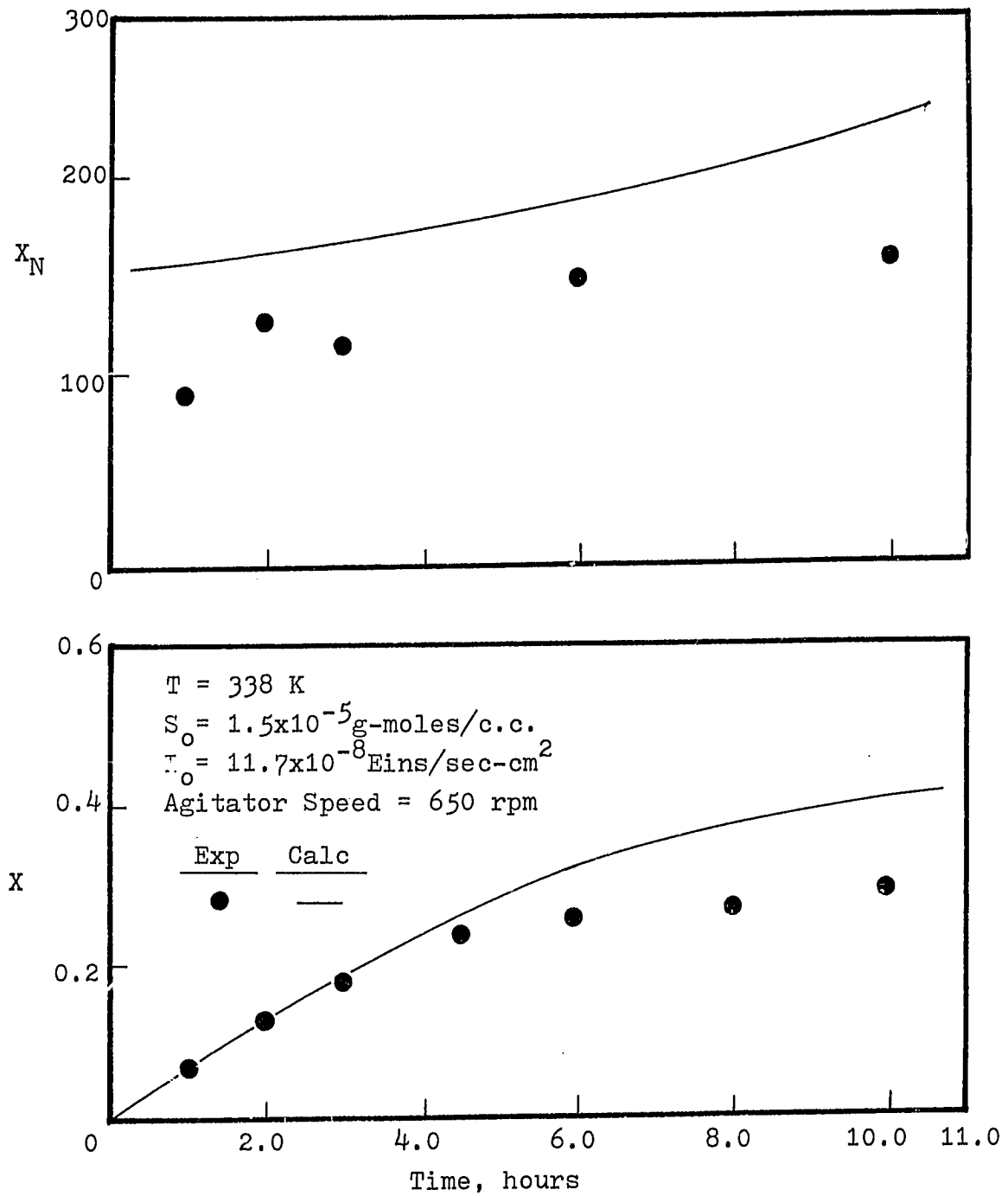

Figure 47. Experimental X and X_N vs. time Data and Prediction of Two Region Model at T = 338 K (I)

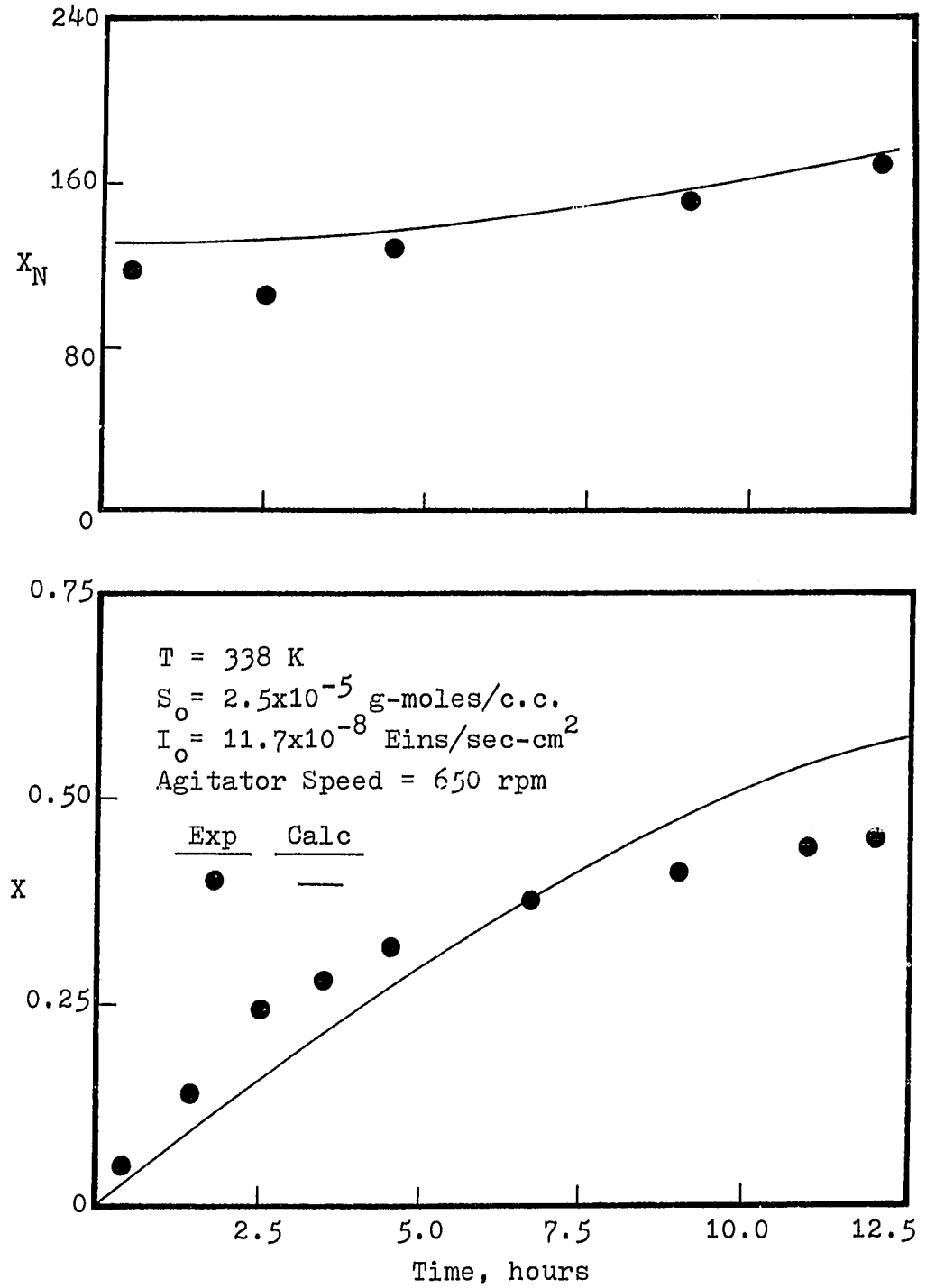

Figure 48. Experimental X and X_N vs. time Data and Prediction of Two Region Model at T = 338 K (II)

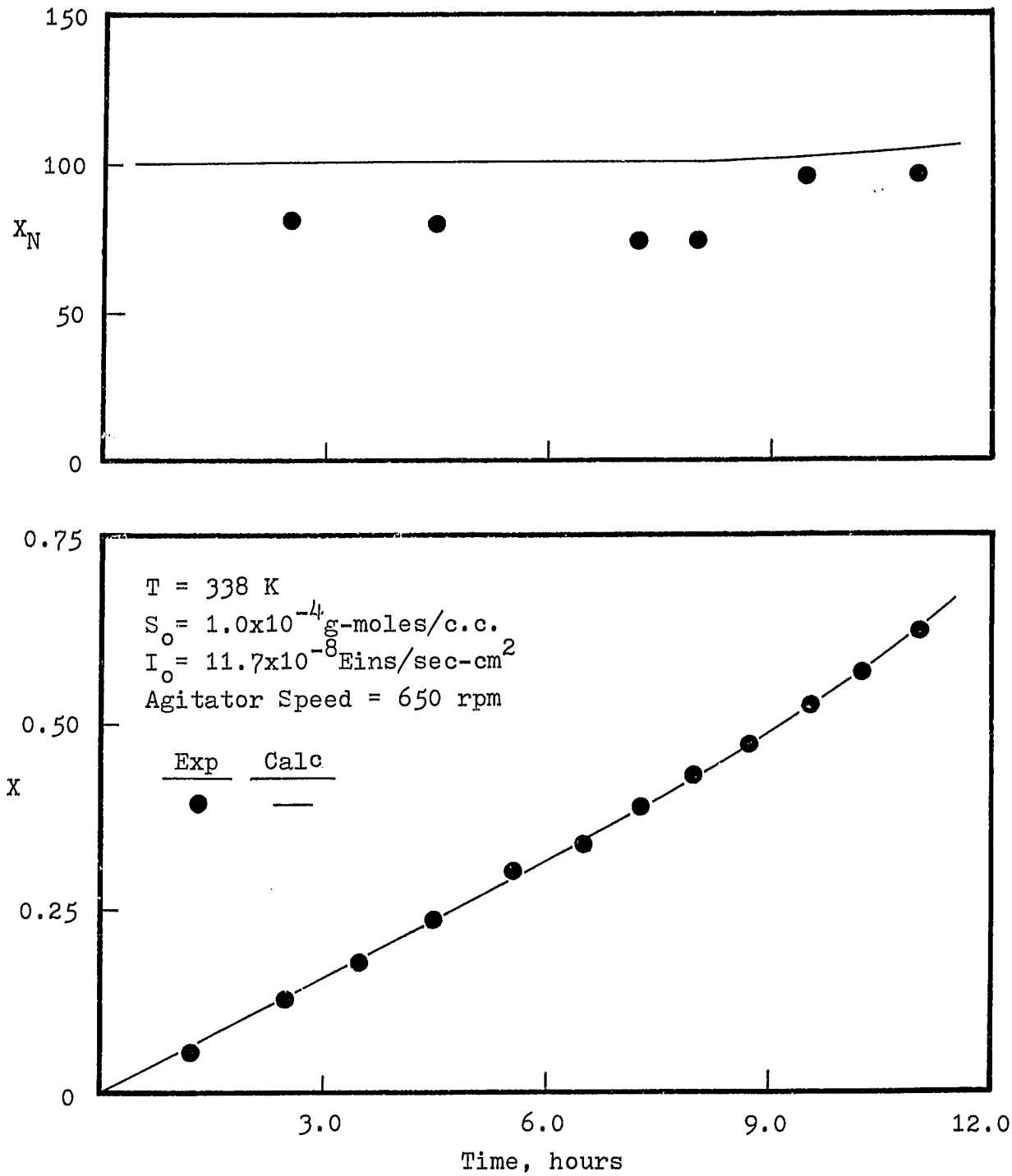

Figure 49. Experimental X and X_N vs. time Data and Prediction of Two Region Model at T = 338 K (III)

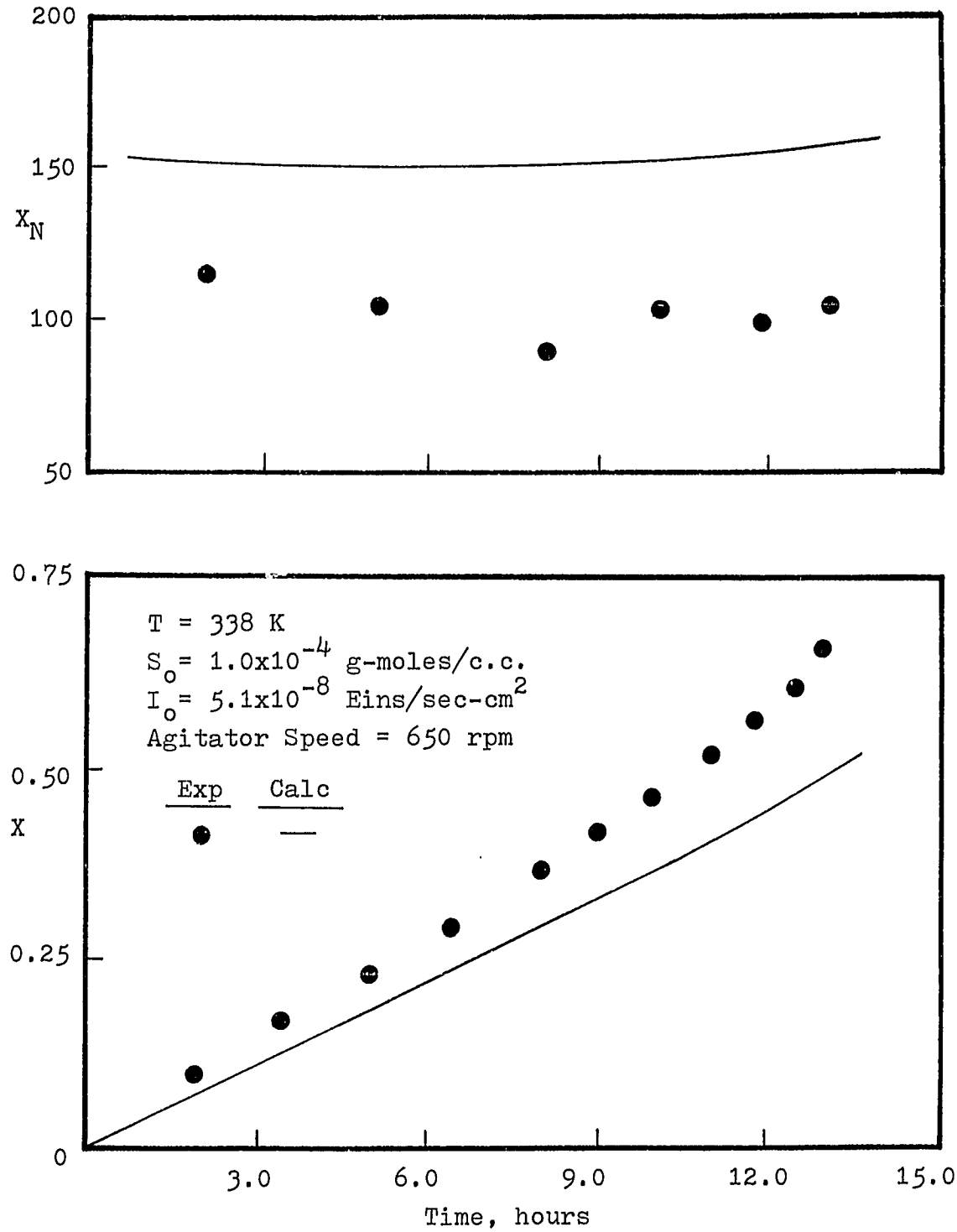

Figure 50. Experimental X and X_N vs. time Data and Prediction of Two Region Model at T = 338 K (IV)

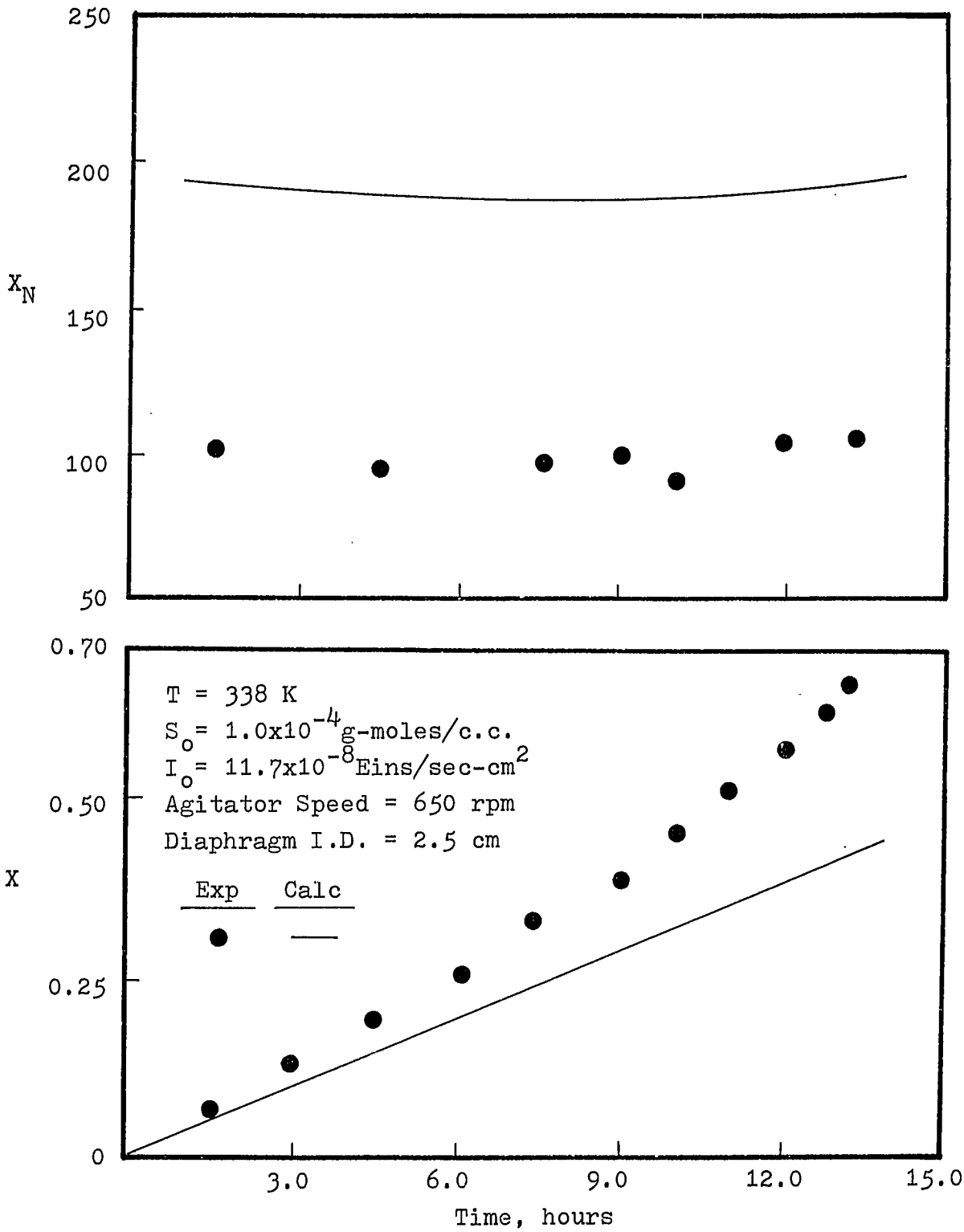

Figure 51. Experimental X and X_N vs. time Data and Prediction of Two Region Model at T = 338 K (V)

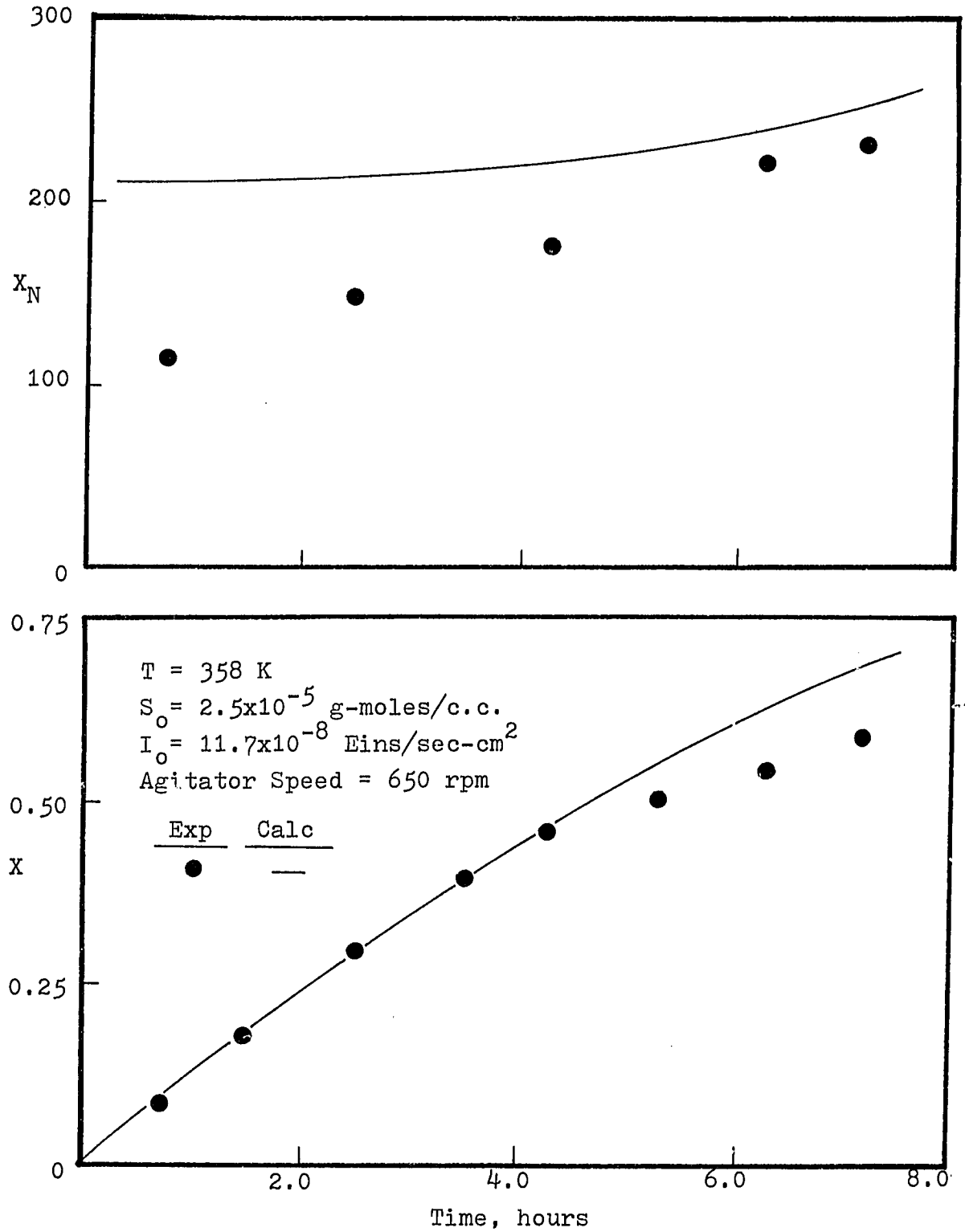

Figure 52. Experimental X and X_N vs. time Data and Prediction of Two Region Model at T = 358 K

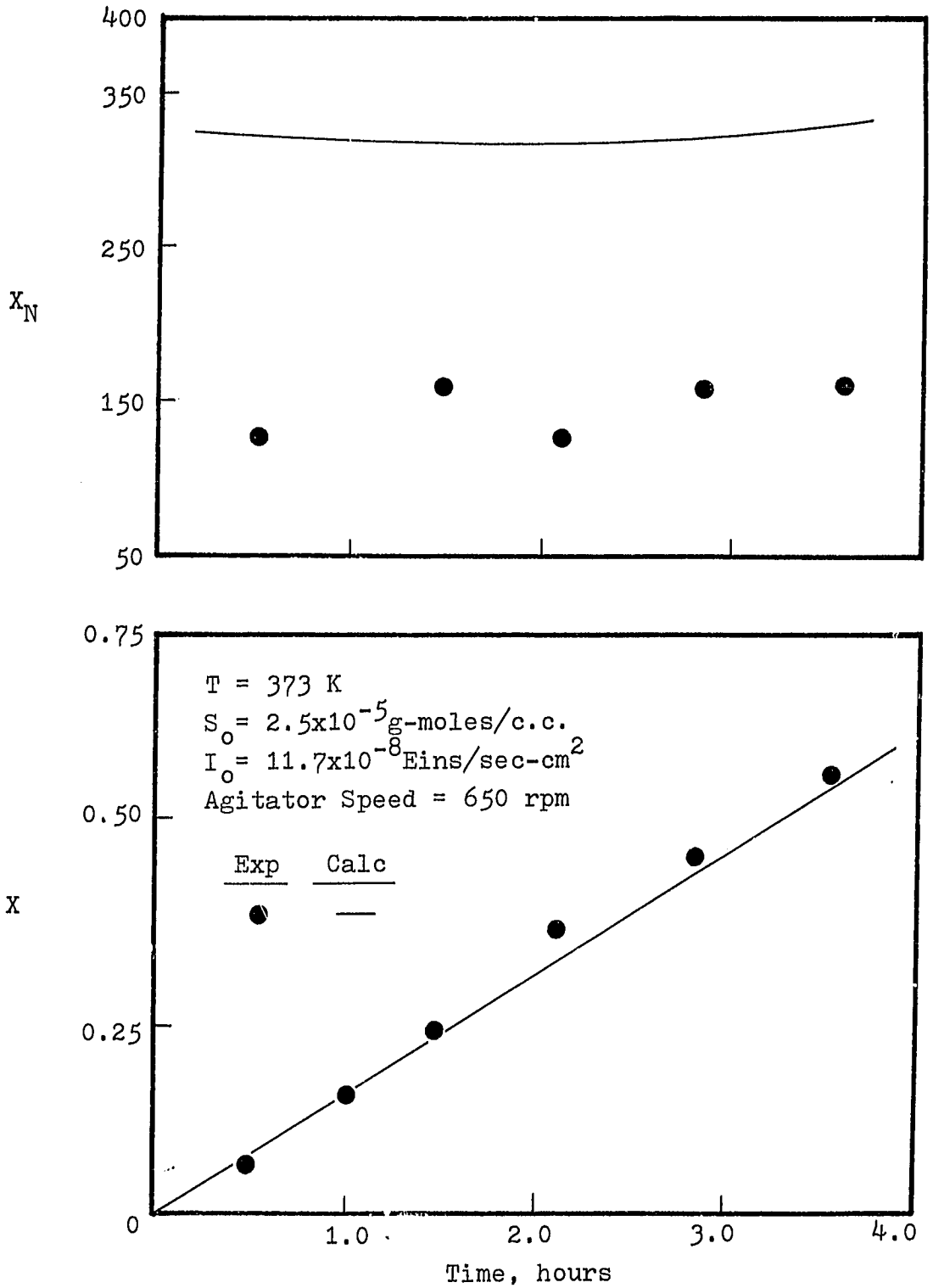

Figure 53. Experimental X and X_N vs. time Data and Prediction of Two Region Model at T = 373 K

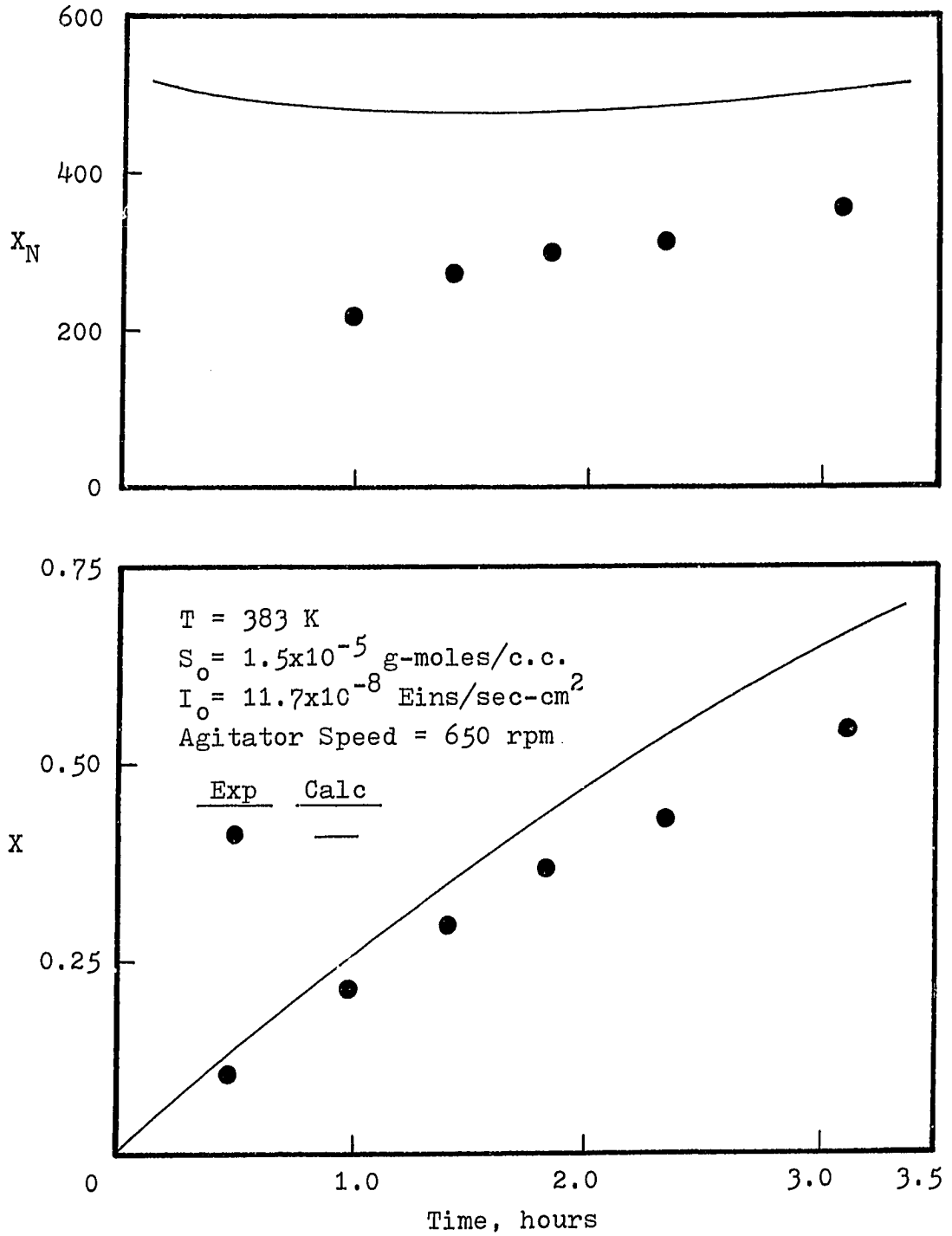

Figure 54. Experimental X and X_N vs. time Data and Prediction of Two Region Model at T = 383 K

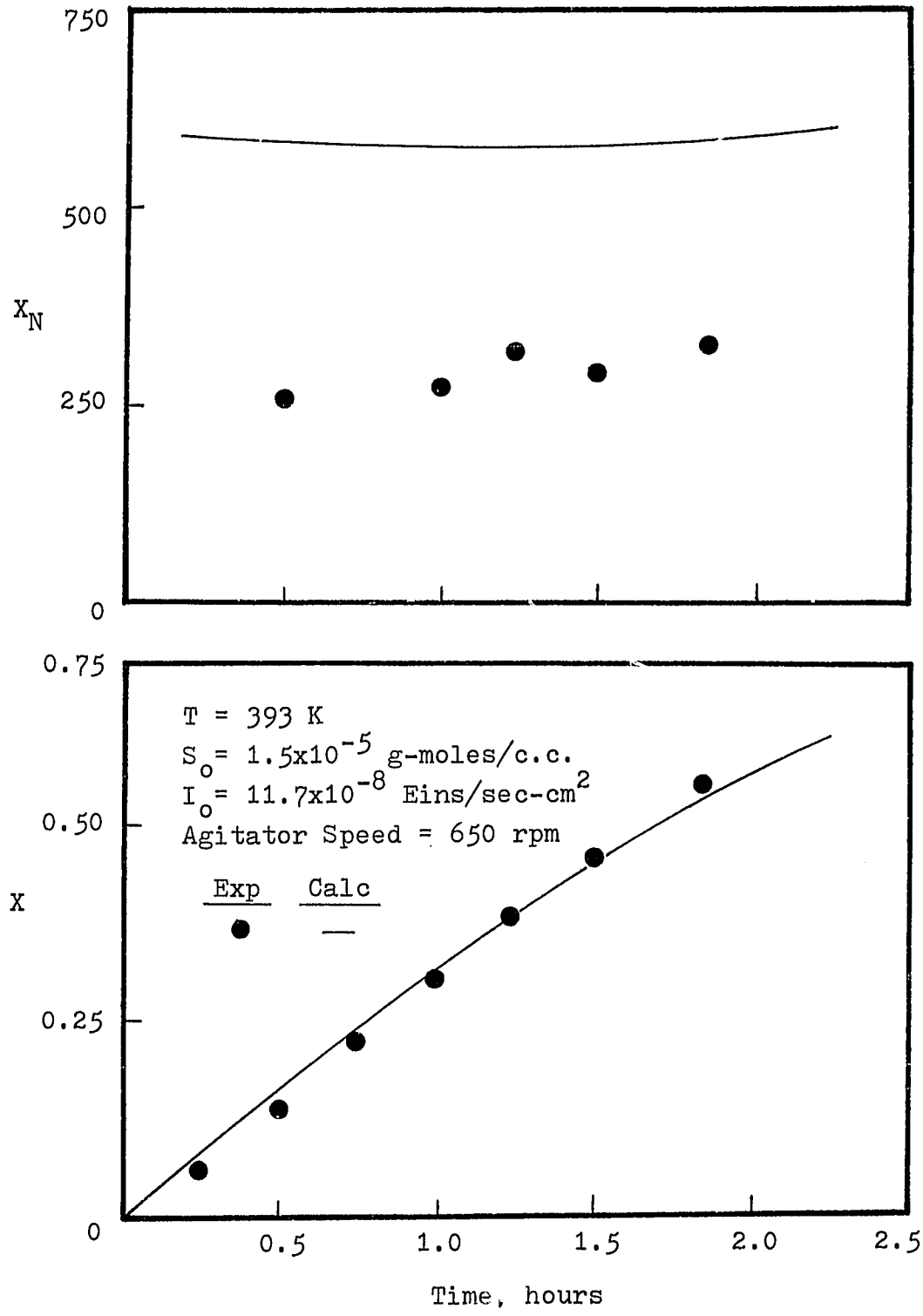

Figure 55. Experimental X and X_N vs. time Data and Prediction of Two Region Model at T = 393 K

this run (low initiation run) are slightly higher than that of a high light intensity run (Figure 49). For the four runs shown in Figures 52 to 55, the predicted conversion curves are in good agreement with the experimental results, while the calculated number average molecular weights are higher. The differences of number average values increases as polymerization temperature increases. The reason for this, as discussed previously is probably because of more hot spots were generated in the reaction mixture which produced a large number of low molecular weight polymer molecules and the resultant molecular number average chain lengths become lower.

7-3. Discussion of Experimental CSTR Results

Experimental results of an adiabatic CSTR in terms of reacion temperature, fractional conversion, number and weigh average chain lengths are presented in Figures 20 and 21. The solid lines are the predicted curves using a perfect mixing model of equations (8), (49), (50), (53), (54), and (56). For all the adiabatic runs, a very low sensitizer concentration was used (S_o=0.5x10^{-5}g-moles/cc). As indicated in Figure 28, the light intensity profile along the reactor path length is almost uniformly distributed, which leads to an assumption of constant initiation rate. constant initiation rate may be assumed. For metastable state, the predicted reaction temperature s are higher than the experimental data. This is probably because

of some heat loss may occur from the reactor system which requires a higher temperature (more heat generated) to reach the metastable state.

In the case of isothermal CSTR, a two region model was used for calculation since the applied sensitizer concentration was higher than that of an adiabatic experiment. For a two region flow pattern reactor (Figure 56), the material balance equations can be described as follows:

for sensitizer:

$$\frac{dS_I}{dt} = \frac{Q\ S_o}{(V_I+V_{II})} + \frac{(1+\epsilon X_{II})S_{II}-(1+\epsilon X_I)S_I}{\theta_I} - \phi_s{}^I a_{sI} - \frac{Q\ S_I}{(V_I+V_{II})} \qquad (116)$$

$$\frac{dS_{II}}{dt} = \frac{Q\ S_o}{(V_I+V_{II})} + \frac{(1+\epsilon X_I)S_I-(1+\epsilon X_{II})S_{II}}{\theta_{II}} - \phi_s{}^I a_{sII} - \frac{Q\ S_{II}(1+\epsilon \bar{X})}{(V_I+V_{II})} \qquad (117)$$

where $$\bar{X} = \frac{V_I X_I + V_{II} X_{II}}{(V_I+V_{II})}$$

for monomer:

$$\frac{dm_I}{dt} = \frac{Q\ m_o}{(V_I+V_{II})} + \frac{(1+\epsilon X_{II})m_{II}-(1+\epsilon X_I)m_I}{\theta} - k_p m_I \Sigma R_{iI} - \frac{Q\ m_o}{(V_I+V_{II})} \qquad (118)$$

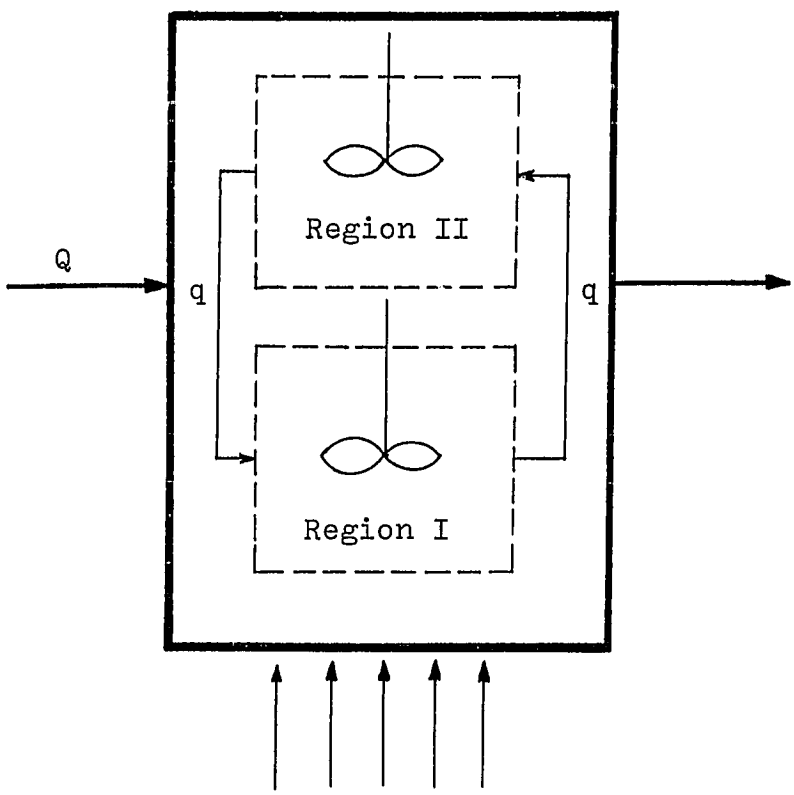

Figure 56. Schematic Diagram of a Continuous Flow Pattern Reactor

$$\frac{dm_{II}}{dt} = \frac{Q\ m_o}{(V_I+V_{II})} + \frac{(1+\epsilon X_I)m_I-(1+\epsilon X_{II})m_{II}}{\theta_{II}}$$

$$- k_p m_{II} \Sigma R_{iII} - \frac{Q\ m_{II}(1+\epsilon \bar{X})}{(V_I+V_{II})} \qquad (119)$$

for zero-th, first and second moments of the dead polymer, the balance equations are,

$$\frac{d\ \Sigma P_{iI}}{dt} = k_{fmI} m_I \Sigma R_{iI} + \frac{1}{2} k_{tI} \Sigma R_{iI}^2 - \frac{Q\ \Sigma P_{iI}}{(V_I+V_{II})}$$

$$+ \frac{(1+\epsilon X_{II})\ \Sigma P_{iII}-(1+\epsilon X_I)\ \Sigma P_{iI}}{\theta_I} \qquad (120)$$

$$\frac{d\ \Sigma P_{iII}}{dt} = k_{fmII} m_{II} \Sigma R_{iII} + \frac{1}{2} k_{tII} \Sigma R_{iII}^2$$

$$+ \frac{(1+\epsilon X_I)\ \Sigma P_{iI}-(1+\epsilon X_{II})\ \Sigma P_{iII}}{\theta_{II}} - \frac{Q\ \Sigma P_{iI}}{(V_I+V_{II})} \qquad (121)$$

$$\frac{d\ \Sigma iP_{iI}}{dt} = k_{tI} \Sigma R_{iI} \Sigma iR_{iI} + k_{fmI} m_I \Sigma iR_{iI} - \frac{Q\ \Sigma iP_{iI}}{(V_I+V_{II})}$$

$$+ \frac{(1+\epsilon X_{II})\ \Sigma iP_{iII}-(1+\epsilon X_I)\ \Sigma iP_{iI}}{\theta_I} \qquad (122)$$

$$\frac{d\ \Sigma iP_{iII}}{dt} = k_{tII} \Sigma R_{iII} \Sigma iR_{iII} + k_{fmII} m_{II} - \frac{Q\ \Sigma iP_{iII}(1+\epsilon \bar{X})}{(V_I+V_{II})}$$

$$+ \frac{(1+\epsilon X_I)\ \Sigma iP_{iI}-(1+\epsilon X_{II})\ \Sigma iP_{iII}}{\theta_{II}} \qquad (123)$$

$$\frac{d\Sigma i^2 P_{iI}}{dt} = k_{tI}\ \Sigma R_{iI}\ \Sigma i^2 R_{iI} + k_{tI}\ \Sigma i R^2_{iI}$$

$$+ k_{fmI} m_I\ \Sigma i^2 R_{iI} - \frac{Q\ \Sigma i^2 P_{iI}}{(V_I + V_{II})}$$

$$+ \frac{(1+\epsilon X_{II})\ \Sigma i^2 P_{iII} - (1+\epsilon X_I)\ \Sigma i^2 P_{iI}}{\theta_I} \qquad (124)$$

$$\frac{d\Sigma i^2 P_{iII}}{dt} = k_{tII}\ \Sigma R_{iII}\ \Sigma i^2 R_{iII} + k_{tII}\ \Sigma i R^2_{iII}$$

$$+ k_{fmII} m_{II}\ \Sigma i^2 R_{iII} - \frac{Q\ \Sigma i^2 P_{iII}(1+\epsilon \bar{X})}{(V_I + V_{II})}$$

$$+ \frac{(1+\epsilon X_I)\ \Sigma i^2 P_{iI} - (1+\epsilon X_{II})\ \Sigma i^2 P_{iII}}{\theta_{II}} \qquad (125)$$

Expressions for active sensitizer, zero-th, first and second moments of active polymer are the same as that of a batch reactor.

The above equations from (116) to (125) were derived from batch equations. As a comparison with the experimental CSTR results, Figure 57 shows that both xperimental and predicted conversion and number average chain length versus residence time. This figure indicates a very good agreement is obtained for lower steady state X and X_N values. However, prediction of metastable steady state reactor performances

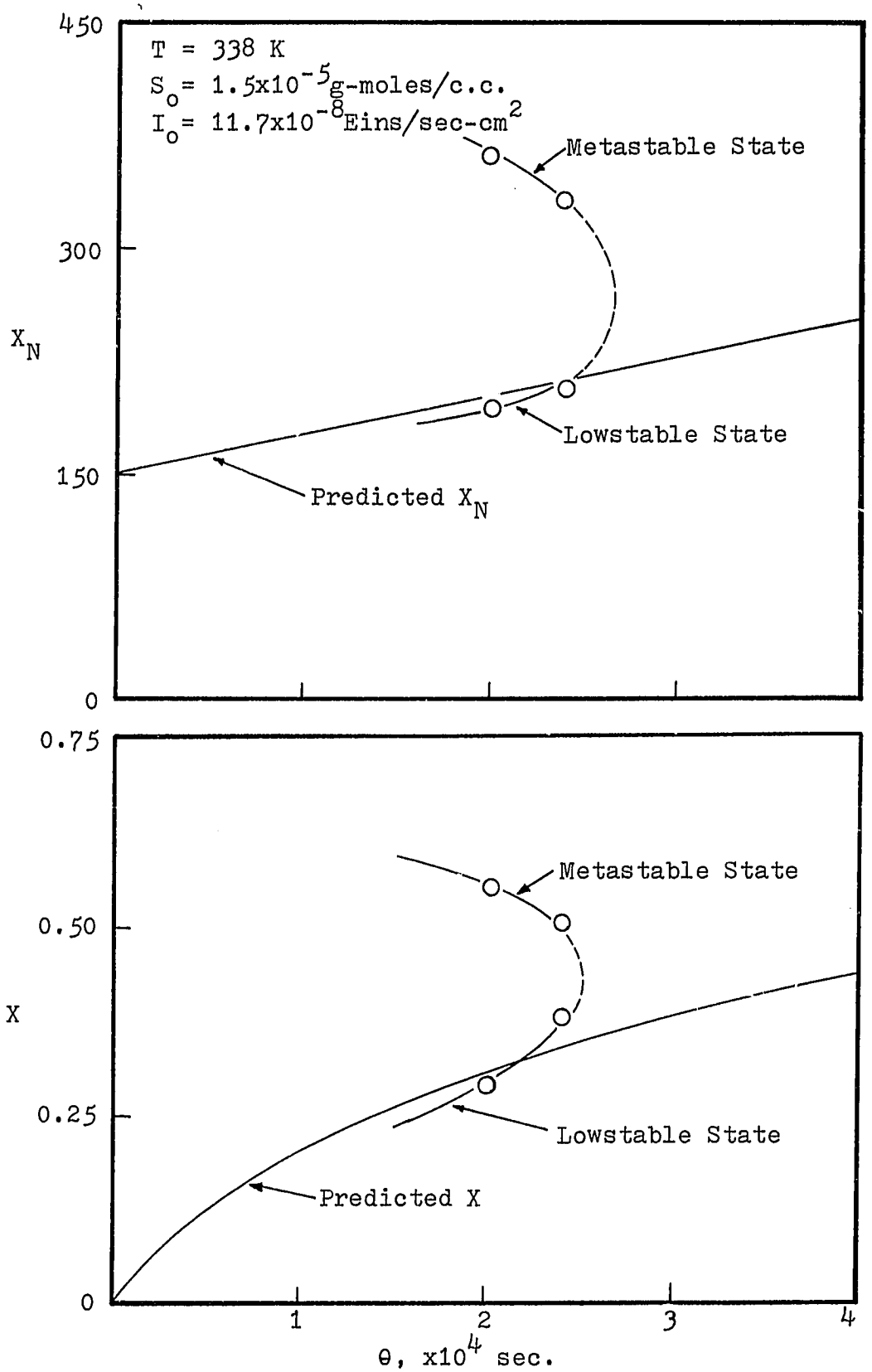

Figure 57. Comparison of Experimental Results with Predicted Two Region Model - Isothermal Conditions

has not been successful. The two basic models of backmixing, one applies to continuous or differential equations, the other one is applicable to stagewise calculations. In both cases, the results is a reduction of polymerization rate as shown in the predicted conversion versus reaction time curve, and the possible multiple steady state region induced by gel effect being eliminated.

The experimental batch data show that, for high sensitizer concentration runs (constant initiation rate) the polymerization rate increases as conversion increases. However, in this study which shows that gel effect is not that pronounced in comparison with the published results [9]. This probably can explain there is a mixing effect in a larger reactor performance. The above observation may lead to the conclusion that in the continuous operation, unstable region can either be reduced or totally vanished.

Mixing may affect other aspect of the polymerization rate which can be seen from the other experimental results. Comparing two different runs shown in Figures 10 and 49 which were carried out at two agitation speeds. For the lower stirring speed run shown in Figure 10 (350 rpm), the observed polymerization rate is faster than that of a higher agitation speed (650 rpm). This is probably because that under lower agitation speed, the amount of heat generated due to exothermic

reaction may not be efficient to transfer to the outside of the reactor and possibly, some local hot spots formed. In addition to this, lower mixing rate may decrease the termination reaction rate. The above two factors might be increasing the observed polymerization rate. During the experimental work, mixing becomes a difficult problem at high conversion level. Very often, the agitator can not be maintained at the same speed as that of a lower conversion run. This may result in unstable region observed.

CHAPTER 8

CONCLUSIONS

From this study, following conclusions can be made:

(1) In both adiabatic and isothermal continuous stirred tank reactors, multiple steady states exist.

(2) For both adiabatic and isothermal continuous stirred tank reactors operating in the metastable state regions, the fractional conversion and the polymer molecular weight are greater than the corresponding lower steady states.

(4) For a given conversion level, the reaction time for both adiabatic and isothermal continuous stirred tank reactors is less than for an equivalent batch reactor. The molecular number averages of the flow systems at metastable steady state are greater than that obtained in a batch system.

(5) An experimental technique has been developed to determine metastable state conversion. Molecular weight averages and molecular weight distribution up to 65% conversion were measured.

(6) The reactor can be accurately controlled at the metastable state by using a simple on-off regulation of UV light.

(7) Temperature and concentration stabilities presented in this work offer a fundamental knowledge for the design,

simulation, and optimization of photopolymerization reactor systems.

(8) A mathematical model was developed to correlate the imperfect mixing of a photopolymerization reactor. For batch data, this model overpredicts the molecular number average chain lengths and for some low sensitizer concentration runs, which overpredicts conversion due to incomplete information of absorsed light intensity in the reactor. Application of this model to the continuous system, prediction of conversion and number average chain lengths are in good agreement with lower steady state results. However, prediction of metastable state operations has not been successful.

(9) Exact multiplicity and uniqueness criteria were established for photopolymerization of styrene in a continuous stirred tank reactor. Experimental results support the derived criteria for multiplicity.

For further investigation of photopolymerization systems, the following suggestions are offered:

(1) The light intensity equation used in this study is a simplified one which neglects the effects such as reflection, refraction, and the finite size of the actual lamp. Some fundamental study should be done accounting for these

effects in an imperfectly mixed photo reactor.

(2) For this study, data were taken in the temperature range of 305 K to 393 K. To avoid the thermal effect on number average chain lengths, heat removal from the reactor system is important. For further study particularly at higher temperature, a cooling coil is suggested to place at the center of the reactor to maintain temperature homogenity. However, design of the coil may become complicated if zones of low light intensity and stagnation are to be avoided.

APPENDIX A

CALCULATION OF MULTIPLE STEADY STATES IN AN ISOTHERMAL AND CONTINUOUS STIRRED TANK REACTOR

Example: Consider photopolymerization of styrene at 65 C. The following values of the parameters are known:

$\phi_s = 0.012$ g-moles/Eins

$m_o = 8.31 \times 10^{-3}$ g-moles/cc

$I_{as} = 1.69 \times 10^{-8}$ Eins/sec-cm^3

$(k_p/k_t^{1/2})_o = 0.028$

$A_1 = 0.863$

$A_2 = 3.69$

$A_3 = -0.376$

From equation (19),

$X_A = 0.41$

$X_B = 4.52$

and

$A_1 - 1 < 0$

$A_3 < 0$

Hence, the necessary conditions (Case 2, Table 1) are satisfied. The four roots of equation (22) are: -0.372, 0.471, 0.779 and 6.520, and $X_1 = 0.7785$ and $X_2 = 0.471$, corresponding to $\theta_1 = 1.35 \times 10^4$ sec and $\theta_2 = 1.55 \times 10^4$ sec. Thus, multiplicity is guaranteed by limiting θ between θ_1 and θ_2.

APPENDIX B

CALCULATION OF MULTIPLE STEADY STATES IN AN ADIABATIC AND CONTINUOUS STIRRED TANK REACTOR

Example: Suppose that the photopolymerization of styrene carried out in an adiabatic CSTR, the following values of parameters are known;

$m_o = 8.31 \times 10^{-3}$ g-moles/cc

$\Delta H = 16683$ g-cal/g-mole

$\phi_s = 0.072$ g-moles/Eins

$C_p = 0.376$ g-cal/cm^3-K

$A_1 = 2.57 - 5.05 \times 10^{-3}\ T$

$A_2 = 9.56 - 1.76 \times 10^{-2}\ T$

$A_3 = -3.03 + 7.85 \times 10^{-3}\ T$

$(k_p)_o = 1.051 \times 10^{10}\ \mathrm{Exp}(-3557/T)$

$(k_t)_o = 1.255 \times 10^{12}\ \mathrm{Exp}(-844/T)$

$T_o = 298$ K

$I_{as} = 1.15 \times 10^{-8}$ Eins/sec-cm^3

From equations (30) and (31),

$T = 298 + 368.7\ X$

$\lambda = 368.7$

$b = 0.383$

$C_1 = 1.065$

$C_2 = 2.45$; $C_3 = -7.18$

The equation $\ell(X) = 0$ has two real roots between 0 and 1, $X_1 = 0.54$ and $X_2 = 0.093$. Hence, the necessary conditions for multiplicity is satisfied. From equation (44), $\theta_1 = 838$ sec. and $\theta_2 = 2970$ sec. Thus, multiplicity is guaranteed for limiting θ between θ_1 and θ_2.

APPENDIX C

SUMMARY OF EXPERIMENTAL RESULTS

- ADIABATIC CSTR

TABLE 5

ADIABATIC CSTR EXPERIMENT 1

S_o = 0.5×10^{-5} g-moles/c.c.

T_o = 298 K

θ = 2000 sec.

Optical Path: 1 neutral density filter
1 color filter

Diaphragm I.D. = 4.7 cm

LOW STABLE STATE

Sample	1	2	3	4	5
T(K)	344.1	344.1	344.1	344.1	344.1
X	0.055	0.057	0.057	0.057	0.058
X_N	-	-	-	138	123
X_W	-	-	-	359	371
PD	-	-	-	2.60	3.02

METASTABLE STATE

Sample	1	2	3	4	5
T(K)	397.4	397.4	397.4	396.3	397.4
X	0.323	0.324	0.325	0.325	0.320
X_N	495	474	528	565	529
X_W	1775	1502	1632	1659	1838
PD	3.59	3.17	3.09	2.94	3.48

TABLE 6

ADIABATIC CSTR EXPERIMENT 2

$S_o = 0.5 \times 10^{-5}$ g-moles/c.c.

$T_o = 298$ K

$\theta = 2000$ sec.

Optical Path: 1 neutral density filter
1 color filter

Diaphragm I.D. = 3.5 cm

LOW STABLE STATE

Sample	1	2	3	4
T(K)	343.1	343.1	342.4	342.4
X	0.036	0.036	0.037	0.036
X_N	-	97	107	-
X_W	-	235	302	-
PD	-	2.42	2.82	-

METASTABLE STATE

Sample	1	2	3	4	5
T(K)	407.5	408.0	408.6	408.6	407.9
X	0.388	0.387	0.410	0.407	0.406
X_N	620	461	498	563	617
X_W	1914	1573	1644	1754	1799
PD	3.09	3.41	3.31	3.12	2.92

TABLE 7

ADIABATIC CSTR EXPERIMENT 3

$S_o = 0.5 \times 10^{-5}$ g-moles/c.c.

$T_o = 298$ K

$\theta = 2000$ sec.

Optical Path: 1 neutral density filter
1 color filter

Diaphragm I.D. = 2.5 cm

LOW STABLE STATE

Sample	1	2	3	4	5
T(K)	340.7	340.8	340.8	340.8	340.8
X	0.024	0.017	0.013	0.017	0.026
X_N	-	-	-	120	104
X_W	-	-	-	337	315
PD	-	-	-	2.81	3.03

METASTABLE STATE

Sample	1	2	3	4
T(K)	420.8	421.3	421.3	421.3
X	0.526	0.514	0.515	0.520
X_N	1084	883	984	825
X_W	2946	2434	2694	2346
PD	2.72	2.76	2.74	2.85

TABLE 8

ADIABATIC CSTR EXPERIMENT 4

S_o= 0.5×10^{-5} g-moles/c.c.

T_o= 298 K

θ = 4000 sec

Optical Path: 1 neutral density filter
1 color filter

Diaphragm I.D. = 4.7 cm

LOW STABLE STATE

Sample	1	2	3	4
T(K)	361.9	361.9	361.9	361.9
X	0.103	0.102	0.105	0.112
X_N	-	-	210	209
X_W	-	-	559	599
PD	-	-	2.66	2.87

METASTABLE STATE

Sample	1	2	3	4	5
T(K)	381.9	381.3	381.3	380.8	381.9
X	0.210	0.205	0.206	0.205	0.210
X_N	328	330	415	631	453
X_W	968	1093	1101	1147	1130
PD	2.95	3.31	2.65	2.66	2.49

TABLE 9

ADIABATIC CSTR EXPERIMENT 5

$S_o = 0.5 \times 10^{-5}$ g-moles/c.c.

$T_o = 298$ K

$\theta = 4000$ sec.

Optical Path: 1 neutral density filter
1 color filter

Diaphragm I.D. = 3.5 cm

LOW STABLE STATE

Sample	1	2	3	4	5
T(K)	357.5	357.5	357.5	357.7	358.0
X	0.085	0.089	0.091	0.099	0.095
X_N	-	-	-	211	191
X_W	-	-	-	583	595
PD	-	-	-	2.76	3.11

METASTABLE STATE

Sample	1	2	3	4	5
T(K)	386.3	386.9	387.4	386.9	386.9
X	0.300	0.292	0.290	0.280	0.280
X_N	593	527	582	565	511
X_W	1504	1364	1449	1550	1544
PD	2.54	2.59	2.49	2.74	3.02

TABLE 10

ADIABATIC CSTR EXPERIMENT 6

$S_o = 0.5 \times 10^{-5}$ g-moles/c.c.

$T_o = 298$ K

$\theta = 4000$ sec.

Optical Path: 1 neutral density filter
1 color filter

Diaphragm I.D. = 2.5 cm

LOW STABLE STATE

Sample	1	2	3	4	5
T(K)	352.4	352.4	352.4	352.4	352.4
X	0.067	0.068	0.067	0.069	0.069
X_N	-	-	-	146	142
X_W	-	-	-	412	447
PD	-	-	-	2.82	3.15

METASTABLE STATE

Sample	1	2	3	4
T(K)	402.4	402.4	401.9	401.9
X	0.380	0.390	0.380	0.382
X_N	573	687	702	577
X_W	1685	2003	1945	1814
PD	2.94	2.92	2.77	3.15

APPENDIX D

SUMMARY OF EXPERIMENTAL RESULTS

- ISOTHERMAL CSTR

TABLE 11

ISOTHERMAL CSTR EXPERIMENT 1

$T = 338$ K

$S_o = 1.5 \times 10^{-5}$ g-moles/c.c.

$I_o = 11.7 \times 10^{-8}$ Eins/sec-cm^2

$\theta = 24000$ sec.

Agitator Speed = 650 rpm

Optical Path: 1 neutral density filter
1 color filter

LOW STABLE STATE

Sample	1	2	3	4	5
X	0.362	0.378	0.377	0.388	0.390
X_N	206	204	207	197	190
X_W	696	666	685	640	591
PD	3.38	3.26	3.31	3.26	3.11

METASTABLE STATE

Sample	1	2	3	4
X	0.501	0.512	0.527	0.523
X_N	-	370	336	305
X_W	-	1426	1343	1199
PD	-	3.86	4.00	3.93

TABLE 12

ISOTHERMAL CSTR EXPERIMENT 2

$T = 338$ K

$S_o = 1.5 \times 10^{-5}$ g-moles/c.c.

$I_o = 7.0 \times 10^{-8}$ Eins/sec-cm^2

$\theta = 24000$ sec.

Agitator Speed = 650 rpm

Optical Path: 2 neutral density filters
1 color filter

LOW STABLE STATE

Sample	1	2	3	4	5
X	0.333	0.344	0.341	0.339	0.345
X_N	-	233	217	227	225
X_W	-	908	854	824	797
PD	-	3.90	3.94	3.63	3.55

METASTABLE STATE

Sample	1	2	3
X	0.542	0.504	0.554
X_N	340	317	319
X_W	1209	1104	1162
PD	3.56	3.48	3.65

TABLE 13

ISOTHERMAL CSTR EXPERIMENT 3

$T = 338$ K

$S_o = 1.5 \times 10^{-5}$ g-moles/c.c.

$I_o = 5.1 \times 10^{-8}$ Eins/sec-cm^2

$\theta = 24000$ sec.

Agitator Speed = 650 rpm

Optical Path: 3 neutral density filters
1 color filter

LOW STABLE STATE

Sample	1	2	3	4	5
X	0.314	0.323	0.334	0.334	0.330
X_N	-	146	134	118	189
X_W	-	517	472	519	637
PD	-	3.54	3.52	4.39	3.36

METASTABLE STATE

Sample	1	2	3
X	0.567	0.579	0.596
X_N	338	402	425
X_W	1174	1529	1671
PD	3.47	3.80	3.93

TABLE 14

ISOTHERMAL CSTR EXPERIMENT 4

T = 338 K

S_o = 1.5×10^{-5} g-moles/c.c.

I_o = 14.9×10^{-8} Eins/sec-cm^2

θ = 20000 sec.

Agitator Speed = 650 rpm

Optical Path: no neutral density filter
1 color filter

LOW STABLE STATE

Sample	1	2	3	4	5
X	0.332	0.337	0.342	0.343	0.346
X_N	-	238	213	197	204
X_W	-	682	598	598	524
PD	-	2.87	2.80	3.04	2.57

METASTABLE STATE

Sample	1	2	3	4
X	0.552	0.556	0.526	0.546
X_N	358	328	377	339
X_W	1726	1594	1428	1353
PD	4.83	4.86	3.79	3.99

TABLE 15

ISOTHERMAL CSTR EXPERIMENT 5

$T = 338$ K

$S_o = 1.5 \times 10^{-5}$ g-moles/c.c.

$I_o = 11.7 \times 10^{-8}$ Eins/sec-cm^2

$\theta = 20000$ sec.

Agitator Speed = 650 rpm

Optical Path: 1 neutral density filter
1 color filter

LOW STABLE STATE

Sample	1	2	3	4
X	0.272	0.268	0.279	0.286
X_N	-	203	183	187
X_W	-	637	583	597
PD	-	3.14	3.19	3.19

METASTABLE STATE

Sample	1	2	3
X	0.612	0.582	0.599
X_N	332	375	392
X_W	1409	1412	1421
PD	4.24	3.77	3.62

TABLE 16

ISOTHERMAL CSTR EXPERIMENT 6

$T = 338$ K

$S_o = 1.5 \times 10^{-5}$ g-moles/c.c.

$I_o = 7.0 \times 10^{-8}$ Eins/sec-cm^2

$\theta = 28000$ sec.

Agitator Speed = 650 rpm

Optical Path: 2 neutral density filters
1 color filter

LOW STABLE STATE

Sample	1	2	3	4	5
X	0.446	0.457	0.466	0.461	0.447
X_N	-	-	327	314	326
X_W	-	-	907	845	845
PD	-	-	2.78	2.69	2.59

METASTABLE STATE

Sample	1	2	3	4	5
X	0.487	0.483	0.482	0.473	0.472
X_N	333	364	319	294	295
X_W	1151	1113	1090	1001	970
PD	3.45	3.06	3.42	3.41	3.28

TABLE 17

ISOTHERMAL CSTR EXPERIMENT 7

T = 338 K

S_o = 1.5×10^{-5} g-moles/c.c.

I_o = 5.1×10^{-8} Eins/sec-cm^2

θ = 28000 sec.

Agitatot Speed = 650 rpm

Optical Path: 3 neutral density filters
1 color filter

LOW STABLE STATE

Sample	1	2	3	4	5	6
X	0.327	0.332	0.348	0.350	0.355	0.363
X_N	-	-	266	253	257	283
X_W	-	-	884	876	836	878
PD	-	-	3.33	3.46	3.25	3.10

METASTABLE STATE

Sample	1	2	3	4	5
X	0.506	0.521	0.522	0.525	0.540
X_N	429	370	354	310	311
X_W	1551	1355	1301	1090	1075
PD	3.62	3.66	3.68	3.51	3.45

TABLE 18

ISOTHERMAL CSTR EXPERIMENTS 8 and 9

Run no. 8

$T = 338$ K , $S_o = 1.5 \times 10^{-5}$ g-moles/c.c.

$I_o = 5.1 \times 10^{-8}$ Eins/sec-cm^2 , $\theta = 20000$ sec.

Agitator Speed = 650 rpm

Optical Path: 3 neutral density filters, 1 color filter

LOW STABLE STATE

Sample	1	2	3	4	5
X	0.155	0.156	0.163	0.163	0.168
X_N	-	-	-	103	99
X_W	-	-	-	245	254
PD	-	-	-	2.37	2.57

Run No. 9

$T = 338$ K , $S_o = 1.5 \times 10^{-5}$ g-moles/c.c.

$I_o = 7.0 \times 10^{-8}$ Eins/sec-cm^2 , $\theta = 20000$ sec.

Agitator Speed = 650 rpm

Optical Path: 2 neutral density filters, 1 color filter

LOW STABLE STATE

Sample	1	2	3	4	5
X	0.216	0.226	0.228	0.231	0.231
X_N	-	-	-	129	126
X_W	-	-	-	373	379
PD	-	-	-	2.90	3.02

TABLE 19

ISOTHERMAL CSTR EXPERIMENT 10

$T = 358$ K

$S_o = 1.5 \times 10^{-5}$ g-moles/c.c.

$I_o = 11.7 \times 10^{-8}$ Eins/sec-cm^2

$\theta = 12000$ sec.

Agitator Speed = 650 rpm

Optical Path: 1 neutral density filter
1 color filter

LOW STABLE STATE

Sample	1	2	3
X	0.271	0.349	0.320
X_N	185	181	192
X_W	533	523	526
PD	2.89	2.89	2.74

METASTABLE STATE

Sample	1	2	3	4
X	0.585	0.592	0.585	0.585
X_N	317	297	289	319
X_W	808	812	840	845
PD	2.55	2.73	2.91	2.65

TABLE 20

ISOTHERMAL CSTR EXPERIMENT 11

$T = 358$ K

$S_o = 1.5 \times 10^{-5}$ g-moles/c.c.

$I_o = 11.7 \times 10^{-8}$ Eins/sec-cm^2

$\theta = 14000$ sec.

Agitator Speed = 650 rpm

Optical Path: 1 neutral density filter
1 color filter

LOW STABLE STATE

Sample	1	2	3	4
X	0.385	0.392	0.406	0.410
X_N	-	219	248	252
X_W	-	642	715	700
PD	-	2.94	2.88	2.77

METASTABLE STATE

Sample	1	2	3	4
X	0.532	0.527	0.541	0.544
X_N	255	272	259	285
X_W	694	758	762	791
PD	2.72	2.79	2.94	2.78

TABLE 21

ISOTHERMAL CSTR EXPERIMENT 12

$T = 358$ K

$S_o = 1.5 \times 10^{-5}$ g-moles/c.c.

$I_o = 11.7 \times 10^{-8}$ Eins/sec-cm^2

$\theta = 6000$ sec.

Agitator Speed = 650 rpm

Optical Path: 1 neutral density filter
1 color filter

LOW STABLE STATE

Sample	1	2	3
X	0.218	0.222	0.229
X_N	200	197	200
X_W	582	584	578
PD	2.91	2.97	2.88

TABLE 22

ISOTHERMAL CSTR EXPERIMENT 13

$T = 338$ K

$S_o = 2.5 \times 10^{-5}$ g-moles/c.c.

$I_o = 11.7 \times 10^{-8}$ Eins/sec-cm^2

$\theta = 12000$ sec.

Agitator Speed = 650 rpm

Optical Path: 1 neutral density filter
1 color filter

LOW STABLE STATE

Sample	1	2	3	4
X	0.271	0.270	0.274	0.276
X_N	-	129	116	135
X_W	-	423	393	426
PD	-	3.29	3.40	3.16

METASTABLE STATE

Sample	1	2	3
X	0.534	0.556	0.551
X_N	-	140	204
X_W	-	473	611
PD	-	3.37	2.99

APPENDIX E

SUMMARY OF EXPERIMENTAL RESULTS - ISOTHERMAL BATCH

TABLE 23

ISOTHERMAL BR EXPERIMENT 1

T = 305 K

S_o = 1.5×10^{-4} g-moles/c.c.

I_o = 11.7×10^{-8} Eins/sec-cm^2

Agitator Speed = 650 rpm

Optical Path: 1 neutral density filter
1 color filter

Diaphragm I.D. = 4.7 cm

Sample	Time (min)	X	X_N	X_W	PD
1	120	0.030	-	-	-
2	240	0.058	112	277	2.48
3	360	0.083	-	-	-
4	480	0.114	106	316	2.97
5	600	0.140	60	169	2.80
6	690	0.167	60	181	3.00

TABLE 24

ISOTHERMAL BR EXPERIMENT 2

T = 323 K

S_o = 1.0×10^{-4} g-moles/c.c.

I_o = 11.7×10^{-8} Eins/sec-cm^2

Agitator Speed = 650 rpm

Optical Path: 1 neutral density filter
1 color filter

Diaphragm I.D. = 4.7 cm

Sample	Time (min)	X	X_N	X_W	PD
1	90	0.046	-	-	-
2	180	0.089	68	299	4.38
3	270	0.134	-	-	-
4	390	0.200	64	246	3.84
5	510	0.275	-	-	-
6	600	0.323	71	234	3.30
7	690	0.392	-	-	-
8	810	0.458	74	242	3.30
9	930	0.509	-	-	-
10	1050	0.538	81	279	3.45
11	1110	0.552	83	288	3.49

TABLE 25

ISOTHERMAL BR EXPERIMENT 3

T = 338 K

S_o = 1.5×10^{-5} g-moles/c.c.

I_o = 11.7×10^{-8} Eins/sec-cm^2

Agitator Speed = 650 rpm

Optical Path: 1 neutral density filter
1 color filter

Diaphragm I.D. = 4.7 cm

Sample	Time (min)	X	X_N	X_W	PD
1	60	0.059	92	354	3.84
2	120	0.118	126	646	5.11
3	180	0.173	115	380	3.32
4	270	0.219	-	-	-
5	360	0.249	146	525	3.59
6	480	0.260	-	-	-
7	600	0.280	156	567	3.63

TABLE 26

ISOTHERMAL BR EXPERIMENT 4

T = 338 K

S_o = 2.5×10^{-5} g-moles/c.c.

I_o = 11.7×10^{-8} Eins/sec-cm^2

Agitator Speed = 650 rpm

Optical Path: 1 neutral density filter
1 color filter

Diaphragm I.D. = 4.7 cm

Sample	Time (min)	X	X_N	X_W	PD
1	30	0.051	117	598	5.12
2	90	0.150	-	-	-
3	150	0.242	107	339	3.16
4	210	0.277	-	-	-
5	270	0.313	128	395	3.09
6	400	0.364	-	-	-
7	540	0.407	153	576	3.76
8	660	0.425	-	-	-
9	720	0.445	164	634	3.88

TABLE 27

ISOTHERMAL BR EXPERIMENT 5

T = 338 K

S_o = 1.0×10^{-4} g-moles/c.c.

I_o = 11.7×10^{-8} Eins/sec-cm^2

Agitator Speed = 650 rpm

Optical Path: 1 neutral density filter
1 color filter

Diaphragm I.D. = 4.7 cm

Sample	Time (min)	X	X_N	X_W	PD
1	75	0.058	-	-	-
2	150	0.128	80	382	4.75
3	210	0.174	-	-	-
4	270	0.236	79	354	4.48
5	330	0.300	-	-	-
6	390	0.333	-	-	-
7	435	0.382	73	310	4.25
8	480	0.423	74	307	4.17
9	525	0.467	-	-	-
10	570	0.522	96	328	3.43
11	615	0.564	-	-	-
12	660	0.618	95	328	3.45

TABLE 28

ISOTHERMAL BR EXPERIMENT 6

T = 338 K

S_o = 1.0×10^{-4} g-moles/c.c.

I_o = 11.7×10^{-8} Eins/sec-cm^2

Optical Path: 1 neutral density filter
1 color filter

Diaphragm I.D. = 4.7 cm

Sample	Time (min)	X	X_N	X_W	PD
1	120 (D)	0.112	87	443	5.09
2	120 (L)	0.112	97	486	5.03
3	240 (D)	0.211	83	367	4.42
4	240 (L)	0.215	84	395	4.70
5	360 (D)	0.328	82	354	4.33
6	360 (L)	0.331	76	326	4.31
7	480 (D)	0.457	-	-	-
8	480 (L)	0.464	-	-	-
9	570 (D)	0.562	94	380	4.03
10	575 (L)	0.588	78	329	4.24
11	645 (D)	0.670	-	-	-
12	650 (L)	0.673	-	-	-

*** L: Light Region
D: Dark Region

Agitator Speed = 350 rpm

TABLE 29

ISOTHERMAL BR EXPERIMENT 7

T = 338 K

S_o = 1.0×10^{-4} g-moles/c.c.

I_o = 11.7×10^{-8} Eins/sec-cm^2

Agitator Speed = 650 rpm

Optical Path: 1 neutral density filter
1 color filter

Diaphragm I.D. = 2.5 cm

Sample	Time (min)	X	X_N	X_W	PD
1	90	0.070	101	562	5.58
2	180	0.128	-	-	-
3	270	0.188	96	472	4.90
4	360	0.258	-	-	-
5	450	0.323	95	426	4.49
6	540	0.390	99	412	4.15
7	600	0.446	89	383	4.31
8	660	0.501	-	-	-
9	720	0.557	103	382	3.71
10	765	0.604	-	-	-
11	795	0.647	104	377	3.62

TABLE 30

ISOTHERMAL BR EXPERIMENT 8

T = 338 K

S_o = 1.0×10^{-4} g-moles/c.c.

I_o = 5.1×10^{-8} Eins/sec-cm^2

Agitator Speed = 650 rpm

Optical Path: 1 neutral density filter
1 color filter

Diaphragm I.D. = 4.7 cm

Sample	Time (min)	X	X_N	X_W	PD
1	120	0.098	114	654	5.70
2	210	0.166	-	-	-
3	300	0.221	103	470	4.57
4	390	0.287	-	-	-
5	480	0.363	89	334	3.75
6	540	0.417	-	-	-
7	600	0.458	102	415	4.06
8	660	0.513	-	-	-
9	705	0.561	98	387	3.94
10	750	0.601	-	-	-
11	780	0.651	103	389	3.78

TABLE 31

ISOTHERMAL BR EXPERIMENT 9

T = 358 K

S_o = 2.5×10^{-5} g-moles/c.c.

I_o = 0.

Agitator Speed = 650 rpm

Sample	Time (min)	X	X_N	X_W	PD
1	90	0.013	-	-	-
2	150	0.020	378	1630	4.31
3	210	0.030	-	-	-
4	270	0.038	409	1548	3.78
5	336	0.050	-	-	-
6	396	0.060	421	1808	4.29
7	450	0.073	429	1897	4.43

TABLE 32

ISOTHERMAL BR EXPERIMENT 10

T = 358 K

S_o = 2.5×10^{-5} g-moles/c.c.

I_o = 11.7×10^{-8} Eins/sec-cm^2

Agitator Speed = 650 rpm

Optical Path: 1 neutral density filter
1 color filter

Diaphragm I.D. = 4.7 cm

Sample	Time (min)	X	X_N	X_W	PD
1	45	0.087	115	579	5.02
2	90	0.179	-	-	-
3	150	0.292	147	590	4.02
4	210	0.394	-	-	-
5	255	0.457	174	601	3.45
6	315	0.502	-	-	-
7	375	0.543	202	705	3.50
8	430	0.581	231	849	3.68

TABLE 33

ISOTHERMAL BR EXPERIMENT 11

T = 373 K

S_o = 2.5×10^{-5} g-moles/c.c.

I_o = 11.7×10^{-8} Eins/sec-cm^2

Agitator Speed = 650 rpm

Optical Path: 1 neutral density filter
1 color filter

Diaphragm I.D. = 4.7 cm

Sample	Time (min)	X	X_N	X_W	PD
1	30	0.070	129	635	4.95
2	60	0.156	-	-	-
3	90	0.243	159	594	3.75
4	125	0.336	125	514	4.12
5	170	0.464	159	633	3.99
6	215	0.569	163	615	3.77

TABLE 34

ISOTHERMAL BR EXPERIMENT 12

T = 383 K

S_o = 0.

I_o = 0.

Agitator Speed = 650 rpm

Sample	Time (min)	X	X_N	X_W	PD
1	45	0.038	-	-	-
2	90	0.073	-	-	-
3	150	0.129	860	3322	3.86
4	210	0.176	1298	4110	3.17
5	270	0.221	1407	4835	3.44
6	330	0.260	1482	4753	3.21

TABLE 35

ISOTHERMAL BR EXPERIMENT 13

T = 383 K

S_o = 2.5×10^{-5} g-moles/c.c.

I_o = 0.

Agitator Speed = 650 rpm

Sample	Time (min)	X	X_N	X_W	PD
1	45	0.044	1092	3068	2.81
2	90	0.095	-	-	-
3	135	0.120	-	-	-
4	180	0.161	1219	3329	2.73
5	240	0.214	1090	3624	3.33
6	300	0.253	-	-	-
7	360	0.309	1242	3702	2.98

TABLE 36

ISOTHERMAL BR EXPERIMENT 14

T = 383 K

S_o = 0.

I_o = 11.7×10^{-8} Eins/sec-cm^2

Agitator Speed = 650 rpm

Optical Path: 1 neutral density filter
1 color filter

Diaphragm I.D. = 4.7 cm

Sample	Time (min)	X	X_N	X_W	PD
1	60	0.048	972	4733	4.87
2	120	0.096	831	4223	5.08
3	180	0.140	1343	5090	3.79
4	240	0.184	1156	5522	4.78
5	285	0.217	-	-	-
6	330	0.242	1051	5076	4.83

TABLE 37

ISOTHERMAL BR EXPERIMENT 15

T = 383 K

S_o = 1.5×10^{-5} g-moles/c.c.

I_o = 11.7×10^{-8} Eins/sec-cm^2

Agitator Speed = 650 rpm

Optical Path: 1 neutral density filter
1 color filter

Diaphragm I.D. = 4.7 cm

Sample	Time (min)	X	X_N	X_W	PD
1	30	0.102	-	-	-
2	60	0.203	219	924	4.22
3	85	0.283	273	1108	4.06
4	110	0.360	291	1103	3.79
5	140	0.425	310	1136	3.67
6	185	0.531	345	1295	3.75

TABLE 38

ISOTHERMAL BR EXPERIMENT 16

T = 393 K

S_o = 2.5×10^{-5} g-moles/c.c.

I_o = 0.

Agitator Speed = 650 rpm

Sample	Time (min)	X	X_N	X_W	PD
1	30	0.057	-	-	-
2	60	0.100	1529	4364	2.85
3	90	0.160	1601	4400	2.75
4	120	0.183	-	-	-
5	150	0.220	1792	4805	2.68
6	200	0.304	1655	4696	2.84

TABLE 39

ISOTHERMAL BR EXPERIMENT 17

T = 393 K

S_o = 1.5×10^{-5} g-moles/c.c.

I_o = 11.7×10^{-8} Eins/sec-cm^2

Agitator Speed = 650 rpm

Optical Path: 1 neutral density filter
1 color filter

Diaphragm I.D. = 4.7 cm

Sample	Time (min)	X	X_N	X_W	PD
1	15	0.051	-	-	-
2	30	0.131	260	1210	4.66
3	45	0.219	-	-	-
4	60	0.299	275	1150	4.18
5	75	0.372	317	1222	3.85
6	90	0.449	292	1128	3.86
7	110	0.540	328	1161	3.54

TABLE 40

ISOTHERMAL BR EXPERIMENT 18

T = 338 K

S_o = 1.0×10^{-4} g-moles/c.c.

I_o = 11.7×10^{-8} Eins/sec-cm^2

Agitator Speed = 650 rpm

Optical Path: 1 neutral density filter
1 color filter

Diaphragm I.D. = 4.7 cm

Styrene: 80 wt%
Benzene: 20 wt%

Sample	Time (min)	X	X_N	X_W	PD
1	60	0.051	89	277	3.12
2	120	0.104	72	220	3.09
3	210	0.182	60	186	3.10
4	300	0.248	62	207	3.35
5	390	0.340	56	186	3.35
6	570	0.457	67	196	2.94
7	810	0.550	76	216	2.84
8	1050	0.588	71	199	2.79
9	1320	0.602	83	237	2.85
10	1380	0.612	80	238	2.97

APPENDIX F

SUMMARY OF EXPERIMENTAL RESULTS - ADIABATIC BATCH

TABLE 41

ADIABATIC BR EXPERIMENT 1

T_o = 338 K

S_o = 1.0×10^{-4} g-moles/c.c.

I_o = 11.7×10^{-8} Eins/sec-cm^2

Agitator Speed = 650 rpm

Optical Path: 1 neutral density filter
1 color filter

Diaphragm I.D. = 4.7 cm

Sample	Time (min)	T (K)	X	X_N	X_W	PD
1	60	340.8	0.065	83	403	4.88
2	120	343.0	0.151	65	333	5.15
3	180	347.4	0.213	90	362	4.01
4	240	351.9	0.317	70	327	4.64
5	300	360.2	0.420	93	354	3.81
6	345	370.8	0.529	101	367	3.64
7	385	379.7	0.705	148	414	2.80

TABLE 42

ADIABATIC BR EXPERIMENT 2

T_o = 338 K

S_o = 1.0×10^{-4} g-moles/c.c.

I_o = 11.7×10^{-8} Eins/sec-cm^2

Agitator Speed = 650 rpm

Optical Path: 1 neutral density filter
1 color filter

Diaphragm I.D. = 4.7 cm

Styrene: 87 wt%
Benzene: 13 wt%

Sample	Time (min)	T (K)	X	X_N	X_W	PD
1	60	338.0	0.062	-	-	-
2	120	338.6	0.127	68	347	5.07
3	180	343.6	0.178	-	-	-
4	240	347.7	0.242	76	306	4.04
5	300	350.8	0.317	-	-	-
6	360	353.6	0.389	79	291	3.68
7	450	358.6	0.518	-	-	-
8	540	362.4	0.667	87	276	3.18
9	600	364.4	0.728	-	-	-
10	640	367.2	0.794	99	296	2.99

TABLE 43

ADIABATIC BR EXPERIMENT 3

T_o= 338 K

S_o= 0.5×10^{-5} g-moles/c.c.

I_o= 11.7×10^{-8} Eins/sec-cm^2

Agitator Speed = 650 rpm

Optical Path: 1 neutral density filter
1 color filter

Diaphragm I.D. = 4.7 cm

Sample	Time (min)	T (K)	X	X_N	X_W	PD
1	45	338.6	0.033	135	364	2.70
2	90	338.6	0.079	175	441	2.53
3	135	341.3	0.100	191	525	2.74
4	180	344.1	0.112	208	627	3.02
5	240	347.4	0.132	210	694	3.31
6	300	349.1	0.154	241	799	3.32
7	345	347.7	0.178	245	860	3.52

TABLE 44

ADIABATIC BR EXPERIMENT 4

T_o= 393 K

S_o= 1.5×10^{-5} g-moles/c.c.

I_o= 11.7×10^{-8} Eins/sec-cm^2

Agitator Speed = 650 rpm

Optical Path: 1 neutral dendity filter
1 color filter

Diaphragm I.D. = 4.7 cm

Sample	Time (min)	T (K)	X	X_N	X_W	PD
1	15	391.3	0.070	156	608	3.19
2	30	393.0	0.153	-	-	-
3	45	394.0	0.248	202	694	3.44
4	60	394.0	0.342	-	-	-
5	75	394.0	0.418	227	721	3.17
6	90	394.0	0.500	-	-	-
7	105	395.0	0.618	256	741	2.89
8	115	395.7	0.841	-	-	-

NOMENCLATURE

Symbol	Definition
A_1, A_2, A_3	Model Parameters in Equation (26)
AH	Diel-Alder Adduct
C_p	Specific Heat, cal/g-mole
E	Activation Energy, cal/g-mole
g	Defined in Equation (45)
ΔH	Heat of Reaction, cal/g-mole
I_o	Incident Light Intensity, Eins/sec-cm^2
I_{as}	Absorbed Light Intensity, Eins/sec-cm^3
i, j	Number of Monomer Units
k_d	Rate Constant for Reaction of Sensitizer Radical with Monomer, cc/g-mole-sec
$\bar{k}_i$	Rate Constant for Initiation 3rd Order in Monomer, $cc^2/g\text{-}mole^2\text{-}sec$
k_{fm}	Rate Constant for Chain Transfer to Monomer, cc/g-mole-sec
k_p	Propagation Rate Constant, cc/g-mole-sec
k_{tc}	Rate Constant for Termination by Combination, cc/g-mole-sec
k_{td}	Rate Constant for Termination by Disproportionation, cc/g-mole-sec
k_t	$= k_{tc} + k_{td}$
L	Reactor Length, cm

Symbol	Definition
M	Styrene Monomer
m_o	Monomer Concentration in Feed, g-moles/cc
m	Monomer Concentration in Reactor, g-moles/cc
P_i	Concentration of Dead Polymer of Chain Length i Monomer Units, g-moles/cc
PD	Polydispersity
Q	Volumetric Flow Rate, cc/sec
q	Circulation Flow Rate in the Reactor, cc/sec
R_i	Concentration of Free Radical of Chain Length i Monomer Units, g-moles/cc
RS	Radical Scavenger
S_o	Sensitizer Concentration in Feed, g-moles/cc
S	Sensitizer Concentration in Reactor, g-moles/cc
t	Time, sec
T_o	Feed Temperature, K
T	Temperature in Reactor, K
V	Reactor Volume, cc
x	Distance, cm
X	Fractional Conversion
X_N	Number Average Chain Length
X_W	Weight Average Chain Length

Greek Symbol	Definition
α	Defined in Equation (12)
β	Defined in Equation (17)

Greek Symbol	Definition
Ω_{im}	Thermal Initiation Rate, g-moles/cc-sec
Ω_{is}	Photo Initiation Rate, g-moles/cc-sec
Ω_{i}	$= \Omega_{im} + \Omega_{is}$
Ω_{p}	Propagation Rate, g-moles/cc-sec
Ω_{tc}	Termination Rate by Combination, g-moles/cc-sec
Ω_{td}	Termination Rate by Disproportionation, g-moles/cc-sec
Ω_{m}	Monomer Consumption Rate, g-moles/cc-sec
θ	Residence time, second
ϕ_{s}	Quantum Yield of Sensitizer, g-moles/Eins
ϵ	Fractional Change in Volume Between zero and Complete Conversion
ϵ_{m}	Molar Absorptivity of Monomer, cm^2/g-mole
ϵ_{P_i}	Molar Absorptivity of Polymer of Chain Length of j Monomer Units, cm^2/g-mole
ϵ_{s}	Molar Absorptivity of Sensitizer, cm^2/g-mole
ρ	Fluid Density, g/cc

REFERENCES

REFERENCES

1. Knorr, R.S. and O'Driscoll, K.F., "Multiple Steady States, Viscosity, and High Conversion in Continuous Free-Radical Polymerization," J. Appl. Polym. Sci., 14, 2683, (1970).

2. Hui, A.W. and Hamielec, A.E., "Thermal Polymerization of Styrene at High Conversion and Temperature. An Experimental Study," J. Appl. Polym. Sci., 16, 749, (1972).

3. Kawakami, W. and Machi, S., "Effect of Mixing on Nonuniformly Initiated Polymerization by Radiation," AIChE J., 19, 94, (1973).

4. Chen, H.T., Chartier, P.A. and Setthachayanon, S., "Influence of Initiation Mode on Stability and Control of a Chain Reactor," Polym. Engr. Sci., 20, 1197, (1980).

5. Chen, H.T., Kuan, C.N., Setthachayanon, S. and Chartier, P.A., "Photopolymerization in a Continuous Stirred-Tank Reactor: Experiment," AIChE J., 26, 672, (1980).

6. Chen, H.T. and Steenrod, J., "Effect of Mixing on Polymerizations in Batch Reactors: Comparison of Catalytic and Ionizing Radiation Initiations," Polym. Engr. Sci., 15, 357, (1975).

7. Chen, H.T. and Hill, F.B., "Radiation-Induced Polymerizations in Continuous Stirred-Tank Reactors," AIChE J., 17, 933, (1971).

8. Lin, K.F., "Multiplicity and Uniqueness for Binary, Exothermic Reaction in a non-Adiabatic Continuous Stirred Tank Reactor," Chem. Engr. Sci., 35, 1537, (1980).

9. Nishimura, N., "Kinetics of Diffusion-Controlled Free-Radical Polymerizations. II. Bulk Polymerizations of Styrene and Methyl Methacrylate," J. Macromolecular Chem., 1(2), 257, (1966).

10. Boundy, R.H. and Boyer, R.F., "Styrene, It's polymers, Copolymers and Derivativies," Reinhold, NY, (1952).

11. Mendiratta, S.K. and Felder, R.M., "Benzoin- and Benzoin Methyl Ether-Sensitized Photopolymerization of Styrene and Methyl Methacrylate: Quantum Yield and Mixing Effects," AIChE J., 21. 1115, (1975).

12. Felder, R.M. and Hill, F.B., "Mixing Effects in Chemical Reactors - I. Reactant Mixing in Batch and Flow Systems," Chem. Engr. Sci., 24, 385, (1969).

13. Houston, T. and Logan, R.S., "Development of a Photo-Chlorination Reactor," Chem. Engr. Prog., 68, 76, (1972).

14. Klink, A., Lago, J. and Paul, E., "A Photochemical Reactor System," Chem. Engr. Prog., 68, 81, (1972).

15. Kawakami, W. and Isbin, H.S., "Effect of Agitation on Radiation Chemical Reactions Involving Chloral Hydrate Aqueous Solutions," AIChE J., 16, 502, (1970).

16. Carnahan, B., Luther, H.A. and Wilkes, J.O., "Applied Numerical Methods," New York, NY, (1969).

17. Norrish, R.G.W. and Smith, R.R., "Catalyzed Polymerization of Methyl Methacrylate in the Liquid Phase," Nature, 150, 336, (1942).

18. Trommsdorf, E., Kohle, H. and Lagally, P., "Polymerization of Methyl Methacrylate," Makromol. Chem., 1, 169, (1948).

19. Lin, D.J., "Continuous Photopolymerization Reactor in Periodical Operation," M.S. Thesis, New Jersey Inst. Tech. (1981).

20. Bamford, C.H. and Dewar, M.J.S., "Polymerization. I. Method for Determining the Velocity Constants in Polymerization Reactions and its Application to Styrene II. Method for Investigating the Relation Between the Molecular Weights and Intrinsic Viscosities of Polymers, and its Application to Polystyrene," Proc. Roy. Soc. (London), A192, 309, (1948).

21. Pryor, W.A. and Coco, J.H., "Computer Simulation of the Polymerization of Styrene. The Mechanism of Thermal Initiation and the Importance of Primary Radical Termination," Macromolecules, 3, 500, (1970).

22. Yemin, L. and Hill, F.B., "Measurement of Mixing of Chain Centers in a Nonuniformly Initiated Photopolymerization," Ind. Engr. Chem. Fundamental, 8, 210, (1969).

23. Jacob. S.M. and Dranoff, J.S., "Light Intensity Profiles in a Perfectly Mixed Photoreactor," AIChE J., 16, 359, (1970).

24. Muller, A.C., Eichacker, J.C. and Hill, F.B., "The Effects of Partial Illumination and Mixing on the Sensitized Photopolymerization of Methyl Methacrylate," BNL-16455, (1971).

25. Vejtasa, S.A. and Schmitz, R.A., "Steady State Multiplicity and Stability in an Adiabatic Stirred Reactor," AIChE J., 16, 410, (1970).

26. Ausikaitis, J. and Engel, A.J., "Steady State Multiplicity and Stability in an Adiabatic Controlled Cycled Stirred Reactor," AIChE J., 20, 256, (1974).

27. Guha, B.K., Narsimhan, G. and Agnew, J.B., "Transient Behavior of an Adiabatic Continuous-Flow Stirred Tank Reactor," Ind. Engr. Chem. Fundamentals, 14, 146, (1975).

28. Chang, M. and Schmitz, R.A., "Feedback Control of Unstable States in a Laboratory Reactor," Chem. Engr. Sci., 30, 837, (1975).

29. Hoftyzer, P.J. and Zwietering, Th.N., "Characteristics of a Reactor for the Homogeneous Polymerization of Ethylene," Chem. Engr. Sci., 14, 241, (1961).

30. Warden, R.B. and Amundson, N.R., "Stability and Control of Addition Polymerization Reactions," Chem. Engr. Sci., 17, 725, (1962).

31. Hashimoto, S. and Kawakami, W., "Experimental Study on Control of Radiation Polymerization by Dose Rate Regulation," Ind. Engr. Chem., Process Des. Dev., 15, 244, (1976).

32. Schmidt, A.D. and Ray, W.H., "Multiple Steady States and Dynamics of a CSTR for Solution Polymerization," Presented at 73rd Annual Meeting of AIChE, Chicago, (1980).

33. McGovern, J.J., Grim, J.M. and Teach, W.C., "Determination of Monomer in Polystyrene, Spectrophometric and solubility Methods," Anal. Chem., 20, 312, (1948).

34. Newell, J.E., "Residual Monomer in Polystyrene, Spectrophotometric Analysis," Anal. Chem., 23, 445, (1951).

35. Parker, C.A., "A New Sensitive Chemical Actinometer I. Some Trials with Potassium Ferrioxalate," Proc. Roy. Soc., (London), A220, 104, (1953).

36. Hatchard, C.G. and Parker, C.A., "A New Sensitive Chemical Actinometer II. Potassium Ferrioxalate as a Standard Chemical Actinometer," Proc. Roy. Soc., (London), A235, 518, (1956).

37. Setthachayanon, S., "Photopolymerization of Styrene in a Continuous Stirred-Tank Reactor," M.S. Thesis, New Jersey Inst. Tech. (1980).

38. Marr, G.R. and Johnson, E.F., "The Pumping Capacity of Impellers in Stirred Tank," AIChE J., 9, 383, (1963).

39. Ross, R.T. Jr. and Laurence, R.L., "Continuous Casting and Polymerization of Methyl Methacrylate," AIChE Symposium Series, 72, 80, (1976).

40. Jain, R.L., W.W. Graessley and J.S. Dranoff, "Design and Analysis of a Photoreactor for Styrene Polymerization," paper presented at the 3rd Joint Meeting AIChE and Puerto Rican Inst. Chem. Eng., San Juan (1970).

41. Sandru, D., and J.M. Smith, "Photopolymerization of Acrylamide in an Annular Flow Reactor," ibid., 19, 558 (1973).

42. Ibarra, M., and J.M. Smith, "Induction-Period Kinetics in Acrylamide Photopolymerization," AIChE J., 20, 404, (1974).

43. Hill, F.B., and H.T. Chen, "Radiation Initiation of Exothermic Reactions," paper presented at 164th ACS National Meeting, New York, (1972).